HAPLOINSUFFICIENCY OF THE TRIPARTITE MOTIF-CONTAINING PROTEIN 32 INHIBITS UVB-INDUCED PAPILLOMA FORMATION

A Thesis By

Aaron Marcus Wortham

Presented to the Department of Cell, Developmental & Cancer Biology

and Oregon Health & Science University

School of Medicine

in partial fulfillment of

The requirements for the degree of

Master of Science

June 2016

School of Medicine

Oregon Health & Science University

CERTIFICATE OF APPROVAL

This is to certify that the Master's thesis of

Aaron Marcus Wortham

has been approved

_____

Committee Chair

_____

Mentor/Advisor

_____

Member

_____

Member

_____

Member

TABLE OF CONTENTS

CHAPTER I: INTRODUCTION

Part 1: Cutaneous Squamous Cell Carcinoma

Part 2: Trim32

CHAPTER II: APPROACH

Aim 1: Determine if modifying the expression of Trim32 *in vivo* affects tumor development induced via two-stage chemical carcinogenesis.

Aim 2: Determine if Trim32 deficiency *in vivo* affects UVB-induced tumorigenesis in SKH1-E mice.

Aim 3: Determine if Trim32 deficiency *in vivo* inhibits UVB-induced cellular proliferation and apoptosis in SKH1-E mice.

CHAPTER III: METHODS AND MATERIALS

CHAPTER IV: RESULTS

LIST OF FIGURES AND TABLES

APPENDIX I: COAUTHORED PUBLICATION

ABBREVIATIONS

129S;B6	wild type mice on a mixed 129S5/SvEvBrd x C57BL/6J background
Ago1	argonaute 1
cSCC	cutaneous squamous cell carcinoma
D2;B6	wild type mice on a mixed DBA/2 x C57BL/6J background
DAG	diacylglycerol
DMBA	7,-12-dimethylbenz[a]anthracene
EGFR	epidermal growth factor receptor
ERK	extracellular signal-regulated kinase
HaCaT	a human keratinocyte cell line containing homozygous *TP53* inactivating mutations that was cultured in high calcium and at a high temperature (Ha = human adult; Ca = Calcium; T = Temperature)
HNSCC	head and neck squamous cell carcinoma
IκBα	inhibitor of NF-κB, α
IKK	IκB kinase
JNK	Jun-N terminal kinase
MAPK	mitogen-activated protein kinase
MED	minimal erythemal dose
NF-κB	nuclear factor kappa-light-chain-enhancer of activated B cells
NHL	NCL-1, HT2A and Lin-41
Piasy	protein inhibitor of activated STATs, y

PKC	protein kinase C
PS	phosphatidylserine
RING	really interesting new gene
RISC	RNA-induced silencing complex
ROS	reactive oxygen species
SEM	standard error of the mean
SCC	squamous cell carcinoma
SD	standard deviation
STAT	signal transducer and activator of transcription
TNFα	tumor necrosis factor, α
TPA	12-tetradecanoylphorbol-13-acetate
TRIM32	tripartite motif 32
UVA	ultraviolet light A
UVB	ultraviolet light B

ACKNOWLEDGEMENTS

As with all lives, there are countless sources of inspiration, motivation, and advice that I must pay tribute to. I would be remiss if I didn't start by acknowledging my parents, Doreen and Steven Wortham. I have no idea how I got to where I'm at today, but clearly they have made the most important impact (after all, I wouldn't exist if it wasn't for them). For that, I am inexpressively grateful.

Along with the two captains, I would like to mention my other lifelong comrades, the Sisters Wortham. A more eclectic group of siblings is hard to find. A soldier, a researcher, a musician. An evangelical, an atheist, and somewhere in between. And, of course, our leader, who fell far too early, all of us becoming a little lost in her absence. But like all good leaders, her presence remains and her influence is still felt.

To Amber and Tabitha: may we continue to unite in our differences. To Trina, who lives inside anybody fortunate enough to know her: I hope I would have made you proud. Perhaps one day you will throw open the gates, and we'll see each other with smiling faces.

A writer once instructed his readers to treat their significant other like a proverbial partner in crime. With that in mind, I would next like to thank my confidant, S. Chelsea

Hoffer. You have taken me, demons and all, on a most interesting journey, and I can't wait to see what comes next. You grab the cash, I'll handle the crowd.

I also would like to recognize my mentors at Oregon Health & Science University: Dr. Molly Kulesz-Martin, who gave me the opportunity to perform research, and my thesis advisory committee, Dr. Melissa Wong, Dr. Arup Indra, Dr. Mushui Dai, and Dr. R. Stephen Lloyd. Your input and encouragement has been invaluable during my time here. Also, a big thank you to Dr. Caroline Enns for giving me time to work on my thesis when I should have been managing her mouse colonies.

ABSTRACT

Cutaneous squamous cell carcinoma (cSCC) arises when keratinocytes in the epidermis of the skin undergo malignant conversion, often as a result of cumulative UV exposure. In the United States, cSCC is the second most common malignancy, with over half a million new cases each year. Although cSCC is usually detected at an early stage, the surgical removal of cSCC lesions can cause a high degree of morbidity. In addition, the presence of regional or distant metastases at diagnosis is associated with a large increase in mortality, with the five-year survival rate being less than 10% for patients with metastatic disease. Moreover, immunocompromised patients have a significant increased risk of reoccurrence and mortality, and patients being treated for other cancers have been known to develop cSCCs as a side effect to certain targeted therapies.

For patients with metastatic disease, treatment options are limited to chemotherapeutic agents or cetuximab, an EGFR inhibitor. One obstacle encountered while trying to develop new therapies is the controversial role of several kinases and transcription factors such as JNK and NF-κB. In the

case of NF-κB, numerous publications have demonstrated opposing functions for the transcription factor, and the precise nature of the protein's activity in cSCC is still unknown. A deeper understanding of pathways involved during the development of the disease would not only help clarify these findings, but may also lead to the creation of new targeted therapies.

The Tripartite Motif protein 32 (Trim32) has been shown to be upregulated soon after keratinocytes become initiated *in vitro*. Its expression has also been shown to increase in both human and mouse cSCC. However, whether Trim32 plays an active role during malignant progress remains to be determined. In order to further our understanding of the nature of Trim32, we performed a two-stage chemical carcinogenesis on Trim32 deficient and K14-Trim32 transgenic mice. Results from these experiments were inconclusive, but a decrease in the expression of Trim32 did trend with an inhibition of tumorigenesis.

To clarify these initial observations, we backcrossed the deficient and transgenic mice onto the hairless SKH1-E strain, which would allow us to study the effect Trim32 has on the UV response. Untreated *Trim32$^{-/-}$* mice were observed to have a lower body weight and significantly thinner

epidermis. When a UVB carcinogenesis assay was performed, we noted a dramatic decrease in tumor multiplicity and burden in both *Trim32*$^{+/-}$ and *Trim32*$^{-/-}$ mice, as well as a delay in tumor formation for the *Trim32*$^{-/-}$ mice. When skin was collected after a single dose of 2.240 kJ/m^2 UVB, DNA synthesis was inhibited 24 hrs after exposure, and skin thickening was strongly delayed for up to 48 hrs. These results suggest that Trim32 has an important role during the progression of cSCC. Further investigations into the mechanisms by which Trim32 acts are necessary to determine which pathways are being affected.

CHAPTER I: INTRODUCTION

Part 1: Cutaneous Squamous Cell Carcinoma

A. Causes and Risk Factors

Cutaneous Squamous Cell Carcinoma (cSCC) is defined as the malignant proliferation of epidermal keratinocytes in the skin. In the United States, cSCC is second most common type of cancer and accounts for approximately 20% of all nonmelanoma skin malignancies. Since most cancer registries do not track non-melanoma skin cancers, the exact prevalence of cSCC in not known, but it is estimated that half a million cases occur each year (Karia et al., 2013; Rogers et al., 2010). Cutaneous SCC develops mostly on sun exposed skin, with over half of all cases presenting on the head and neck, followed by occurrences on the arms, legs, and trunks (English et al., 1998). The primary causal factor for most cSCC is cumulative exposure to UVA and UVB radiation (primarily sun exposure) over the course of an individual's lifetime. As a result, most occur in older (more than 45 years of age), light skinned, non-Hispanic, white populations (Karagas et al., 1999), and, similarly for other epithelial type of cancers, incidence stochastically increases with age.

While UVB radiation (290 – 320 nm wavelength) is the most common culprit, studies have implicated multiple environmental risk factors in the development of cSCC. Exposure to the lower energy UVA radiation (320 – 400 nm), the primary emission of tanning beds and PUVA (psoralen and UVA) phototherapy, has been correlated with a

large increased risk for developing cSCC (Stern and PUVA Follow-Up Study, 2012; Wehner et al., 2012). Other potential risk factors exist, such as human papilloma virus (HPV) infection, tobacco smoking, and ionizing radiation. However, epidemiological studies on these factors have yielded conflicting results (Chahoud et al., 2015; Kishikawa et al., 2005; Leonardi-Bee et al., 2012). More investigations are needed in order to confirm or dismiss these possibilities.

B. Cellular Effects of UV Radiation

i. Initiation. UVB radiation is directly absorbed by DNA, inducing the formation of cyclobutane pyrimidine dimers (thymine dimers) and pyrimidine (6-4) pyrimidone photodimers (6-4 photoproducts) in the genome of irradiated cells (Cadet et al., 1986; Hart et al., 1977). These pyrimidine dimers can occur between adjacent cytosines and/or thymidines. If left unrepaired by the cell, UVB-induced DNA lesions can stall transcription, leading to the generation of C→T transitions, often in the *TP53* tumor suppressor gene. In contrast, UVA is very poorly absorbed by DNA and therefore acts indirectly by causing the formation of reactive oxygen species (ROS). These free radicals can damage DNA by producing 8-oxo-deoxyguanosine (8-oxo-dG) lesions, which will induce G→T transversions if not repaired (Kielbassa et al., 1997). Contrary to the canonical role of UVA, a recent study demonstrated that exposure to UVA or UVB will result in the formation of C→T mutations (Kappes et al., 2006), and others have observed pyrimidine dimers as the predominant DNA lesion in human primary keratinocytes exposed to UVA *in vitro* (Mouret et al., 2006). While these results highlight

the importance of UVA in cSCC, it remains to be determined which lesion is the primary product when skin is exposed to the UVA rays from sunlight.

As a response to the formation of lesions on DNA, keratinocytes will activate several cellular pathways to remove damaged DNA, inhibit cell cycle progression, stimulate inflammation, and induce apoptosis (Li et al., 1996; Lu et al., 1999). Pyrimidine dimers formed after UV irradiation can be repaired by either the Global Genomic Nucleotide Excision Repair pathway (GG-NER), or the Transcription Coupled Nucleotide Excision Repair pathway (TC-NER) (Laat et al., 1999). As its name implies, the TC-NER is activated when RNA Polymerase II is stalled during transcription by a lesion on the genome. Alternatively, GG-NER is capable of repairing photoproducts by scanning the entire genome for helix distortions. TC-NER and GG-NER also differ in their dependence on p53 activity. When human fibroblasts are null for *TP53*, or are homozygous for a p53 inactivating mutation, the cells fail to activate GG-NER, resulting in an accumulation of C→T transitions (Wani et al., 1999). TC-NER, however, is capable of repairing photoproducts in a p53-independent manner.

The most common mutations in cSCC occur in the *TP53* tumor suppressor gene. Multiple studies have shown that *TP53* mutations can be found in 50-90% of all cSCC (Giglia-Mari and Sarasin, 2003). These mutations often occur on both alleles, resulting in a loss of heterozygosity. Interestingly, the mutations in each allele are usually at different locations, but almost always consist of C→T transitions, confirming that an accumulation of UVB exposure is what drives the transformation of keratinocytes to a

3

malignant state (Tornaletti and Pfeifer, 1994).

Other tumor suppressors have a much more controversial role in the development of cSCC. One such gene, *CDKN2A*, encodes for several tumor suppressors using alternate splicing and an alternate reading frame (Sherr, 2004). One of these proteins, $p16^{INK4}$, is a cyclin-dependent kinase inhibitor that hinders progression through G1 phase of the cell cycle. Several studies have shown that $p16^{INK4}$ is mutated at low frequencies in cSCC (Kubo et al., 1997; Soufir et al., 2000). More commonly, cSCC tumor samples will display a loss of the short arm of chromosome 9, which contains the *CDKN2A* gene (Popp et al., 2002). Interestingly, an increase in $p16^{INK4}$ staining intensity has been observed in some invasive cSCC when compared to benign precursors such as actinic keratoses (Hodges and Smoller, 2002). This may indicate that loss of $p16^{INK4}$ occurs very late in cSCC progression, or that there are multiple, independent pathways a cSCC cells can use to become invasive.

ii.   Promotion. UV-induced mutation events, also known as the "initiation" step of carcinogenesis, occur in tandem with the activation of several pro-inflammatory pathways. The stimulation of signaling cascades by an agent that promotes proliferation and inflammation is termed "promotion" and is necessary for tumor formation. With respects to UV-induced carcinogenesis, promotion occurs when a chromophore (such as tryptophan, DNA, or RNA) absorbs UV light, producing photoproducts that function as ligands for proteins that sense UV-induced damage. In the case of tryptophan, UVB absorption produces the photoproduct 6-formylindolo[3,2-b]carbazole, which was

recently shown to directly activate the cytoplasmic aryl hydrocarbon receptor (AhR) complex, allowing it to translocate to the nucleus and stimulate the transcription of cytochrome P450 1A1 (Fritsche et al., 2007). In the same report, it was demonstrated that knocking out AhR in mice inhibits internalization of EGFR and activation of ERK1/2 after UVB exposure.

Activation of the MAPK/ERK signaling cascade is one of the main pro-inflammatory responses that occurs after UVB irradiation and is capable of inducing apoptosis or cell survival (Muthusamy and Piva, 2010; Schieke et al., 2005). Of the multiple kinases acting in this pathway, p38α is the best studied and, feasibly, the most relevant to the UV response. When primary, cultured keratinocytes are exposed to high levels of UVB radiation (2.0 kJ/m^2), they will undergo apoptosis in a phosphorylated p38α-dependent manner (Hildesheim et al., 2004). Conversely, when a lower dose of UVB is used (0.3 kJ/m2), phosphorylated p38α inhibits apoptosis by sequestering p53 in the cytoplasm (Chouinard et al., 2002). Production of ROS through UVA or UVB treatments can also activate p38α by means of the receptor tyrosine kinase EGFR (Van Laethem et al., 2006).

Several other MAPKs are critical for a complete UV response. Jun-N terminal kinase (JNK) activity is upregulated via phosphorylation 15 to 30 min after human keratinocytes are exposed to 0.3 kJ/m^2 UVB *in vitro* (Chouinard et al., 2002). Like many of the pathways involved in carcinogenesis, the exact consequences of the JNK phosphorylation remains elusive and seems to be contradictory at times.

Phosphorylation of JNKs has been demonstrated to be both anti- and pro-apoptosis, with outcome being dependent upon multiple factors including cell line, UV type, and UV dose (Karin and Gallagher, 2005; Tournier et al., 2000). To explain this phenomenon, some have postulated that continuous activation of JNKs leads to TNFα-induced apoptosis, while a short, transient activation will lead to TNFα-induced cell proliferation (Chen et al., 1996). Another group of MAPKs, the ERK proteins, have been shown to be more consistently oncogenic when activated. Upregulation of ERK1/2 generated anti-apoptotic signals in HaCaT cells, and induces the expression of matrix metalloproteinases, which are involve in tumor progression and metastasis, in cSCC cell lines (He et al., 2004; Ramos et al., 2004).

An additional well-studied UV-response pathway involves the NF-κB family of transcription factors (Baeuerle and Baltimore, 1996). The NF-κB family consist of five members, which are further split into two subfamilies: 1) the Rel proteins p65 (RelA), RelB, and c-Rel; and 2) the NF-κB proteins p50/p105 (NF-κB1), and p52/p100 (NF-κB2). These proteins have been shown to form heterodimers between a Rel and a NF-κB protein, or homodimers between two NF-κB subunits. The main heterodimer that has been consistently shown to have an important role in cSCC, p65/p50, is often referred to simply as NF-κB in the literature, a practice that will be replicated here.

Like the Jun-N terminal kinases, the exact role of NF-κB during the development of cSCC is controversial and most likely dependent on multiple extracellular and intracellular factors. After UVB exposure, NF-κB is capable of being activated by the

6

increase in ROS (DNA-independent) and the presence of pyrimidine photoproducts (DNA-dependent) (Bender et al., 1998; Simon et al., 1994). The activation of NF-κB has been shown to have opposing effects, sometimes within the same model system. Indeed, when mice contain a transgene that overexpress an inhibitor of NF-κB (IκB-α) in keratinocytes, there is both an increase in apoptosis in the basal layer of the skin and the spontaneous formation of invasive cSCC (Hogerlinden et al., 1999). However, others have shown that UVB can induce NF-κB activation in a process that does not involve removal of IκB-α (Lewis and Spandau, 2007). Given these contradictory results, further investigations are needed before developing targeted treatments involving the MAPK or the NF-κB pathways.

C. Treatments

Treatments of cSCC lesions are carried out with relative ease with a low risk of morbidity and an even lower risk of mortality (discussed below). The large majority of cSCCs present with low risk of metastasis or reoccurrence and can be removed using several therapies (Veness, 2006). For small (less than 20 mm in diameter), well-defined, low-risk cSCC, surgical excision is a preferred method of removal, allowing for histological assessment of the specimens' margins post-surgery, which ensures removal of the entire tumor (Brodland and Zitelli, 1992). If a patient is not a candidate for surgical excision (for example, in the case of elderly patients or if the tumor is located in a cosmetically sensitive area), there are several other methods that can be used, including cryotherapy, electrosurgery, and radiation therapy (Lansbury et al.,

2013). These methods are often more sparing of normal, healthy tissue, yielding superior cosmetic results when compared to surgical excision. One important limitation of these alternative methods is the inability to perform a histological analysis of the tumor margins.

For large (greater than 20 mm in diameter), high-risk lesions (for example, reoccurring tumors or lesions on immunocompromised patients), the highly specialized Mohs surgery procedure is the preferred method (Connolly et al., 2012). Mohs surgery involves complete and continuous histological assessment of the margins for the removed tumor during the surgery. This procedure minimizes the amount of normal tissue removed from the patient and ensures complete removal of the tumor. For cSCC, Mohs surgery is highly successful, with one study reporting a reoccurrence rate of 3% (Lansbury et al., 2013).

If the patient presents with locoregional or systemic metastases, or if the primary tumor is unresectable, treatment options are limited. For metastatic disease, chemotherapy, particularly cisplatin-based combinations, is a common regimen (Sadek et al., 1990). Several recent studies have attempted to use cetuximab, a monoclonal antibody to the EGFR receptor, as an adjuvant therapy for metastatic disease, or as a neoadjuvant therapy for unresectable tumors (Maubec et al., 2011; Reigneau et al., 2015). Both of these treatment options have had limited success, as discussed below.

D. Prognosis

Most cases of cSCC present locally and with an excellent prognosis, but a low percentage (1-5%) form nodal or distant metastases (Brougham et al., 2012). Patients who develop metastases are subjected to a high frequency of mortality, with the five-year survival rate between 25 to 35 percent for regional lymph node metastases and less than 10 percent for distant metastases (Rowe et al., 1992). Given the high occurrence of this disease, some researchers have concluded that deaths from cSCC in the southern United States are as frequent as deaths from other common cancers, including melanoma, non-Hodgkin lymphoma, renal cancer, and bladder cancer (Karia et al., 2013). In addition, there are several groups of patients that are at an elevated risk of developing aggressive cSCC. Thirty-five percent of heart transplant recipients will develop skin cancer within 10 years of the transplantation as a result of chronic immunosuppression (Brewer et al., 2009). When compared to immunocompetent patients with cSCC, immunocompromised patients are more likely to acquire local or distant metastases that have an increased aggressiveness, resulting in a low three-year survival rate (Martinez J et al., 2003). Given the high mortality and lack of available treatments for patients with metastatic cSCC (cetuximab is the only targeted therapy used to treat the disease (Maubec et al., 2011)), further investigations into the pathways involved in the development of cSCC is warranted. One protein that has recently shown potential to play a significant role in these pathways is the Tripartite Motif-containing protein 32 (Trim32).

Part 2: Trim32

A. The TRIM Superfamily

Trim32 is a member of a large and functionally diverse group of scaffolding proteins collectively termed the Tripartite Motif superfamily (the TRIM superfamily). Using sequence homology, more than 70 members of this superfamily have been identified. The defining characteristic common to all of these genes is the highly conserved order of domains known as the RBCC motif, which consists of three zinc-binding regions: a RING domain, one or two B-Box domains, and a Coiled-Coil domain (**Figure 1**) (Nisole et al., 2005). The three domains in this "tripartite motif" are all protein-interacting regions, but their functions can be diverse or, for some motifs, unknown.

i. The RING domain. The RING domain (an acronym standing for "Really Interesting New Gene") is a zinc-binding motif located 10-20 amino acids from the N-terminal portion of most TRIM family proteins (Ozato et al., 2008). The RING domain of several proteins, Trim32 included, has been shown to contain E3 ubiquitin ligase activity. This allows for the protein containing the RING domain to catalyze the transfer of ubiquitin from an E2 ubiquitin-conjugating enzyme to a lysine residue of a substrate protein specified by the E3 ligase (Ciechanover, 1994). The ubiquitination process may then continue, forming a chain of covalently-linked ubiquitins on the substrate. The polyubiquitin chain formed often targets the substrate for degradation via the proteasomal pathway. In the case of Trim32, its expression has been shown to up-regulate the ubiquitination, and subsequent degradation, of several proteins important to oncogenesis, including p53, Abl-interactor 2, and the X-linked Inhibitor of Apoptosis
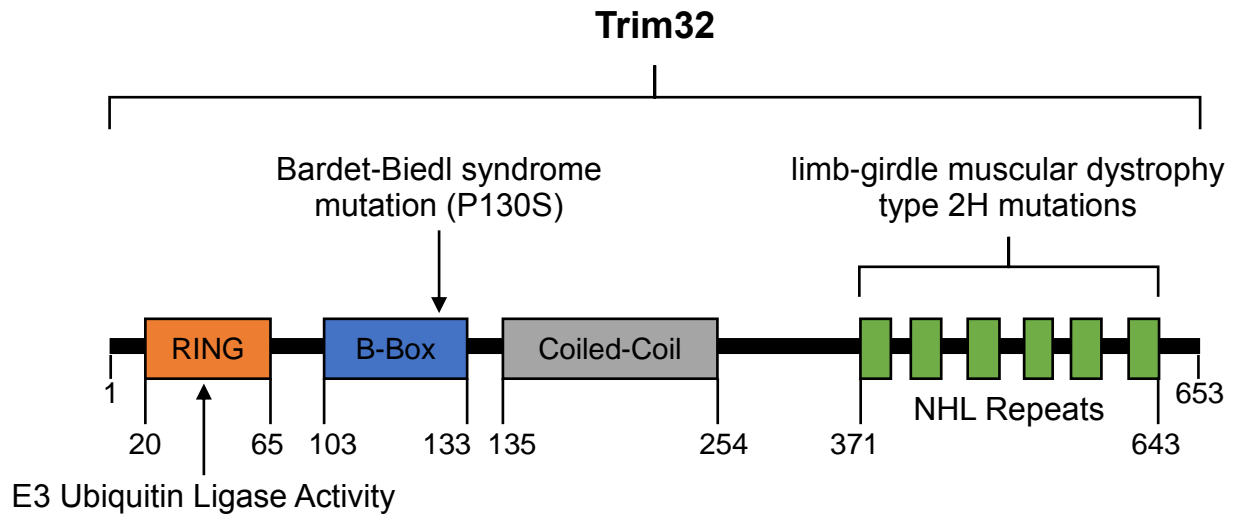
Figure 1. Domain schematic for TRIM32. The TRIM32 protein contains the three domains of the "tripartite motif" near its N-terminus: the RING, B-Box, and Coiled Coil domains. The RING domain harbors E3 ubiquitin ligase activity, while the function of the B-Box and Coiled-Coil remains unknown. A missense mutation in the B-Box domain is linked to the ciliopathy Bardet-Biedl syndrome. As a member of the TRIM C-VII family, TRIM32 contain six NHL repeats near its C-terminus. The NHL repeats are important for regulating miRNA activity, and have been shown to be active in differentiation and quiescence of neural progenitor cells (Fatima et al., 2016). Several mutations and deletions in the NHL repeats are linked to the inheritable disease limb-girdle muscular dystrophy type 2H. Schematic modified from Chiang et al., 2006.

(XIAP) (Kano et al., 2008; Liu et al., 2014; Ryu et al., 2011). One protein, the E3 SUMO ligase and putative tumor suppressor PIASy, was shown not only to be ubiquitinated by Trim32 *in vitro* in a RING domain-dependent manner, but its protein levels were also inversely correlated with Trim32 in cSCC (Albor and Kulesz-Martin, 2007; Albor et al., 2006). In addition, Albor et al. (2006) demonstrated that TRIM32 and PIASy have opposing effects on NF-κB activation, with TRIM32 inducing and PIASy inhibiting the ability of NF-κB to stimulate transcription. These studies suggest that Trim32 might play a prominent role during the progression of cSCC by inhibiting the activity of putative tumor suppressors via proteasomal degradation.

ii. B-Box and Coiled-Coil domains. The function of the B-Box and Coiled-Coil domains are not well understood. Like the RING domain, the B-Box motifs are zinc-containing regions. Using high-density SNP arrays, a homozygous missense mutation in the B-Box domain of Trim32 (P130S) was shown to be present in a group of patients with Bardet-Biedl syndrome, a rare ciliopathy with severe and pleotropic symptoms (Chiang et al., 2006). How the mutated allele contributes to ciliopathy is still unknown, but it was recently shown that Trim32 interacts with another gene linked to a ciliopathy, Glis2 (Ramachandran et al., 2014). The Coiled-Coil region has no known function in Trim32, but has been shown to be necessary for homomeric and heteromeric interacts among other TRIM family members (Ozato et al., 2008).

iii. C-terminal domains. The TRIM superfamily has been divided into 11 sub-classes based on the presences (or absence) of various C-terminal domains (Short and Cox, 2006). As a member of the TRIM C-VII family, Trim32 contains six NHL repeats near its C-terminus (Ozato et al., 2008). Similar to the three domains of the RBCC motif, the NHL repeats contain protein-binding capabilities. Several deletions, missense and nonsense mutations in this region are believed to be the cause of the autosomal recessive disorder limb-girdle muscular dystrophy type 2H (LGMD2H) (Kudryashova et al., 2011; Neri et al., 2013). Uniquely, the NHL repeats of Trim32 have also been shown to be necessary for Trim32 to regulate neural differentiation and quiescence by modulating the activity of miRNAs and proteins associated with proliferation (Hillje et al., 2011, 2013; Schwamborn et al., 2009). In neural stem cells, TRIM32 binds to and is inhibited by protein kinase C ζ (PKCζ). During differentiation, the ubiquitination of PKCζ by TRIM32 and the decrease in PKCζ expression allows for TRIM32 to translocate into the nucleus. There, TRIM32 binds to and ubiquitinates c-Myc, which inhibits proliferation and induces differentiation. Schwamborn et al. (2009) also showed that the NHL domain of TRIM32 binds to Argonaute 1 in differentiating neurons, increasing its affinity for the miRNA Let-7a, which promotes differentiation and quiescence. These studies provide evidence supporting the hypothesis that an increase in TRIM32 expression and activity induces the differentiation of neural progenitors, a finding that contrasts with previous studies showing a RING domain-dependent increase in proliferation, motility, and survival (Kano et al., 2008; Liu et al., 2014). Given this dual nature of Trim32, it is likely that this gene has multiple and varying functions in different tissues and possibly in different cancers.

B. Trim32 in Diseases and Disorders

i. Trim32 and innate immunity. The initial discovery of TRIM32 (then called HT2A) used a yeast two-hybrid system to a direct interaction between Trim32 and the activation domain of the lentiviral Tat proteins (Fridell et al., 1995). The same study also demonstrated that exogenous TRIM32 can bind to HIV-1 Tat in the nucleus of mammal COS cells. Exactly how TRIM32 affects Tat activity was unknown until a much later study investigated the effect of TRIM32 in human neural precursor cells (Fatima et al., 2016). TRIM32 is most highly expressed in brain tissue (Horn et al., 2004), and its expression has been shown to increase in differentiating mouse neural progenitor cells (Schwamborn et al., 2009). Likewise, HIV-1 infection of human neural precursor cells (hNPCs) also induces differentiation and quiescence (Mishra et al., 2010), leading to HIV-1 associated neurocognitive disorders such as dementia (Maschke et al., 2000). Fatima et al. (2016) showed that the HIV-1 Tat protein and TRIM32 work in synergy to inhibit proliferation. Infection with HIV-1 Tat inhibits the expression of the miR-155. As a result, *TRIM32* mRNA, which contains a miR-155 binding sequence in its 3' untranslated region, is stabilized, allowing for an increase in protein levels and for TRIM32 to translocate to the nucleus, where it inhibits c-Myc.

ii. Genetic disorders associated with Trim32. Since the mid-1990s, a missense mutation in the third NHL repeat of *TRIM32* (p.D487N) has been correlated with a rare form of limb-girdle muscular dystrophy (Frosk et al., 2002). In a study published more recently (Saccone et al., 2008), the *TRIM32* gene in 310 patients with limb-girdle muscular dystrophy was sequenced, and three new mutations were identified: a

missense mutation in the first NHL repeat (p.R394H), a deletion in the fifth NHL repeat (p.D588del), and a deletion in the fourth NHL repeat that results in a truncated protein (p.T520YfsX13). The presence of multiple *TRIM32* mutations in patients with LGMD2H is supportive of the hypothesis that TRIM32 plays a functional role in the development of the disorder. To further support this premise, Kudryashova et al. (2009) created a Trim32-deficient mouse and observed a mild sarcotubular myopathy in the deficient animals. A later study by the same investigators used a knock-in mouse that carried the D489N mutation in *Trim32* (Kudryashova et al., 2011). While the mRNA levels of *Trim32* were similar to wild type mice, the protein levels of TRIM32 were severely reduced in the primary myoblasts of the knock-in mice, suggesting that the mutation destabilized the protein.

iii. Trim32 expression in tumors. As it relates to cSCC, there is mounting evidence that Trim32 has oncogenic activities. The first study to implicate Trim32 in cancer was published by Horn et al. in 2004. Using a clonal epidermal model for mouse carcinogenesis, the investigators showed that Trim32's expression is increased in initiated keratinocytes and stays elevated as the disease progresses to malignant cSCC. In addition, Horn et al. analyzed Trim32 mRNA expression in mouse tumors produced using two-stage chemical carcinogenesis. When compared to un-irradiated ventral skin, 24% of the samples had an increase in Trim32 protein levels. When the same analysis was done using tumors that formed after chronic UVB irradiation, 100% of the tumor samples had a 2 to 6 fold increase in Trim32 protein levels. The later of these two analyses is significant given that cumulative sun exposure (particularly UVB

radiation) is the main cause of cSCC in humans (as opposed to intermittent acute sun exposure, which is the most important risk factor for basal cell carcinoma and melanoma) (Armstrong and Kricker, 2001). In addition, Horn et al. analyzed the TRIM32 mRNA levels in 21 tumor samples from patients with head and neck squamous cell carcinoma and compared the results to adjacent tissue isolated from the same patient. They found that 21% of the samples had elevated TRIM32 mRNA levels. Since the adjacent tissue likely contains initiated keratinocytes, it's plausible that overexpression of Trim32 was underreported in the analysis. To support this hypothesis, Horn et al. compared TRIM32 mRNA expression levels in the adjacent mucosa to its expression levels in normal mucosal tissue isolated from sleep apnea patients. They found that relative TRIM32 mRNA levels were significantly higher in the adjacent, initiated mucosa when compared to normal mucosa tissue. A later study from the same group showed an inverse relationship between Trim32 and the putative tumor Piasy in cSCC (Albor and Kulesz-Martin, 2007), adding evidence to the possibility that Trim32 expression facilitates the survival and proliferation of transformed keratinocytes.

iv. Oncogenic activity of Trim32 *in vitro*. In addition to the *in vivo* expression analyses, Horn et al. investigated Trim32's function using the 291 cells, a normal mouse keratinocyte cell line. After growing keratinocytes in a media that induces terminal differentiation, they observed an increase in colony formation in 291 cells overexpressing Trim32, suggesting that Trim32 expression helps keep keratinocytes in a more proliferative state. Trim32-overexpression also protected 291 cells from UVB-induce apoptosis, and when engrafted onto the dorsal skin of mice, Trim32

overexpression increased skin thickening as a response to UVB radiation and TPA treatments.

Other investigations have corroborated these results. In 2008, Kano et al. showed that overexpression of Trim32 *in vitro* induced the degradation of the putative tumor suppressor Abi2. In addition, suppression of cellular proliferation by Abi2 overexpression was rescued by co-overexpression with Trim32. In the same study, they showed that Trim32 expression also suppresses apoptosis induced by cisplatin treatment and increases cell motility in NIH 3T3 cells. A separate group later demonstrated that Trim32 and the potent tumor suppressor p53 form a negative feedback loop (Liu et al., 2014). In response to stressors such as 5-fluorouracil, p53 directly upregulates Trim32 expression, which in turn catalyzes the ubiquitination of p53. This response was shown to lead to a suppression of p53-mediated apoptosis, cell cycle arrest, and senescence. However, given that p53 mutations occur early on in cSCC development (Giglia-Mari and Sarasin, 2003), it is still unknown how important this feedback loop is in tumorigenic keratinocytes.

v.   The effects of Trim32 on cSCC *in vivo*. All of the studies mentioned above share a similar theme: they relied of correlative data (as in the case of Horn et al.), or they perform overexpression and knockdown studies *in vitro*. More direct *in vivo* evidence is needed to confirm the role of Trim32 in cancer in general, and cSCC in particular. The focus of this thesis is to determine whether the endogenous expression of Trim32 is important for the development and/or progression of cutaneous squamous cell tumors *in*

vivo. Given the results from previous studies, it is my hypothesis that a deficiency in Trim32 expression will result in an inhibition of UVB-induced proliferation and cell survival, leading to a decrease in tumorigenesis. To approach this study, I proposed the three aims discussed in the next chapter.

CHAPTER II: APPROACH

Aim 1: Determine if modifying the expression of Trim32 *in vivo* affects tumor development induced via two-stage chemical carcinogenesis.

A. DMBA/TPA Chemical Carcinogenesis

The two-stage chemical carcinogenesis model (also called multi-stage chemical carcinogenesis) is a well established method of inducing papilloma (benign keratinocyte tumors) formation using sequential treatments over the course of several months (Abel et al., 2009). In this model, mice are first treated with a sub-carcinogenic dose of a chemical mutagen such as 7,-12-dimethylbenz[a]anthracene (DMBA). DMBA is an intercalating molecule that frequently induces an activating mutation in the oncogene *Hras1* by causing an A→T transversion in codon 61 (Rehman et al., 2000). Since DMBA is applied at sub-carcinogenic levels, repeated treatments with a promoting agent, such as the phorbol ester 12-*O*-tetradecanoylphorbol-13-acetate (TPA), are necessary to induce papilloma formation. The mechanisms by which TPA induces proliferation are well understood and involve the direct activation of the membrane associated enzyme Protein kinase Cε (PKCε) (Jansen et al., 2001a).

i.   TPA-activation of the Protein Kinase C pathways. Protein kinase C (PKC) is a family of at least 12 serine/threonine kinases. Six of these kinases (α, δ, ε, η, μ, and ζ) are expressed in epidermal keratinocytes (Hashimoto et al., 1994). The *PKC* genes have been divided further into four subfamilies on the basis of activation requirements,

structure, and cofactors (Aziz et al., 2007a). The classical PKC (cPKC) subfamily consists of α, βI, βII, and γ isoforms and must interact with phosphatidylserine (PS), diacylglycerol (DAG) and Ca^{2+} for activation. Novel PKCs (nPKCs), the δ, ε, η, and θ isoforms, require DAG and PS but not Ca^{2+} for activation. The third subfamily, atypical PKCs, works independently of Ca^{2+} and DAG, but still requires PS. A fourth group that is less structurally similar to the others, the PKC-related kinases, are comparable to atypical PKCs in that they only require PS for activation (Mellor and Parker, 1998).

It is well established that DAG and phorbol esters such as TPA are potent activators of PKCs by directly interacting with the C_2 regulatory domain near the N-terminus of cPKCs and nPKCs (Blumberg, 1991). This interaction allows for PKCs to translocate to the plasma membrane, where its C_1 domain binds to PS. The binding of PS induces a conformational change, releasing the "pseudosubstrate" domain from the kinase site, which in turn allows for the PKC to phosphorylate its substrate.

When the interaction between TPA and PKC is studied in PKC-overexpressing mice, the outcome is dependent of the particular PKC transgene. Overexpression of PKCα has been shown to have no effect on DMBA/TPA carcinogenesis, while PKCδ and PKCε have been shown to have opposing effects (Jansen et al., 2001b; Reddig et al., 1999, 2000). Reddig et al, demonstrated in 1999 and 2000 that overexpression of PKCδ inhibits TPA-induced tumor promotion, while PKCε-overexpression strongly promotes tumorigenesis. PKCδ functions in part by increasing the expression of the tumor suppressor AP-1 (Hirai et al., 1994). PKCε activation, however, induces the expression

of oncogenes such as *c-Myc* through its activation of the transcription factor STAT3 (Aziz et al., 2007a). Interestingly, the expression of the endogenous genes for *PKCδ* and *PKCε* remain largely unchanged during mouse skin carcinogenesis (Mills et al., 1992).

ii. The role of Trim32 in DMBA/TPA carcinogenesis. In this study, we applied a DMBA/TPA chemical carcinogenesis protocol previously verified (Abel et al., 2009) to induce the formation of papillomas in genetically engineered mouse models (GEMMs). In order to look at the effect of Trim32, we utilized two GEMMs: a TRIM32-deficient strain and a *K14-Trim32* transgenic strain, which uses the *K14* promoter to selectively overexpress Trim32 in keratinocytes. Since Horn et al. and other investigators have associated Trim32 with an oncogenic role in cancer, we hypothesized that removal of the *Trim32* gene would result in a decrease in papilloma formation, a decrease in the size of the papillomas, and an increase in time until papillomas become observable. Overexpression of Trim32 in the *K14-Trim32* transgenic mice would have the opposite effect, causing an increase in papilloma size and numbers, and a decrease in the time to papilloma formation.

B. Limitations

i. Inducing carcinogenesis on mixed inbred strains. For this experiment, we used K14-Trim32$^{tg/tg}$, K14-Trim32$^{tg/+}$, Trim32$^{-/-}$, and Trim32$^{+/-}$ mice, in addition to their wild type littermates. The K14-Trim32 transgenic mice were maintained on a DBA/2 x

C57BL/6J mixed inbred strain, and the TRIM32-deficient mice were maintained on a 129S5/SvEvBrd x C57BL/6J mixed inbred strain. Performing a chemical carcinogenesis with mice on a mixed inbred strain presents with several complications since the amount of tumorigenesis induced by chemical treatments of DMBA and TPA varies widely amongst mouse strains (Abel et al., 2009). If an initiating dose of 100 nmol DMBA and a twice weekly promoting dose of 4 µg TPA is applied to C57BL/6, DBA/2, or 129/SvEv mice, the percentage of mice that form papillomas is expected to be 42%, 83%, and 100%, respectively (Reiners and Singh, 1997; Sundberg et al., 1997). Likewise, the number of papillomas per mouse in the three strains also varies, with C57BL/6 being the most resistant (2.2 papillomas per mouse) and 129/SvEv being the most susceptible (10 papillomas per mouse).

An additional complication was the unknown generation of our two colonies. Consequently, we could not accurately predict the background strain percentage for each mouse, nor could we predict the average tumor incidence. Also, given the large number of mice on the experiment, it was unfeasible to undergo background strain characterization. As a result, we decided to randomly divide the mice into two treatment groups: a group treated once weekly with TPA (Group A) and a group treated twice weekly (Group B). Nevertheless, this had the added advantage of letting us analyze the effects of TRIM32 on TPA-induced proliferation.

Treatment with TPA induces thickening of the mouse epidermis via its activation of PKC (Lewis and Adams, 1987). In order to determine if Trim32 affects TPA-induced

proliferation, Horn et al. (2004) overexpressed Trim32 or green fluorescent protein (GFP) in 291 mouse keratinocytes and subsequently engrafted the cells onto the back of nude mice. The engrafted mice were then treated with 2 µg TPA once weekly for 20 weeks. When tissue was collected and analyzed 5 weeks after the last treatment, Trim32-overexpressing epidermis had a prolonged TPA-induced thickening when compared to the GFP control. Therefore, we hypothesized that, compared to wild type controls, K14-Trim32 mice would have disproportionate increase in papilloma formation in the twice weekly treatment group. Removal of the *Trim32* gene would inhibit TPA-induced proliferation, resulting in a dramatic decrease in tumorigenesis in the TRIM32-deficient mice.

ii. Characterization of the *K14-TRIM32* transgene. The K14-Trim32 transgenic mouse strain was recently generated at Oregon Health and Science University Transgenic Facility using the established method of performing a pronuclear injection of the transgene into an embryo (Gordon and Ruddle, 1981). Using this technique, multiple copies of the injected transgene will randomly integrate into the zygotic genome. We previously verified the expression of the transgene (data not shown), but the number and locations of the transgene insertion sites remains unknown. We were able to differentiate between *K14-TRIM32$^{tg/tg}$* and *K14-TRIM32$^{tg/+}$* through selective breeding, but without knowing the insertion site of the transgene, it is difficult to establish any potential phenotypic complications arising from the proximity of the transgene to other endogenous elements.

In addition to proximity effects, it is possible for the transgene of a GEMM to be expressed in unexpected tissues, and the levels of expression can vary between sexes, generations, and even littermates (Heffner et al., 2012). Furthermore, a higher copy number of the transgene can lead to an increase or an inhibition of expression as a results of unintended epigenetic events (Garrick et al., 1998; Williams et al., 2008). Therefore, without further investigations into locations and frequency of the *K14-TRIM32* transgene, it is not possible to say conclusively that any phenotype observed is a direct result of Trim32 over-expression in keratinocytes. Further characterizations are needed in order to validate the model.

Aim 2: Determine if TRIM32 deficiency *in vivo* affects UVB-induced tumorigenesis in SKH1-E mice.

i.   UVB versus DMBA/TPA carcinogenesis. While very useful for studying initiation and promotion of papillomas, the two-stage chemical carcinogenesis model is limited in its ability to simulate cSCC formation in humans. Only a low percentage of human cSCCs harbor Ras activating mutations (one publication gave a high estimate of 9% for Hras , 7% for Nras, and 5% for Kras) (Ratushny et al., 2012; Uribe and Gonzalez, 2011). Furthermore, the primary cause of human cSCC, UV radiation, induces C→T transitions, particularly in the *TP53* gene (Popp et al., 2002). With this knowledge, we decide to perform a UVB carcinogenesis experiment previously characterized (Dickinson et al., 2011) with the *K14-Trim32* transgenic and TRIM32-deficient mice. Since both of the mouse models were initially on a background strain resistant to UVB-

induced tumorigenesis (DBA/2 x C57BL/6J for *K14-Trim32* transgenic mice and 129S5/SvEvBrd x C57BL/6J for TRIM32-deficient mice), we backcrossed both strains onto the hairless, albino SKH1-Elite strain.

ii. SKH1-Elite Mice. The SKH1-Elite hairless mice (Crl:SKH1-Hr^{hr}), an albino, outbreed strain captured from the wild, has been used in research, particularly UV radiation studies, since the mid-1970s (Forbes et al., 1978). This strain contains the spontaneous autosomal recessive mutation *hairless* in the *Hr* gene (Hr^{hr}) (Benavides et al., 2009). The wild type HR protein functions as a transcriptional co-repressor of several nuclear receptors, including the thyroid hormone receptor and the vitamin D receptor (Potter et al., 2001). The *hr* allele is the result of a modified polytropic retrovirus that was stably integrated into intron 6 of the gene, causing aberrant splicing and subsequent degradation of more than 90% of the mRNA transcript (Stoye et al., 1988). The first hair coat of SKH1 mice develops normally. However, at around 2 weeks of age the animals will begin a rapid and complete loss of hair starting at the eyelids and proceeding caudally (Panteleyev et al., 1998). During this process, there is a well-defined boundary between hairless and haired skin. Between 3 and 4 weeks of age, the animals become completely hairless. A second wave of hair growth may occur between 5 and 6 weeks of age, but the hair will be very sparse and abnormal. After complete hair loss, SKH1 mice are also prone to form utriculus, a flask-shaped structure of hyperkeratotic epithelium localized around the infundibulum of hair shafts, and dermal cysts. With age, the animals will form enlarged sebaceous glands and dermal granulomas.

Similar to the *hairless* allele, the *nu* allele for the *Foxn1* gene also results in hairless phenotype in an autosomal recessive manner (Pelleitier and Montplaisir, 1975). Since $Foxn1^{nu/nu}$ mice (also called nude mice) are athymic and, therefore, immunocompromised, some have wondered if SKH1 mice also have an immunodeficiency. Indeed, SKH1 mice are susceptible to spontaneous skin abscesses as a result of β-hemolytic Group G *Streptococcus* infection (Rojas et al., 2002). However, a recent study showed that the immune profile of SKH1 mice is similar to that of C57Bl/6 mice (Schaffer et al., 2010). Furthermore, both strains showed similar tumorigenic potential when crossed with a mouse model for rhabdomyosarcoma. Additional studies are needed in order to understand why SKH1 mice are more susceptible to skin abscess formation. Changes to the skin microbiome is one possible explanation.

iii. UVB carcinogenesis on SKH-Trim32 deficient mice. After backcrossing onto the SKH1 strain, $Trim32^{-/-}$ and $Trim32^{+/-}$ mice, along with SKH1 wild type littermates, were subjected to UVB treatments three times a week. When UVB-induced papillomas were previously analyzed by Horn et al. (2004), they observed overexpression of Trim32 mRNA in all tumors analyzed. Given these findings and the *in vitro* data showing Trim32's effect on cell survival and proliferation, we hypothesized that a deficiency in TRIM32 will cause an increase in the time to tumor development. Likewise, we hypothesize that removal of the *Trim32* gene will decrease the total number of papillomas formed and will inhibit the growth of individual papillomas.

Aim 3: Determine if TRIM32 deficiency _in vivo_ inhibits UVB-induced cellular proliferation and apoptosis in SKH1-E mice.

i.   The response of SKH1-E mice to an acute UVB treatment. In response to single, lose dose of UVB radiation (1.80 kJ/m^2), the skin of SKH1 mice quickly undergoes several cellular and histological changes (Lu et al., 1999). The expression of p53 rises almost immediately, peaking at between 8 and 12 hours after irradiation. An increase in DNA synthesis, as measured by BrdU-labeled cells, is also observed quickly (within 1 hour), but is followed by an almost complete loss (greater than 90%) of BrdU-incorporation from 6-12 hours post-irradiation, which coincides with peak p53 expression. Between 36 and 48 hours post-treatment, p53 expression decreases and BrdU-labeled cells rises rapidly, peaking at around 48 hours. As a result, epidermal thickness reaches its maximum at approximately 96 hours.

Given that Trim32 expression has been shown to affect both p53 stability (Liu et al., 2014) and proliferation (Albor et al., 2006; Horn et al., 2004; Kano et al., 2008), it's plausible that the effects of UVB radiation will be altered in the skin of SKH-Trim32$^{-/-}$ mice. To test this premise, we irradiated SKH-Trim32$^{-/-}$ mice and SKH1-E wild type mice with a single minimal erythemal dose of UVB (1 MED, equivalent to 2.240 kJ/m^2 UVB) and collected skin samples 3-72 hours post-treatment. We hypothesize that a deficiency in TRIM32 will increase the stability of p53, resulting in an inhibition of DNA synthesis

and a decrease in skin thickening as a result of UVB irradiation. The exact methods and

materials used for all of the aims listed above will be discussed in the next chapter.

CHAPTER III: METHODS AND MATERIALS

A. Animal Husbandry. Mice were bred and maintained in the animal house facilities of the Department of Comparative Medicine (DCM) at Oregon Health and Science University (OHSU), Portland, Oregon. All animals were housed in individually ventilated cages in a positive-pressure room maintained at 25°C with a 45% relative humidity and a 12 hour 6:00 AM – 6:00 PM light cycle. Water and rodent diet were provided by DCM and given ad libitum. All experimental protocols present in this thesis were approved by the Institutional Animal Care and Use Committee at OHSU.

B. Mouse Models. Transgenic mice containing a Trim32 transgene under the regulation of the K14 promoter (*K14-Trim32*) were developed in our laboratory and initially maintained on a mixed DBA/2 x C57BL/6J background. TRIM32-deficient (*Trim32$^{-/-}$*) mice on a mixed 129S5/SvEvBrd x C57BL/6J background were obtained from and previously characterized by Dr. Melissa Spencer at the University of California at Los Angeles (Kudryashova et al., 2009). The presence of the genes and alleles were determine by PCR using the following primers: 5' primer for wild type and Trim32 null allele, 5'-GGAGAGACACTATTTCCTAAGTCA-3'; 3' primer for the wild type allele, 5'-GTTCAGGTGAGAAGCTGCTGCA-3'; 3' primer for the Trim32 null allele, 5'-GGGACAGGATAAGTATGACATCA-3'; 5' primer for the *K14-Trim32* transgene, 5'-AGAACTCCTGGGCTTTCGAT-3'; 3' primer for the *K14-Trim32* transgene, 5'-CAGGAGCTTCTCCAGACACTG-3'. The TRIM32-deficient colony was maintained as

heterozygotes in order to maximize breeding potential. *K14-Trim32^{tg}*, *Trim32^{+/-}*, *Trim32^{-/-}*, and their wild type (WT) littermates were used for two-stage chemical carcinogenesis while on their mixed backgrounds. Subsequently, the animals were backcrossed 10 generations onto the hairless SKH1-Elite strain obtained from Charles Rivers. After backcrossing, the weights of the *Trim32^{-/-}, Trim32^{+/-}*, and SKH1 WT mice were monitored weekly from 3 to 13 weeks of age. The SKH1 wild type, heterozygous, and TRIM32 null mice were then subjected to UVB carcinogenesis.

C. DMBA/TPA Chemical Carcinogenesis. The timeline for the experiment is shown in **Figure 2**. 20 mg/ml stock solutions of DMBA and TPA (Sigma-Aldrich) were prepared in DMSO (40x and 800x, respectively) and stored at -20°C. On the day of treatment, the stock solutions were diluted to a 1x working solution with acetone to achieve the final concentrations per mouse as indicated below. Initiation with DMBA was perform on seven week old mice, when the animals' hair is in telogen phase (Abel et al., 2009). At that time, *Trim32^{+/-}*, *Trim32^{-/-}*, and wild type littermates on a mixed 129S5/SvEvBrd x C57BL/6J background, as well as *K14-Trim32^{tg/tg}*, *Trim32^{tg/+}*, and their wild type littermates on a mixed DBA/2 x C57BL/6J background, were shaved and treated topically with 200 µl of the 1x DMBA solution (100 µg of DMBA) on their dorsal skin. Mice were then isolated for 2 weeks to ensure complete degradation of the carcinogen. At that point, the animals were split into two groups: Group A, which received once weekly treatment with TPA, and Group B, which received twice weekly treatment with TPA (see **Table 1**). For each treatment, mice were shaved and received 200 µl of the 1x TPA solution (5 µg TPA). Mice

	D2;B6-Tg(K14-Trim32)				129S;B6-Trim32KO			
	Wild Type	$Trim32^{tg/+}$	$Trim32^{tg/tg}$	Total	Wild Type	$Trim32^{+/-}$	$Trim32^{-/-}$	Total
Group A	17	18	16	51	9	15	13	37
Group B	17	19	16	52	11	16	14	41

Table 1. Mouse numbers for DMBA/TPA chemical carcinogenesis experiment. 100µg of DMBA at 7-9 weeks of age. Two weeks after initiation, mice were randomized into two groups: Group A received 5µg TPA once a week, and Group B received 5µg TPA twice a week. D2;B6-Tg(K14-Trim32) = K14-Trim32 transgenic mice on a mixed DBA/2 x C57BL/6J background; 129S;B6-Trim32KO = TRIM32-deficient mice on a mixed 129S5/SvEvBrd x C57BL/6J background; D2;B6 and 129S;B6 signifies wild type mice from each colony.
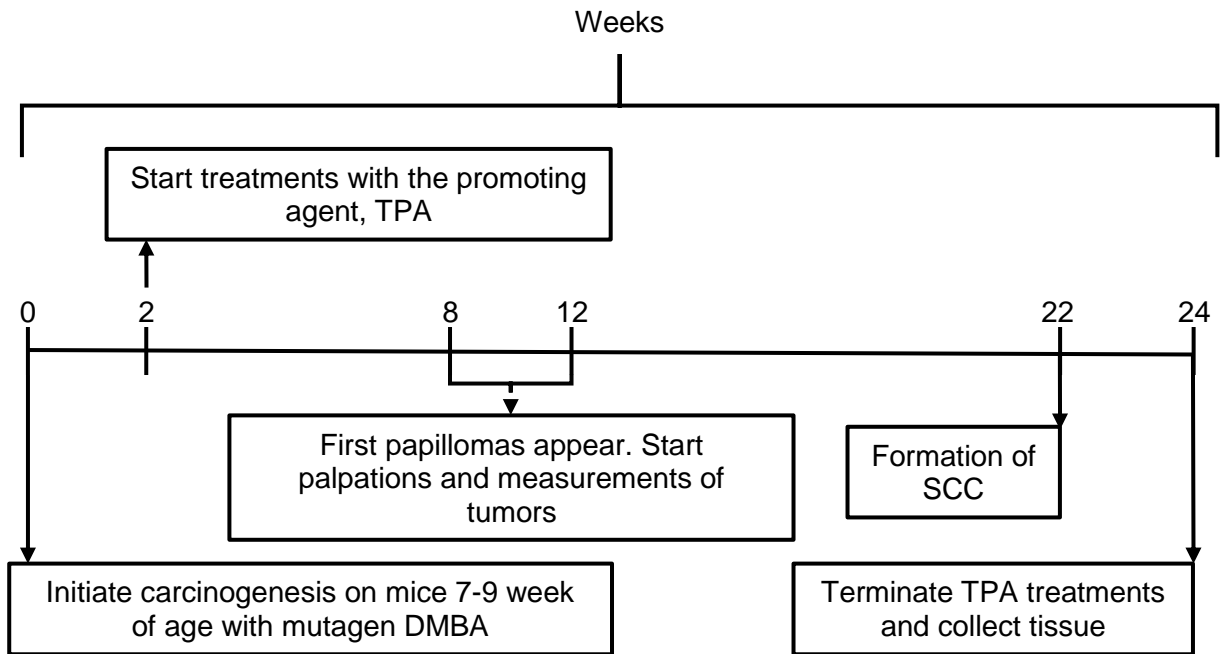
Figure 2. Timeline of DMBA/TPA chemical carcinogenesis. Mice aged 7-9 weeks old are treated with a sub-carcinogenic dose of the mutagen DMBA. After a two week incubation period, mice were treated weekly or twice weekly with 5 μg of the PKC-activator TPA. First papillomas are observed between 6-10 weeks after start of promotion. Squamous cell carcinomas form at very low rates after ≈ 20 weeks of promotion. Experiment is terminated and tissue collected 22 weeks after start of promotion.

were monitored for tumor growth weekly. Once a week, tumors at least 1 mm in diameter were counted and two measurements were taken (length and width) using digital calipers. Tumor volume was estimated using the following equation (Bernacki et al., 1987): $0.4 \times (\text{long axis}) \times (\text{short axis})^2$. In total, 181 mice were used in this experiment. TPA treatments continued for 30 weeks for the TRIM32-deficient colony and 35 weeks for the *K14-Trim32* transgenic colony. Upon completion, animals were sacrificed, and skin was collected using three different techniques: 1) snap freezing in liquid nitrogen for protein analyses, 2) storage in RNA*later* (ThermoFisher Scientific) for qPCR analyses, and 3) fixation in 10% formalin (Sigma-Aldrich) for immunohistochemistry (IHC). Both dorsal and ventral skin was collected, representing treated and untreated skin.

D. UVB Carcinogenesis. Tumorigenesis induced by chronic UVB irradiation was performed as previously described (Dickinson et al., 2011) using the following mice: 9 female and 16 male SKH-Trim32$^{-/-}$; 16 female and 15 male SKH-Trim32$^{+/-}$; and 13 female and 14 male SKH1-E wild type mice (**Figure 3**). Mice were placed beneath three UVB broadband lamps (Phillips FS20T12/UVB) and received 0.9 kJ/m^2 of irradiation three times for the first week. The animals then continued to receive three treatments a week while the UVB dose was increased by 25% each week, until a dose of 2.75 kJ/m^2 was reach. In total, 28 weeks of UVB treatments were applied. Mice were monitored for tumor growth weekly. Once a week, tumors at least 1 mm in diameter were counted and two measurements were taken (length and width) using digital calipers. Tumor volume
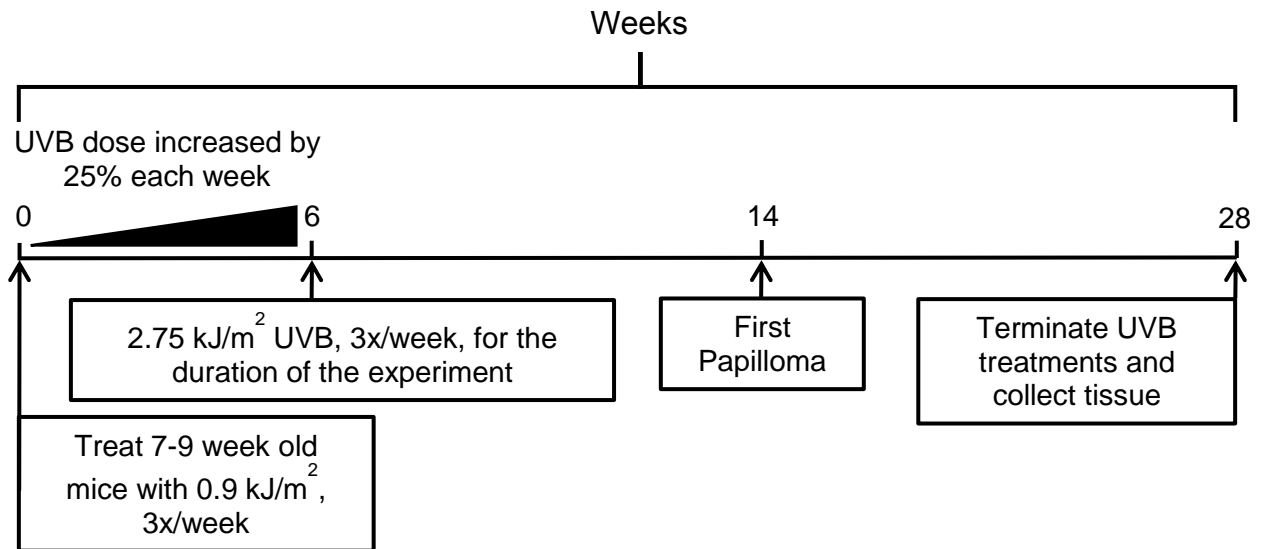
Figure 3. Timeline of UVB carcinogenesis. 7-9 week old SKH-Trim32$^{-/-}$, SKH-Trim32$^{+/-}$, and wild type SKH1-E mice were irradiated with a suberythemal dose of UVB, 3 times a week, increasing the dose by 25% each week until a maximum dose of 2.75 kJ/m2 was reached. First papillomas was observed after 14 weeks of treatment. Irradiations were stopped and tissue was collected after 28 weeks of treatment.

was estimated using the following equation: $0.4 \times (\text{long axis}) \times (\text{short axis})^2$. At the end of the experiment, animals were sacrificed, and skin was collected using three different techniques: 1) snap freezing in liquid nitrogen for protein analyses, 2) storage in RNA*later* (ThermoFisher Scientific) for qPCR analyses, and 3) fixation in 10% formalin (Sigma-Aldrich) for immunohistochemistry (IHC). Both dorsal and ventral skin was collected, representing treated and untreated skin.

E. Acute UVB Exposures. For irradiation with a single dose of UVB, mice were anesthetized with isoflurane and irradiated on their dorsal skin with one minimal erythemal dose of UVB (2.240 kJ/m^2). Animals were sacrificed 3, 6, 12, 24, 48, and 72 hours after irradiation. Dorsal skin was then collected using three different techniques: 1) snap freezing in liquid nitrogen for protein analyses, 2) storage in RNA*later* (ThermoFisher Scientific) for qPCR analyses, and 3) fixation in 10% formalin (Sigma-Aldrich) for immunohistochemistry (IHC).

Samples fixed with 10% formalin (Sigma) were stored overnight at 4°C, then transferred to 70% ethanol kept at 4°C until further processing. For immunohistochemistry, as well as hematoxylin and eosin (H&E) staining, fixed samples were washed with phosphate buffer saline (PBS) 3 times, then dehydrated using increasing concentrations of ethanol (50%, 70%, 95%, and 100%). Samples were subsequently cleared with xylenes by first submerging in a 50:50 xylene and ethanol solution, and finally a 100% xylene solution. After dehydration, samples were paraffined, and sections 5 μm thick were cut using a microtome (Leica). Sections were transferred to a slide and rehydrated using

35

decreasing concentrations of xylenes and ethanol. In order to measure epidermal thickness, sections were stained using Mayer's hematoxylin solution and eosin Y alcohol solution (Sigma), and slide covers were sealed using Cytoseal XYL (ThermoFisher). Images of stained sections were captured using a 20x lens and analyzed using FIJI (ImageJ).

In order to quantify the percentage of keratinocytes in S phase, animals were injected with 1 ml Bromodeoxyuridine (BrdU) labeling reagent (Invitrogen) per 100 g or body weight 2 hours prior to sacrifice. BrdU, a thymidine analogue, is incorporated into proliferating cells during S-phase and can be detected using α-BrdU monoclonal antibodies that are conjugated to horseradish peroxidase (Soames et al., 1994). The addition of 3,3'-diaminogenzidine (DAG) to slides containing a peroxidase-conjugated antibody will results in a localized dark brown stain. For more prominent staining, the α-BrdU antibody can be conjugated to biotin, and a streptavidin-peroxidase compound can be added to antibody-bound slides. For this project, BrdU incorporation was detected using a BrdU staining kit from Invitrogen. After staining, 2 to 3 random sections of the epidermis were images using a 20x lens (Leica), and the amount of labeled and unlabeled basal keratinocytes were quantified for each field of view.

F. Statistical Analyses. Tumor latency data was plotted using a Kaplan-Meier estimator (survival curve) and statistical significance was determined using a log-rank (Mantel-Cox) test (GraphPad Prism). Statistical analyses for tumor multiplicity and tumor burden data was done for each time point using the Mann-Whitney *U* tests

36

(GraphPad Prism). Significance for epidermal thickness, body weight, RNA weight, was also calculated using the Mann-Whitney U tests. For percent BrdU-labeled keratinocytes, a student's t-test was used (GraphPad Prism). Error bars represent the standard error of the mean (SEM) or the standard deviation (SD) as indicated in the figure legends. Outliers were determined using Grubb's test (http://graphpad.com/quickcalcs).

CHAPTER IV: RESULTS

Part 1: Two-Stage Chemical Carcinogenesis Using Mixed Inbred Strains

i. Chemically-induced tumorigenesis was strongly inhibited in D2;B6-Tg(K14-Trim32) mice. While performing DMBA-initiated, TPA-promoted chemical carcinogenesis, we quickly observed that the 129S;B6-Trim32KO wild type littermates were much more susceptible than those in the D2;B6-Tg(K14-Trim32) colony (**Figure 4**). When 129S;B6 and D2;B6 wild type mice in Group A were compared, the time to tumor formation was significantly decreased for the 129S;B6 wild type mice (**Figure 4A**). In the twice weekly treatment groups, there was no significant different in tumor latency between 129S;B6 and D2;B6 wild type mice (**Figure 4B**). However, there was a significant difference in the average tumor multiplicity and average tumor burden for both treatment groups, with 129S;B6 mice being far more sensitive than the D2;B6 wild type mice (**Figures 4C – 4F**). Remarkably, tumor multiplicity for the 129S;B6 mice was not significantly different between the once weekly and twice weekly treatment groups, suggesting that the initiating dose of DMBA was the limiting factor for determining the number of papillomas in these mice.

The difference in vulnerability of the WT littermates to chemically-induced carcinogenesis is most likely caused by the varying percentage of inbred strains present in each mouse. As described in the Limitations section of Chapter 2, the C57BL/6 and DBA/2 inbred strains are less sensitive than the 129/SvEv strain to DMBA/TPA

38
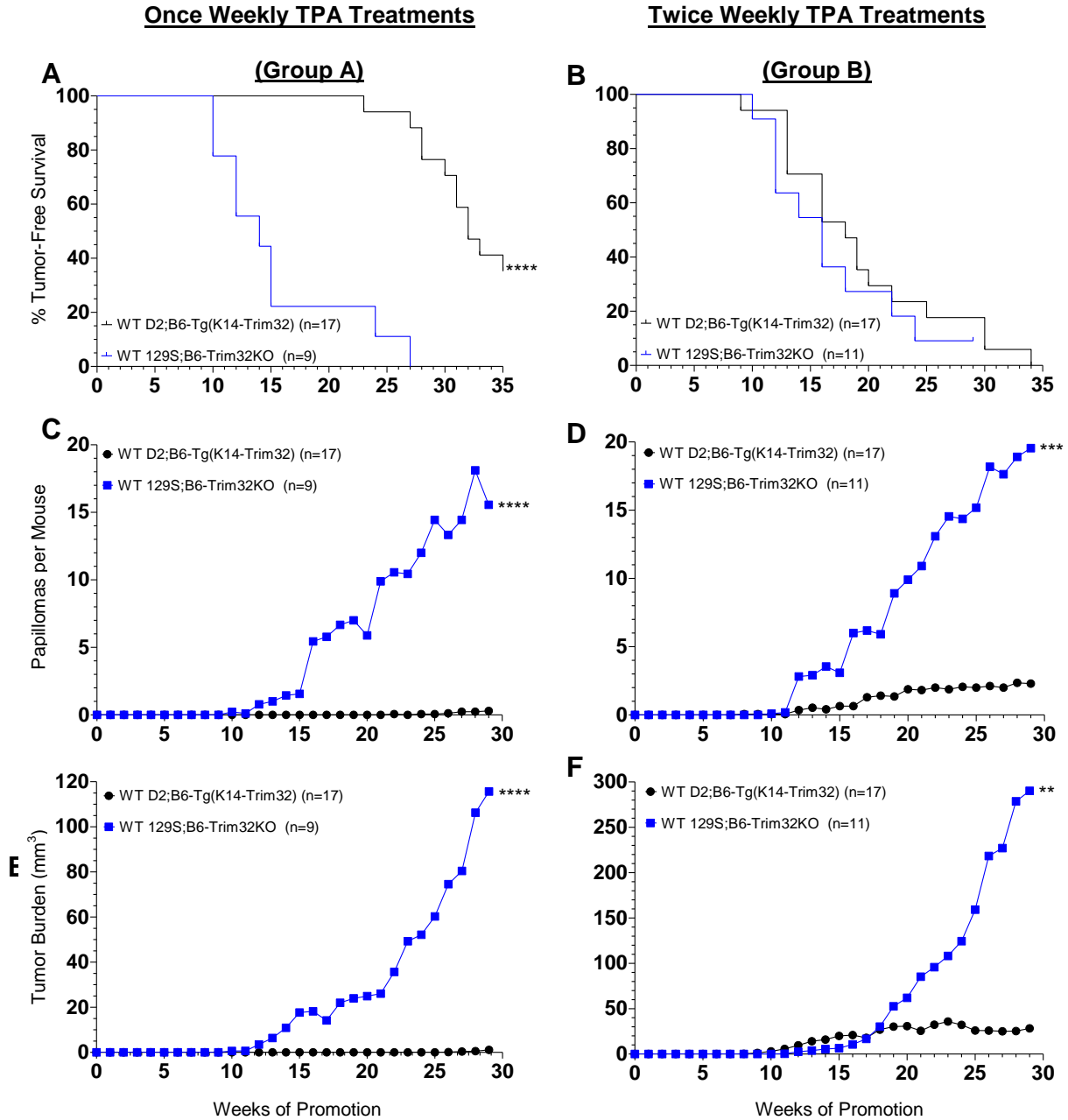
Figure 4. Susceptibility of D2;B6-Tg(K14-Trim32) and 129S;B6-Trim32KO wild type littermates to DMBA/TPA chemical carcinogenesis. (A and B) Tumor latency was significantly greater for D2;B6 mice, compared to 129S;B6 mice, in Group A (32 vs. 14 weeks). However, there was no significant difference in tumor latency between D2;B6 and 129S;B6 mice in Group B (18 vs. 16 weeks). **(C and D)** After 29 weeks of TPA treatments, tumor multiplicity (average number of papillomas per mouse) was significantly lower for D2;B6 mice when compared to 129S;B6 mice in both Group A (0.2941 vs. 15.56) and in Group B (2.294 vs. 19.55). **(E and F)** Tumor burden was also significantly lower for D2;B6 mice in Group A (1.094 vs. 115.7 mm^3) and in Group B (28.28 vs. 290.1 mm^3). Tumor multiplicity and tumor burden was calculated as described in Material and Methods. **p $\leq$ 0.01; ***p $\leq$ 0.001; ****p $\leq$ 0.0001.

carcinogenesis (Reiners et al., 1984; Sundberg et al., 1997). Therefore, it would be anticipated that the D2;B6-Tg(K14-Trim32) colony would be less effected by topical treatments of DMBA and TPA when compared to 129S;B6-Trim32KO mice. In concordance, the percentage of mice that formed tumors in Group A was relatively low for the D2;B6-Tg(K14-Trim32) colony (64.71%, 62.50%, and 44.44% for D2;B6, *K14-TRIM32*$^{tg/tg}$, and K14-TRIM32$^{tg/+}$ littermates, respectively). While tumor latency was significantly decreased in the mice treated twice weekly with TPA, tumor multiplicity remained low, with less than 1 tumor per mouse on average for the D2;B6-Tg(K14-Trim32) mice in Group A, and less than 2 tumors per mouse on average for those in Group B (**Figures 4A – 4D**). It is probable that this low level of tumor formation would not yield a strong enough resolution for differences between genotypes to be observed. However, we did observe a significant decrease in the tumor multiplicity of *K14-Trim32*$^{tg/+}$ mice when compared to D2;B6 littermates (**Figure 6B**). It remains unknown if this difference was caused by the presence of the transgene or the varying percentage of inbred strains in the mice.

ii. Chemically-induced tumorigenesis was variable but significantly inhibited in *Trim32*$^{+/-}$ and *Trim32*$^{-/-}$ mice. On average, mice from the 129S;B6-Trim32KO colony had a much greater response to DMBA/TPA chemical carcinogenesis (**Figure 4**). However, the level of tumorigenesis varied greatly when individual mice were analyzed. After 29 weeks of promotion, the range of tumor multiplicity for 129S;B6 mice in Group A and B was 44 and 38 tumors per mouse, respectively. *Trim32*$^{+/-}$ and *Trim32*$^{-/-}$ mice had a similar variability. Nevertheless, we were still able to detect statistically significant

differences between the genotypes. When treated once weekly with TPA, tumor latency was significantly longer in both $Trim32^{+/-}$ and $Trim32^{-/-}$ mice (20 and 19 weeks, respectively) when compared to 129S;B6 littermates (14 weeks, **Figure 5C**). For tumor multiplicity, only $Trim32^{+/-}$ mice in Group A had a significant decrease when compared to 129S;B6 littermates (3.067 versus 15.56 tumors per mouse, **Figure 6C**). We did observe a similar reduction in the $Trim32^{-/-}$ mice in Group A (7.846 tumors per mouse), however, this decrease was not significant. Tumor burden for Group A was correspondingly affected, with an average of 23.96, 74.34, and 115.7 mm^3 for $Trm32^{+/-}$, $Trim32^{-/-}$, and 129S;B6 littermates, respectively (**Figure 7C**). As with the tumor multiplicity, only $Trim32^{+/-}$ mice in Group A had a significant decrease. When mice were treated twice weekly with TPA, there was no difference in tumor latency or tumor multiplicity between the genotypes (**Figure 5D and 6D**). There was, however, a significant decrease in tumor burden for $Trim32^{-/-}$ mice when compared to 129S;B6 littermates (116.5 mm^3 versus 290.1 mm^3, **Figure 7D**), and $Trim32^{+/-}$ mice, while not statistically significant, did show a decrease as well (191.6 mm^3).

The larger decrease in tumorigenesis for $Trim32^{+/-}$ mice in Group A was unexpectedly larger than reduction in $Trim32^{-/-}$ mice. As with the D2;B6-Tg(K14-Trim32) colony, the most probable explanation for these results is a varying percentage of the two inbred strains in individual specimens. Unfortunately, as mentioned in Chapter 2, it was unfeasible to confirm this hypothesis given the large number of mice on the experiment. Still, we did observe a trend in which Trim32 deficiency reduces tumorigenesis induced by DMBA and TPA. Given these findings, we next backcrossed both the over-
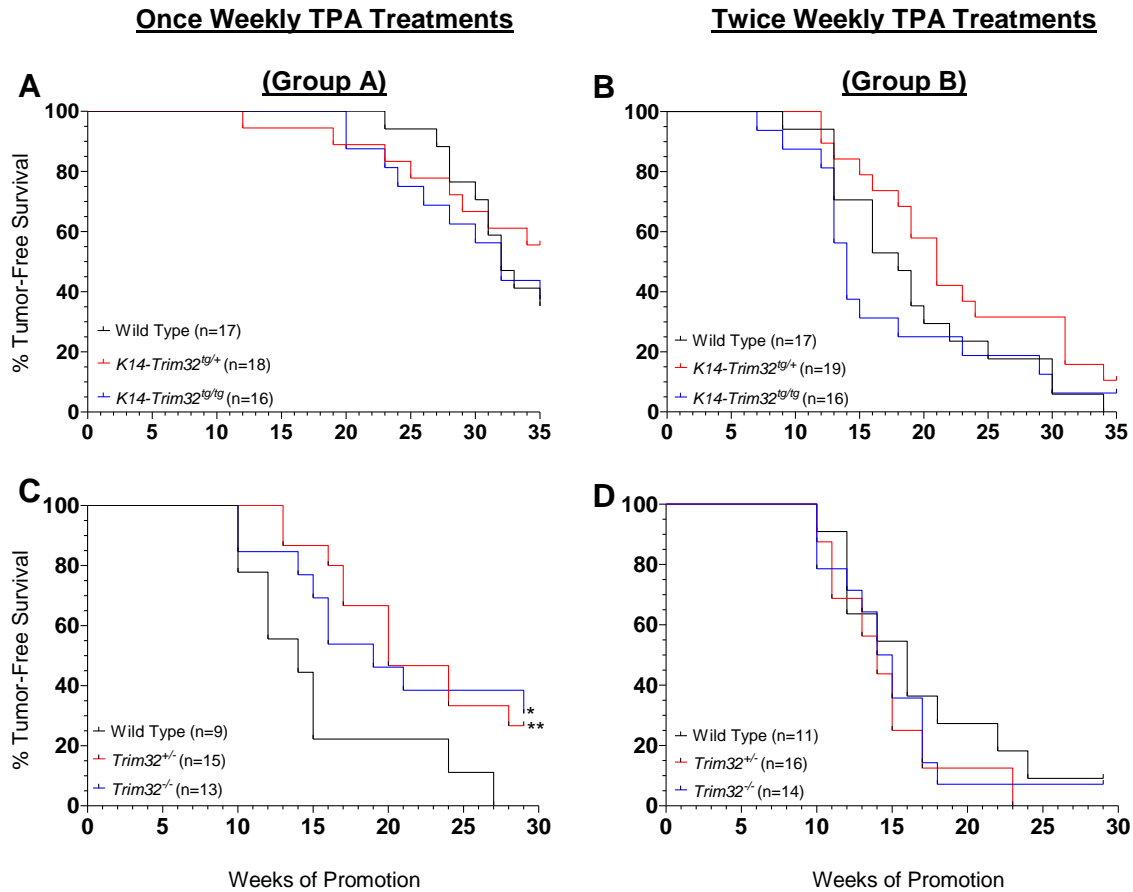
Figure 5. Tumor latency for DMBA/TPA chemical carcinogenesis of *K14-TRIM32^{tg/tg}*, *K14-TRIM32^{tg/+}*, *TRIM32^{+/-}*, *TRIM32^{-/-}*, and WT littermates. Mice were subject to DMBA/TPA chemical carcinogenesis as described in Materials and Methods. *K14-Trim32* transgenic, TRIM32-deficient, and wild type littermates were divided into two groups: **(A and C)** Group A, once weekly 5 µg TPA treatments, and **(B and D)** Group B, twice weekly 5 µg TPA treatments. Papillomas ≥ 1 mm in diameter were counted. The appearance of papillomas was plotted using Kaplan-Meier curves, and statistical significance was determined using a Mantel-Cox test. *p ≤ 0.05; **p ≤ 0.001.

Once Weekly TPA Treatments   **Twice Weekly TPA Treatments**

A (Group A)

Papillomas per Mouse

- ▲ Wild Type (n=17)
- ■ *K14-Trim32*$^{tg/+}$ (n=18)
- ● *K14-Trim32*$^{tg/tg}$ (n=16)

B (Group B)

- ▲ Wild Type (n=17)
- ■ *K14-Trim32*$^{tg/+}$ (n=19)
- ● *K14-Trim32*$^{tg/tg}$ (n=16)

C

Papillomas per Mouse

- ▲ Wild Type (n=9)
- ■ *Trim32*$^{+/-}$ (n=15)
- ● *Trim32*$^{-/-}$ (n=13)

D

- ▲ Wild Type (n=11)
- ■ *Trim32*$^{+/-}$ (n=16)
- ● *Trim32*$^{-/-}$ (n=14)

Weeks of Promotion
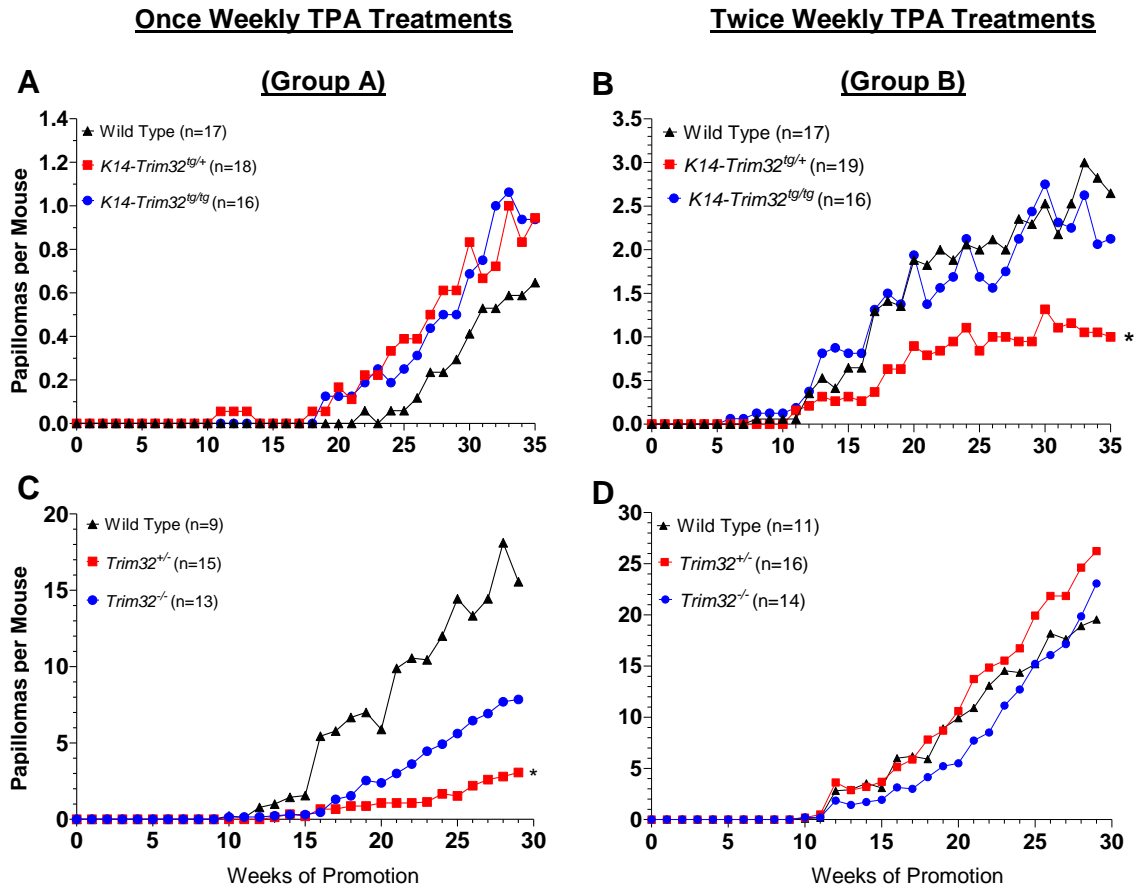
Figure 6. Tumor multiplicity for DMBA/TPA chemical carcinogenesis of *K14-TRIM32*$^{tg/tg}$, *K14-TRIM32*$^{tg/+}$, *TRIM32*$^{+/-}$, *TRIM32*$^{-/-}$, and SKH1-E mice. Mice were subject to DMBA/TPA chemical carcinogenesis as described in Materials and Methods. *K14-Trim32* transgenic, TRIM32-deficient, and wild type littermates were divided into two groups: **(A and C)** Group A, once weekly 5 µg TPA treatments, **(B and D)** Group B, twice weekly 5 µg TPA treatments. Papillomas ≥ 1 mm in diameter were counted, and the average number of papillomas per mouse was recorded weekly. Statistical significance was determined by Mann-Whitney *U* test. *p ≤ 0.05.
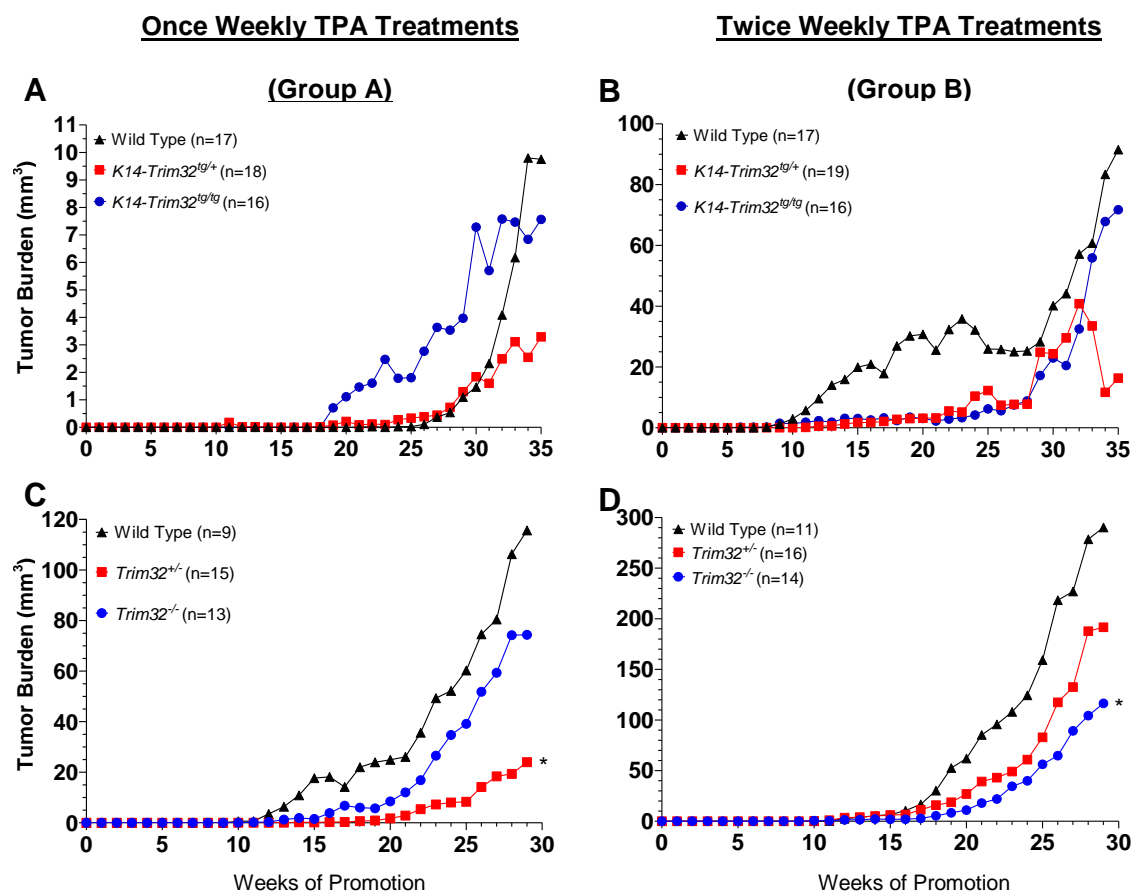
Figure 7. Tumor burden for DMBA/TPA chemical carcinogenesis of *K14-TRIM32^{tg/tg}*, *K14-TRIM32^{tg/+}*, *TRIM32^{+/-}*, *TRIM32^{-/-}*, and WT littermates. Mice were subject to DMBA/TPA chemical carcinogenesis as described in Materials and Methods. *K14-Trim32* transgenic, TRIM32-deficient, and wild type littermates were divided into two groups: **(A and C)** Group A, once weekly 5 µg TPA treatments, **(B and D)** Group B, twice weekly 5 µg TPA treatments. Papillomas ≥ 1 mm in diameter were counted and two measurements (length and width) were recorded. Tumor volume was estimated using the equation: $0.4 \times (\text{long axis}) \times (\text{short axis})^2$. Tumor burden (total tumor volume per mouse) was measured weekly, and the average tumor burden per mouse was plotted. Statistical significance was determined by Mann-Whitney *U* test. *p ≤ 0.05.

expressing and deficient colonies onto the SKH1-Elite hairless strain in order to perform a UVB carcinogenesis study. As discussed above, earlier discoveries showed that Trim32 is more consistently over-expressed in UVB-induced tumors (Horn et al., 2004). Therefore, we hypothesized that chronic UVB irradiations of TRIM32-deficient mice on a single background strain would yield more consistent evidence for Trim32 deficiency in inhibition of tumorigenesis.

Part 2: UVB-Induced Carcinogenesis on SKH-Trim32KO Mice

Trim32$^{+/-}$ **and** *Trim32*$^{-/-}$ **mice on a SKH1-E background display a decrease in body weight.** The TRIM32-deficient mice used in this study were previously characterized by Kudryashova et al. (2009) while on the mixed 129/SvEvBrd x C57 BL/6J background. In that report, a decrease in litter size for homozygous KO breeders was noted, as well as a 10% increase in body weight for *Trim32*$^{-/-}$ mice at 8 weeks of age. Interestingly, after 10 generations of backcrossing onto the SKH1-E strain, we observed a strong decrease in body weight for SKH-*Trim32*$^{+/-}$ mice, and the difference was twice as pronounced in the SKH-*Trim32*$^{-/-}$ mice (**Figure 8**). The percent decrease in body weight was largest at an age of 4 weeks (15.7% and 33.3% for *Trim32*$^{+/-}$ and *Trim32*$^{-/-}$ mice, respectively), but continued to be significantly decreased throughout the animals' life (shown later in **Figure 10**). One possible explanation for the contradictory observations involves the mixed 129/SvEvBrd x C57 BL/6J background used by Kudryashova et al. (2009) for their experiments. 129S mice have a lower body weight than their C57BL/6 counterparts
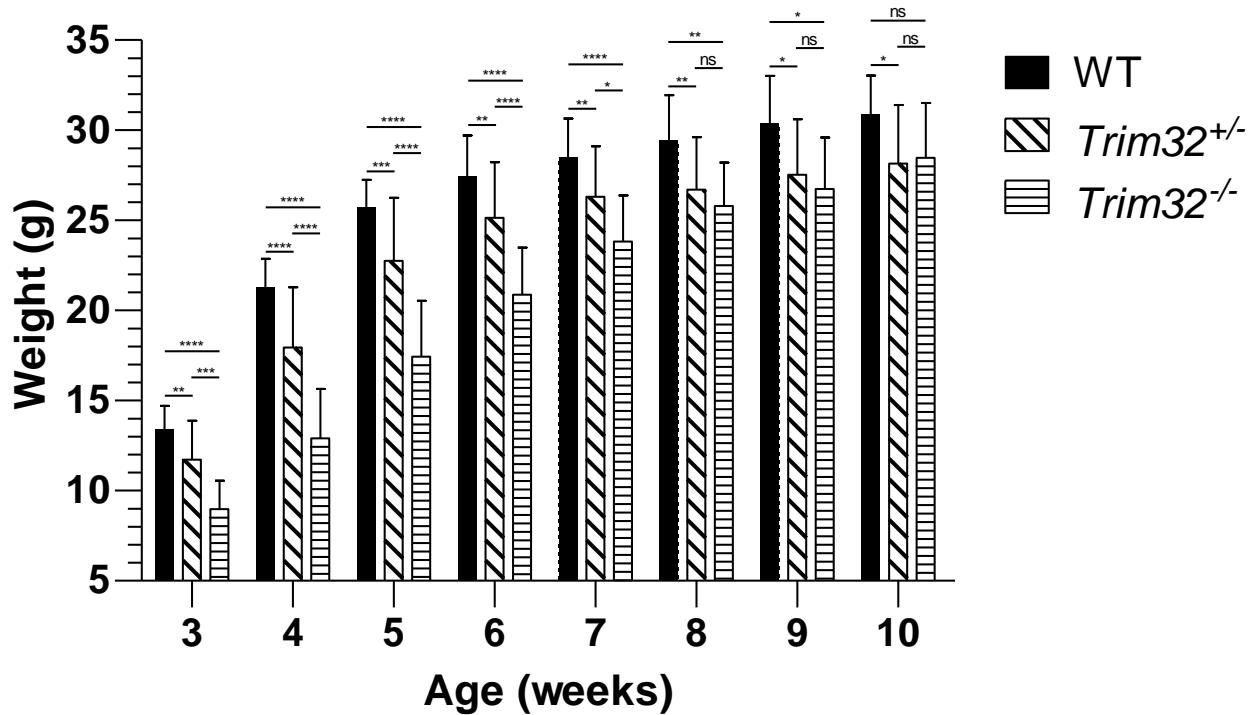
Figure 8. Comparison of body weight of SKH-*Trim32*^{+/-}, SKH-*Trim32*^{-/-}, and WT mice. Body weight of male WT, *Trim32*^{+/-}, and *Trim32*^{-/-} SKH1-E mice was measured weekly. Mean body weight in grams ± SD was plotted for each genotype. The difference in body weight observed reached a maximum at 4 weeks of age (a 15.7% and 39.3% decrease for *Trim32*^{+/-} and *Trim32*^{-/-}, respectively). Statistical significance was determined using Man-Whitney *U* test. (n = 7 – 32; *p ≤ 0.05; **p ≤ 0.01; ***p ≤ 0.001; ****p ≤ 0.0001).

(Reed et al., 2007), and this difference may have affected the initial characterization. Still, we did have other similar findings, such as a difficulty breeding TRIM32-deficient females, which forced us to maintain the colony as heterozygotes.

i. UVB-induced tumorigenesis was significantly inhibited in male SKH1-E mice.

A study designed to characterize gender differences in the SKH1-E strain used thrice weekly treatments of 2.240 kJ/m^2 UVB (1 minimal erythemal dose) to induce papilloma formation on males and females (Thomas-Ahner et al., 2007). In that report, they showed a two week delay in tumor formation for females, which corresponded to a 50% increase in tumor multiplicity and 43% larger tumors for males. For our study, we used a starting dose of 0.9 kJ/m^2 thrice weekly that was increased by 25% until a final dose of 2.75 kJ/m^2 was reached (see Materials and Methods). Using this procedure, the time to the first tumor was approximately 41% shorter for females when compared males, with a mean time of 13.5 and 18 weeks, respectively (**Figure 9A**). After 27 weeks of UVB irradiations, there was also an associated 54.5% increase in the number of papillomas, as well as a 365% increase in the average tumor burden, for WT female mice when compared to WT males (**Figure 9B and 9C**).

The reason behind these two opposing observations is unknown. In their report, Thomas-Ahner et al. (2007) attributed the higher amount of UVB-induced papilloma formation in male mice to a lower antioxidant capacity in the epidermis of the males. To confirm this hypothesis, they measured the levels of 8-oxo-deoxyguanine after UVB exposure and noticed a decrease in male mice when compared to females. They also
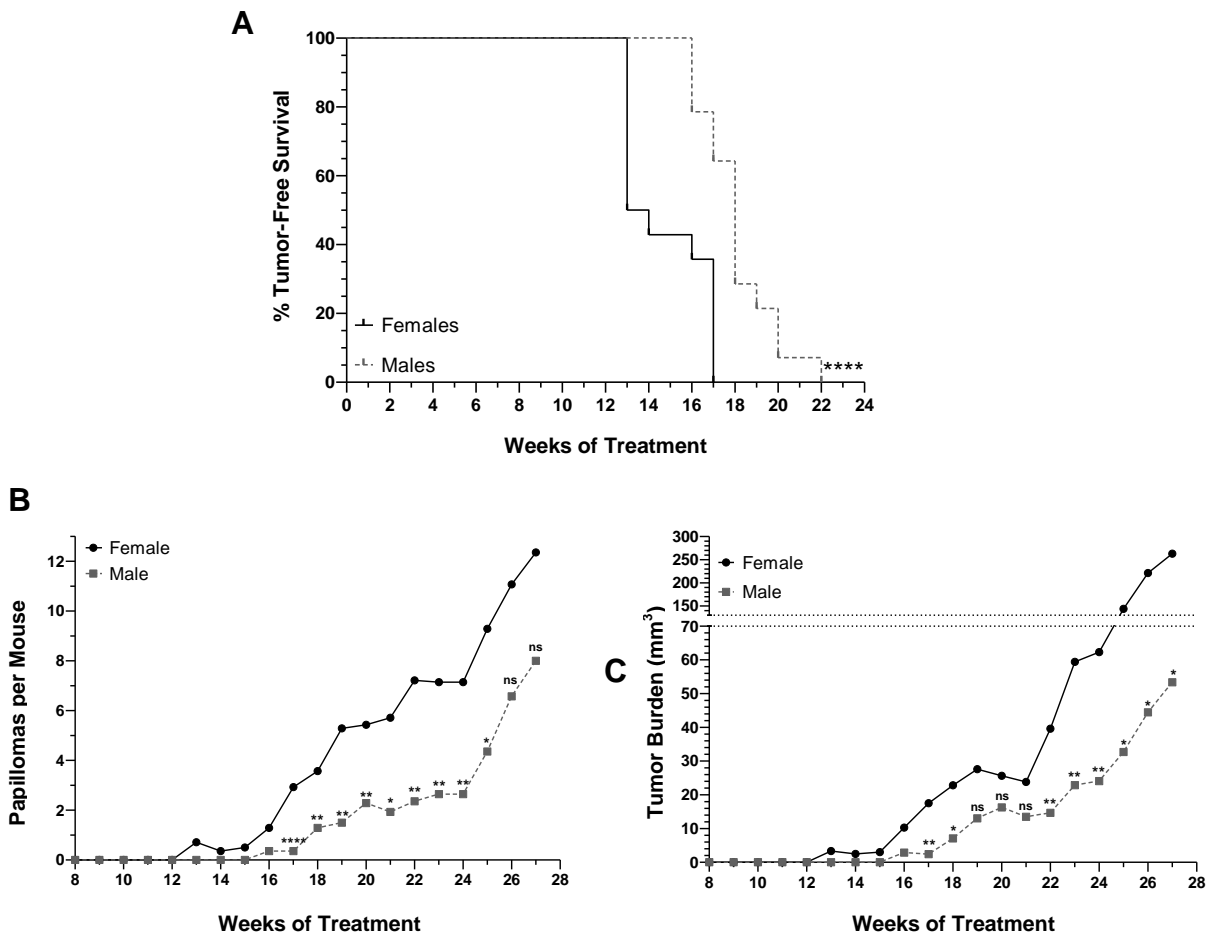
Figure 9. Gender differences for UVB-induced carcinogenesis. SKH1-E WT mice were exposed to UVB treatments as described in Materials and Methods. **(A)** Percent tumor-free survival was plotted using a Kaplan-Meier estimator, and statistical significance was determined using a log-rank (Mantel-Cox) test. **(B)** Papillomas ≥ 1 mm in diameter were counted weekly and the mean papillomas per mouse was plotted as a function of the treatment week. **(C)** The length and width of papillomas ≥ 1 mm in diameter was measured weekly, and the mean of the total tumor volume per mouse (tumor burden) was plotted as a function of the treatment week. tumor volume $= 0.4 \times (\text{long axis}) \times (\text{short axis})^2$. Significance for **(B and C)** was determined using Man-Whitney U test. *p ≤ 0.05; **p ≤ 0.01; ***p ≤ 0.001; ****p ≤ 0.0001; ns = not significant.

observed lower antioxidant potential and lower UVB-induced skin thickening in males compared to females. While a highly prolonged exposure to UVB can cause an accumulation of 8-oxo-dG lesions (Nishigori et al., 2004), the primary mechanism of UVB-induced mutations is through the direct formation of pyrimidine dimers (Kielbassa et al., 1997). Thus, it remains to be determined how significant the difference in antioxidant capacity is to UVB-induced carcinogenesis. One key difference between our study and Thomas-Ahner et al. is the starting dose of UVB. By using a suberythemal dose of UVB (0.9 kJ/m2), we were able to minimize the amount of sunburn during the first few weeks of treatment, giving the dorsal skin of the animals time to acclimate. Our procedure may also have minimized the amount of ROS produced, making pyrimidine dimers an even more significant contributing factor to DNA damage. It is also useful to note that a starting dose of 2.24 kJ/m^2 UVB three times weekly would inevitably cause significant levels of discomfort in the mice and may lead to fighting between males if housed together. Since wounding has been shown to play a significant role in the development of cSCC (Arwert et al., 2012; Roh et al., 2005), it would be interesting to know if this was taken into account.

ii. UVB-induced tumorigenesis was inhibited in SKH-*Trim32*$^{+/-}$ and SKH-*Trim32*$^{-/-}$ mice. The majority of tumors formed for this experiment were small lesions and papillomas. Very few fully invasive cSCCs were detected (data not shown). After 13 weeks of UVB exposures, a single female WT mouse formed one large, ulcerating tumor that grew rapidly for the duration of the experiment, having a final estimated

volume of 2491 mm^3 (**Figure 10C**). While this mouse was statistically an outlier (Grubb's test, $p < 0.01$), the animal was included in all of the analyses.

After 25 weeks of treatments, the mean tumor count for female wild type SKH1-E mice was 9.3 tumors/mouse, equal to what was previously reported (Dickinson et al., 2011). As described above, the tumor count for wild type males was strongly decreased to 4.4 tumors/mouse after 25 weeks of treatment, which may have affected the ability to measure significant differences in this group. Thus, there was no significant difference in the time to tumor formation for male mice, but there was a 24% delay for female *Trim32*$^{-/-}$ mice, increasing from 14.5 weeks for WT females to 18 weeks for *Trim32*$^{-/-}$ females (**Figures 10A and 10B**). For tumor multiplicity, there was a significant decrease in tumor count for female *Trim32*$^{+/-}$ *and Trim32*$^{-/-}$ mice starting at 26 and 17 weeks of treatment, respectively, with the final tumor count for female *Trim32*$^{+/-}$ mice exactly half that of WT females (6.2 and 12.4 tumors/mouse, **Figure 10C**). Female *Trim32*$^{-/-}$ had a very low level of tumor formation, with a final tumor count of 1.7 tumors/mouse, an 86% decrease from WT females. While male *Trim32*$^{+/-}$ mice did not have a significant decrease in tumor multiplicity, the final amount of tumors for male *Trim32*$^{-/-}$ mice was significantly lower than WT males, with a final amount of 3.9 tumors/mouse for KO versus 8.0 for WT (**Figure 9D**). The tumor multiplicity was also significantly different between *Trim32*$^{+/-}$ and *Trim32*$^{-/-}$ mice starting at 17 weeks of treatment for females and 26 weeks of treatment for males.
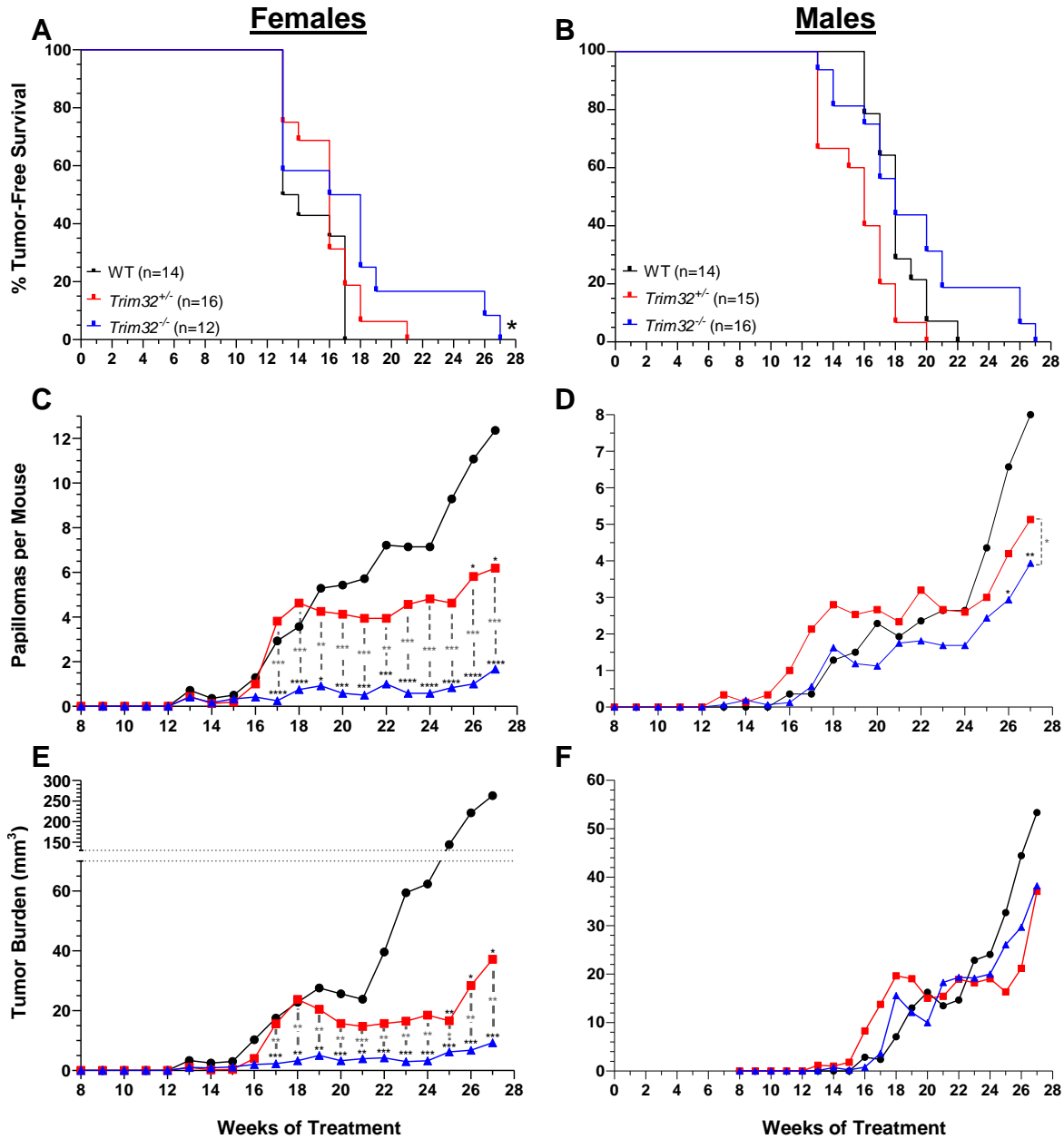
Figure 10. UVB Carcinogenesis of SKH-*Trim32+/-*, SKH-*Trim32-/-*, and SKH1-E WT mice.
Mice were exposed to UVB as described in Materials and Methods. **(A and B)** Percent tumor-free survival was plotted using a Kaplan-Meier estimator and statistical significance was determined using a log-rank (Mantel-Cox) test. **(C and D)** Papillomas ≥ 1 mm in diameter were counted weekly, and the mean number of papillomas per mouse was plotted as a function of the treatment week. **(E and F)** The length and width of papillomas ≥ 1 mm in diameter was measured weekly, and the mean of the total tumor volume per mouse (tumor burden) was plotted as a function of the treatment week. tumor volume $= 0.4 \times (\text{long axis}) \times (\text{short axis})^2$. Significance for **(A–F)** was determined using Man-Whitney U test. Black asterisks represent significance when compared to WT mice. Grey asterisks represent significance between *Trim32+/-* and *Trim32-/-* mice. *p ≤ 0.05; **p ≤ 0.01; ***p ≤ 0.001; ****p ≤ 0.0001.

While tumor burden was unaffected by genotype in males (**Figure 10F**), the results for females were similar to what was measured for tumor multiplicity (**Figure 10E**). Both *Trim32*$^{+/-}$ and *Trim32*$^{-/-}$ females had a significant decrease in tumor burden starting at 25 and 17 weeks of treatments, respectively. After 27 weeks of UVB irradiation, total tumor burden was lowered by 89% in *Trim32*$^{+/-}$ females and 98% in *Trim32*$^{-/-}$ females when compared to WT mice of the same gender. Starting at 17 weeks of treatment, there was also a significant decrease in total tumor volume for *Trim32*$^{-/-}$ females when compared to *Trim32*$^{+/-}$ females. These results indicate not only that TRIM32-deficient mice are resistant to UVB-induced tumorigenesis but also that haploinsufficiency is a feature of the *Trim32* gene. Since removal of one allele can inhibit tumor formation by 50%, it is likely that *Trim32* plays an important role in UVB-induced carcinogenesis.

After 27 weeks of UVB irradiations, treatments were stopped and mice were weighed. Female *Trim32*$^{+/-}$ and *Trim32*$^{-/-}$ mice on the experiment had a 11% and 19% decrease in body weight, respectively, when compared to WT females (**Figure 11C**). This was not unexpected, given the persistent decrease in body weight measured for *Trim32*$^{+/-}$ and *Trim32*$^{-/-}$ mice and shown in **Figure 8**. The lower body weight may mean that *Trim32*$^{+/-}$ and *Trim32*$^{-/-}$ mice have a smaller surface area for their dorsal epidermis, which would affect the results obtained from the UVB carcinogenesis by restricting the amount of papillomas formed. However, after normalizing the data to the average percent body weight for each genotype (relative to WT mice), statistical significance was largely unaffected (data not shown), demonstrating that the differences obtained were not a result of a smaller body size. To further affirm these results, images of representative
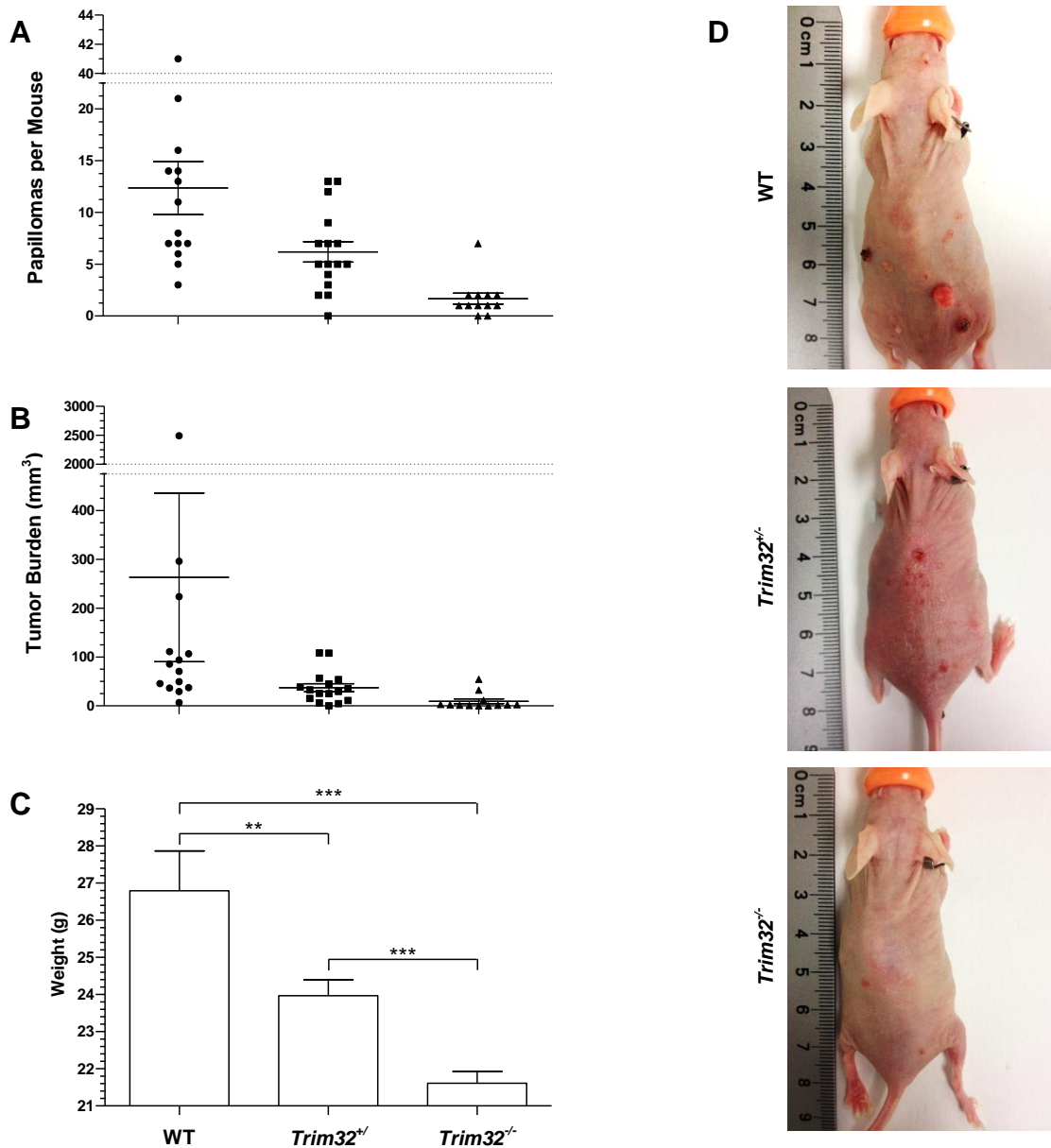
Figure 11. Tumor multiplicity and tumor burden after 28 weeks of UVB irradiation. Scatter plot with mean ± SEM for **(A)** number of papillomas per mouse, and **(B)** tumor burden per mouse. Each dot represents an individual female mouse after 27 weeks of UVB treatment. Tumor burden per mouse is equal to the sum of the tumor volumes, where tumor volume = $0.4 \times (\text{long axis}) \times (\text{short axis})^2$. **(C)** Weight of female mice in grams ± SEM after 27 weeks of UVB treatments. **(D)** Representative female mice after 27 weeks of UVB treatments. **p ≤ 0.01; ***p ≤ 0.001.

females from each genotype were taken, and a very noticeable decrease in tumor formation on the *Trim32*^{+/-} and *Trim32*^{-/-} mice was observed (**Figure 11D**). Altogether, these results demonstrate the crucial role Trim32 plays during the development of cSCC in mice.

Part 3: Acute UVB Response of *Trim32*^{-/-} Mice

i. UVB-induced epidermal thickening is delayed in *Trim32*^{-/-} mice. The lack of tumor formation in *Trim32*^{-/-} mice suggests that prevention of TRIM32 expression decreases the ability of keratinocytes to stimulate cellular proliferation as a result of UVB exposure. This hypothesis is supported by the findings of Horn et al. (2004), who showed that TRIM32 overexpression in engrafted keratinocytes can increase TPA-promoted skin thickening. Likewise, others have correlated an increase in Trim32 activity with cellular proliferation *in vitro* using immortalized cell lines (Kano et al., 2008; Liu et al., 2014). However, it is still unknown if endogenous TRIM32 affects the short-term response of keratinocytes to UVB. Therefore, we next investigated the effect of TRIM32 on the capacity of UVB-irradiated skin to induce proliferation directly after exposure. In order to do so, SKH-*Trim32*^{-/-} and SKH1-E WT mice were irradiated with 2.240 kJ/m^2 UVB, an amount previously determined to be the lowest dose of UVB necessary to cause observable cutaneous inflammation 48 hours after exposure (1 MED) (Wilgus et al., 2000). Dorsal skin was then collected and analyzed 0–72 hours after treatment.

While processing tissue, we consistently noticed a decrease in RNA yield from *Trim32*^{-/-} skin when compared to an equivalent weight of skin from WT mice (**Figure 12A**). The majority of weight in the epidermis of the skin comes from keratins and filaggrins produced in keratinocytes, while the dermis comprises mainly of extracellular collagen and water (McGrath and Uitto, 2010). Therefore, a decrease in RNA yield could be explained by lower ratio of epidermal to dermal mass. To test this hypothesis, we measured the thickness of the epidermis (minus the stratum corneum) before and after irradiation with 1 MED of UVB. Un-irradiated *Trim32*^{-/-} epidermis was found to be 17% thinner than WT epidermis (**Figure 12B and 12C**). When skin was collected 48 hours after UVB exposure, the epidermal thickness of wild type SKH1-E mice had increased by 21%, while there was no significant change in *Trim32*^{-/-} mice. However, at 72 hours post-exposure, while there was still 15% decrease in the mean thickness of *Trim32*^{-/-} epidermis, there was no significant difference between the two genotypes.

Previous reports have shown that the dorsal skin of SKH1-E mice continues to thicken for 96 hours after being irradiated with 1.8 kJ/m^2 UVB (Lu et al., 1999). Our initial goal was to analyze very early molecular changes that occur in the skin after exposure to UVB. However, these results warrant an extended time course, in which would the epidermal thickness would be measured 96 hours after UVB exposure. While, the results in **Figure 12** demonstrate a delay in proliferation for *Trim32*^{-/-} keratinocytes irradiated with UVB, it would be interesting to know if skin thickness stays significantly decreased throughout the UVB response.
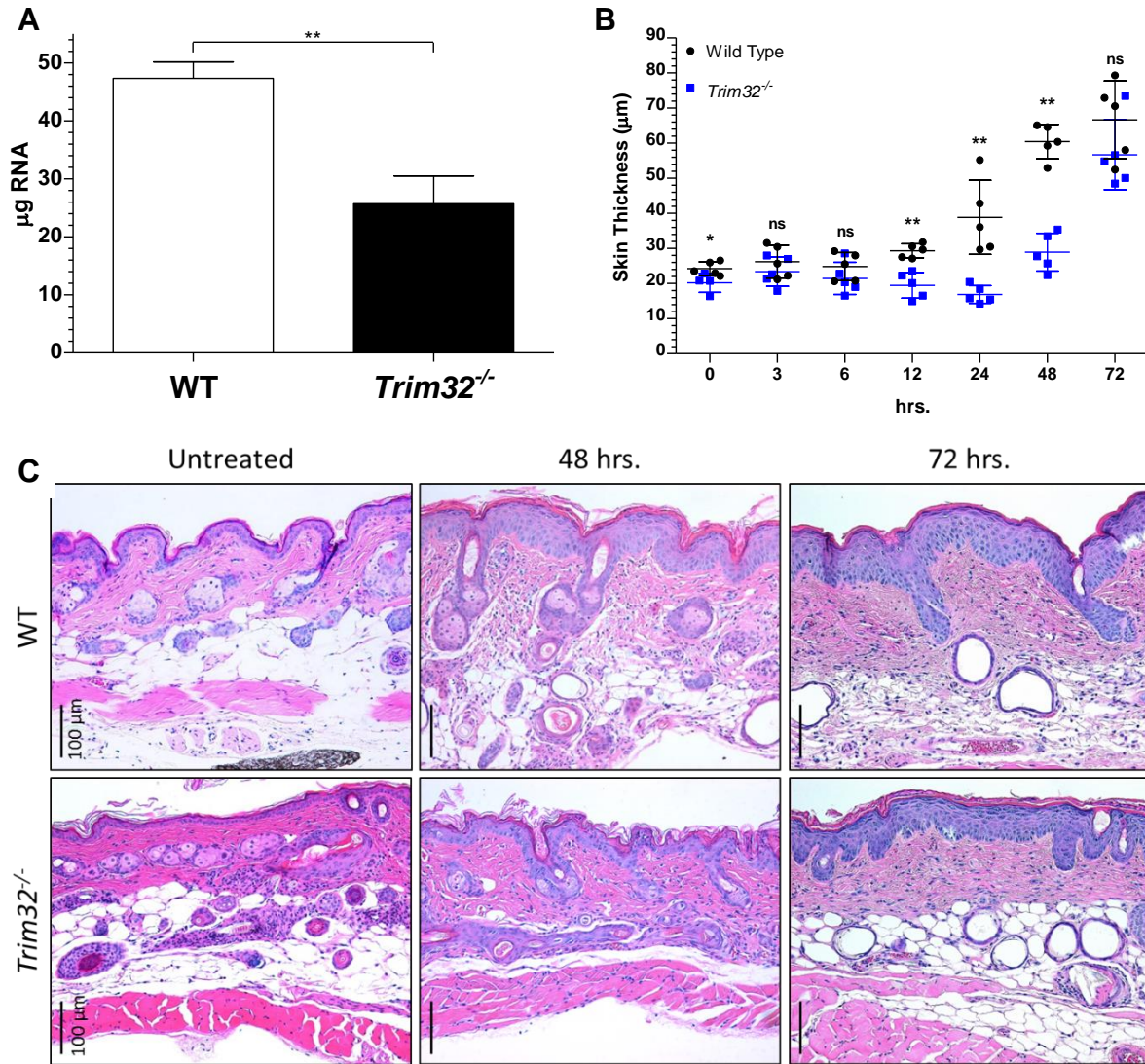
Figure 12. UVB-induced epidermal thickening of WT and *Trim32*^{-/-} mice. Wild type and *Trim32*^{-/-} female mice on the SKH1-E background were irradiated with 2.240 kJ/m^2 UVB (1 MED). Tissue was collected and fixed with 10% formalin 0 – 72 hrs after irradiation. H&E staining was performed as described in Materials and Methods. Measurements were made using a 50 μm grid for comparison. **(A)** Mass of RNA ± SEM acquired from 30 mg skin tissue 48 hrs after irradiation with 1 MED UVB. RNA was isolated as described in Materials and Methods. **(B)** Scatter plot of skin thickness in μm for untreated and UVB-treated WT and *Trim32*^{-/-} mice. Mean ± SD and statistical significance between WT and *Trim32*^{-/-} mice at the corresponding time points are displayed on the graph. n = 4 – 5 mice **(C)** Representative H&E for WT and *Trim32*^{-/-} females at 0, 48, and 72 hrs post-irradiation (20x magnification). *p ≤ 0.05; **p ≤ 0.01; ns = not significant.

ii. UVB-induced DNA synthesis is inhibited in *Trim32*$^{-/-}$ mice. The decrease in epidermal thickness suggests an inhibition of UVB-induced proliferation in *Trim32*$^{-/-}$ keratinocytes. In order to further understand this response, mice were injected with BrdU two hours prior to collection and then stained for BrdU-incorporation. Forty-eight hours after exposure to a 1.8 kJ/m^2 of UVB, the amount of basal keratinocytes in S phase will increase from 1.6% to 51.1% (Lu et al., 1999). Using 1 MED of UVB, wild type SKH1-E mice were found to have 50.8% of its basal keratinocytes labeled with BrdU (**Figure 13**).

However, *Trim32*$^{-/-}$ mice displayed an almost complete inhibition of UVB-induced proliferation 48 hours post-exposure, with only 6.9% of basal keratinocytes staining for BrdU incorporation. These results indicate that the delay in UVB-stimulated epidermal thickening in *Trim32*$^{-/-}$ mice is a result of a decrease or delay in the proliferation potential of keratinocytes. As with the results for epidermal thickening, more time points need to be analyzed before it can be determined if *Trim32*$^{-/-}$ inhibits or delays proliferation.
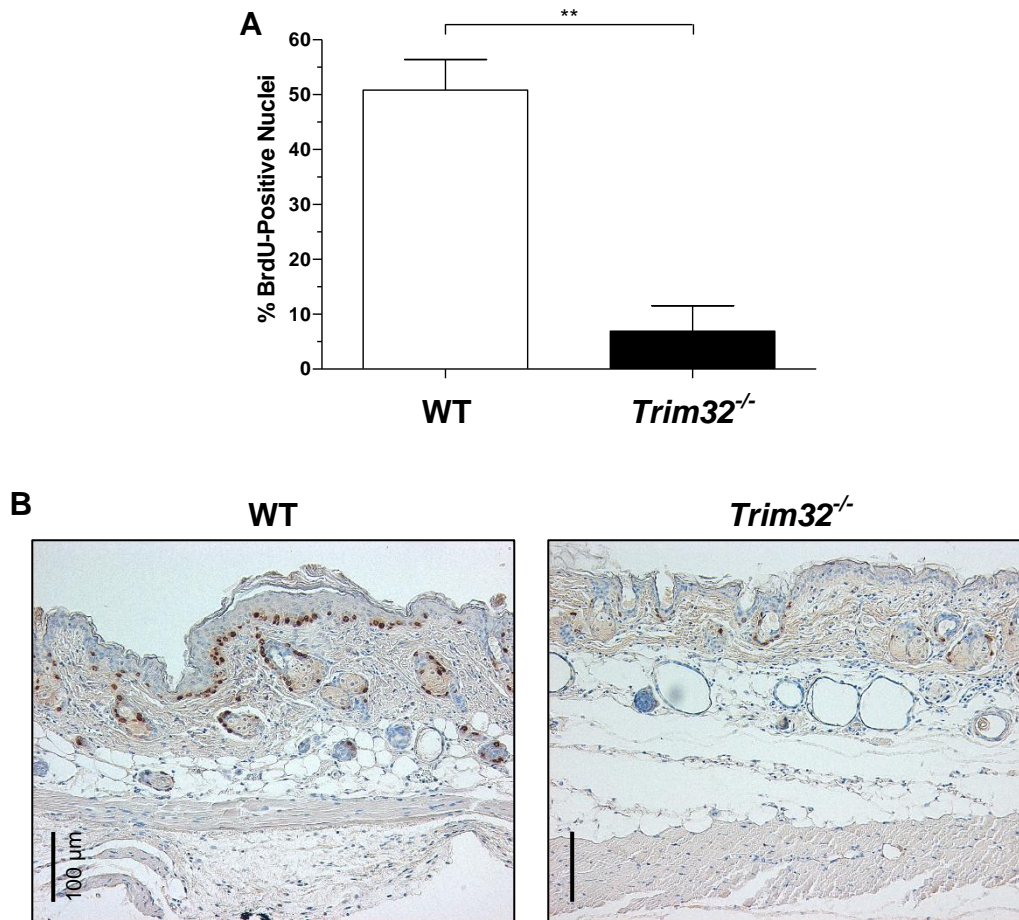
Figure 13. BrdU-labeled cells in the epidermis 24 hrs after UVB irradiation. SKH1-E WT and *Trim32*$^{-/-}$ mice were irradiated with 1 MED of UVB and skin samples were collected 24 hrs post-exposure in 10% formalin. Samples were processed and stained for BrdU incorporation as described in Material and Methods. Two random sections of the epidermis were imaged using 20x magnification for each mouse. Stained and unstained basal nuclei for the entire field of vision was quantified. **(A)** Average percentage of stained basal nuclei for each genotype ± SEM. Statistical analysis was done by student's *t* test. n = 3 **(B)** Representative images of WT and *Trim32*$^{-/-}$ epidermis taken at 20x magnification. **p ≤ 0.01.

CHAPTER V: DISCUSSION

Part 1: Benefits and Limitations of Using Two-Stage Chemical Carcinogenesis

The two-stage chemical carcinogenesis protocol is designed to make the initiation and promotion phases of tumor development independent from one another. This allows investigators to determine the phase of importance when stimulating carcinogenesis in their mouse model of choice. Knocking out or overexpressing a target gene may result in a change in the number of papillomas, the time to papilloma onset, or the size of the resultant papillomas, and these differences can be dependent on the chosen DMBA/TPA regimens. For example, when wild type and *Nrf2* null mice on the C57BL/6 background are initiated with a high dose of DMBA (200 nmol) and promoted with low doses of TPA (8 nmol) twice weekly, there is no significant difference in tumor incidence between the two genotypes (Katiyar et al., 1992). However, when a low dose of DMBA is used (20 nmol) for initiation followed by a high regimen of TPA (16 nmol), papilloma incidence is significantly elevated in *Nrf2$^{-/-}$* mice. NRF2 (Nuclear factor E2–related factor 2) is a basic leucine zipper transcription factor that activates the expression of several antioxidant proteins such as NAD(P)H:quinone oxidoreductase1 (Venugopal and Jaiswal, 1996). It has been well established that chronic treatments with TPA will increase intracellular ROS concentrations by indirectly activating NADPH oxidase (Kamiya et al., 2011). Therefore, the results obtained by Katiyar et al. (2002) highlight the important role of NRF2 in inhibiting oxidative damage in keratinocytes. In addition,

59

since knocking out NRF2 had no effect when a high dose of DMBA was used, it is plausible that NRF2 does not have a significant role in repairing damaged DNA.

Initially, we set out to confirma the ability of TRIM32 to modulate TPA-induced proliferation by splitting the mice into high and low TPA treatment groups, similar to the method demonstrated by Katiyar et al. (2002). Given that overexpression of Trim32 prolongs TPA-induced epidermal thickening (Horn et al., 2004), it was hypothesized that increasing the expression of TRIM32 in keratinocytes through the use of a transgenic mouse model would compensate for a decrease in the dosage of TPA. Conversely, TPA-induced carcinogenesis would be inhibited in *Trim32* null mice. While we were able to observe significant differences between *Trim32$^{+/-}$*, *Trim32$^{-/-}$*, and WT littermates, these results were not conclusive given the high degree of variability in tumor latency, multiplicity, and burden within the Trim32 genotypes. Likewise, the percent increase in tumor multiplicity and tumor burden from Group A (once weekly TPA treatments) to Group B (twice weekly TPA treatments) was highly variable. For instance, the percent increase in tumor multiplicity from Group A to Group B for WT, *Trim32$^{+/-}$*, and *Trim32$^{-/-}$* mice was 25.6%, 755.2%, and 194.0%, respectively (**Figure 6C and 6D**). This was opposed to our initial hypothesis, and the results were further complicated given that *Trim32$^{+/-}$* mice has the largest percent increase. Trim32 transgenic mice had an even more enigmatic response, with mice heterozygous for the transgene displaying a decrease in tumor multiplicity when treated twice weekly with TPA (**Figure 6B**).

Explanations for these events are multifarious. All arms of this experiment contain mice of both sexes. Generally, male and female mice do not display differences in papilloma or SCC formation when carcinogenesis is induced using DMBA and TPA (Reddig et al., 1999; Simanainen et al., 2015). However, male mice are more prone to fighting than females (Lofgren et al., 2012), and wounding has been shown to increase papilloma formation (Abel et al., 2009; DiGiovanni et al., 1993). Furthermore, the repeated shavings and treatments performed in this project would induce a stress response, increasing the likelihood of fighting in both sexes, which could lead to the variable tumor development observed.

The most significant explanation, perhaps, is the mixed inbred strains present in both colonies used for this carcinogenic assay. Moreover, this issue is compounded by the design of the experiment. While the total amount of mice used was relatively large, given the six independent arms attempted there were as few as 11 mice in each treatment group. Much larger groups would be needed in order to overcome the observed variability. In retrospect, it would have been beneficial to exclude the group receiving once weekly TPA treatments, allowing more mice to be assigned to the twice weekly group. As mentioned above, limiting the experiment to females would further decrease the standard deviation. Furthermore, knowing that complications might arise when experimenting on uncharacterized transgenic mice (discussed in Chapter 2), the insertion sites and copy number of the *K14-Trim32* transgene should be examined before using them in any carcinogenic assay.

Implementing the above suggestions would allow us to obtain more significant results by performing experiments that are more controlled. We could then clarify the data obtained by Horn et al. (2004) through analyzing molecular pathways affected by TPA treatments. These investigations could be performed with females from the newly generated SKH-Trim32 deficient colony, which would not only remove most of the impediments encountered with the mixed inbred strains but also have the added benefit of excluding the need for hair removal. Promotion with TPA could be performed with or without an initial treatment of DMBA, followed by an analysis of the PKCε pathway. As discussed in Chapter 2, after direct activation by TPA, PKCε will phosphorylate STAT3, allowing it to translocate to the nucleus and modulate transcription. Activation of PKCε could be measured by quantifying the amount STAT3-positive nuclei in the epidermis of WT and $Trim32^{-/-}$ mice, and by immunoblotting for phospho-STAT3 (Aziz et al., 2007b). Measuring the expression levels of STAT3 target gene such as c-Myc would confirm STAT3 activation.

In addition to chemical carcinogenesis, both PKCε and STAT3 have been shown to influence tumor formation and progression after UV exposure (Aziz et al., 2007b; Sano et al., 2005; Wheeler et al., 2004, 2005). Chronic UV exposure on PKCε-overexpressing mice results in the development of SCCs independent of papilloma formation, a model more closely related to the human condition. STAT3 phosphorylation at Tyr705 and Ser727 is also increased in the UV exposed transgenic mice, resulting in an increase in the expression of the STAT3 target genes cyclin D, c-Myc, Cdc25A, and COX-2. Thus, assessing the effect of Trim32 on the PKCε pathway would be beneficial for further

understanding the development of SCC in humans, and this can be accomplished through the use of two-stage chemical carcinogenesis assays.

Still, there are robust limitations when attempting to relate two-stage chemical carcinogenesis studies to human SCC. As mentioned in Chapter 2, papilloma and SCCs produced via DMBA and TPA treatments contain a high percentage of *HRAS* activation mutations (Abel et al., 2009). *HRAS* mutations are rare in human cancers, but can be found in head and neck squamous cell carcinomas (4.7%) and bladder urothelial carcinomas (5.9%), albeit at low frequencies (Cox et al., 2014). Moreover, while papillomas are almost always the benign precursors in a DMBA/TPA carcinogenesis assay, human SCCs often develop from actinic keratoses (Ratushny et al., 2012). While using a UVB model would still result in a progression from papilloma to SCC, the large majority of tumors obtained would harbor *TP53* mutations, which would affect pathways similar to those affected in humans. Therefore, focusing on a UVB carcinogenesis model instead of chemical carcinogenesis would increase the likelihood of obtaining translatable results.

Part 2: Focusing on UV Carcinogenesis

In Chapter 1, a description of the molecular events that take place after UVB exposure was provided, demonstrating how UVB acts as a "complete carcinogen" throughout the initiation and promotion phases of carcinogenesis (D'Orazio et al., 2013). As a consequence, using UV treatments to induce papilloma formation prohibits the investigators from analyzing the effects of a promoter or an initiator separately.

However, there are several benefits to using UV versus chemical carcinogenesis as a model. As mentioned, human cSCC is caused primarily by cumulative exposure to UV rays throughout an individual's lifetime. Accordingly, the mutagenesis that occurs during UVB treatments on SKH1-E mice is similar to changes that occur in the genome of human cSCC, with *TP53* being the most commonly mutated gene. Furthermore, UV-induced p53 inactivating mutations have been shown to occur at similar frequencies in both human and mouse lesions (Giglia-Mari and Sarasin, 2003; van Kranen et al., 1995; Melnikova et al., 2005).

These similarities highlight the efficacy of using UVB carcinogenesis as a model for human cSCC and justify a focus on discerning the effect of TRIM32 on UVB-irradiated keratinocytes. Moreover, the striking results obtained from performing a UVB carcinogenesis experiment with *Trim32*$^{+/-}$ and *Trim32*$^{-/-}$ mice demonstrate the important role TRIM32 has during the skin's response to UVB. The observed 50% and 86% reduction in tumor numbers for *Trim32*$^{+/-}$ and *Trim32*$^{-/-}$ mice, respectively, not only provide *in vivo* evidence for an oncogenic role for TRIM32 but also demonstrates the occurrence of haploinsufficiency for the *Trim32* gene. This response is in part due to the 44% decrease in UVB-induced basal cell proliferation observed in *Trim32*$^{-/-}$ mice 24 hours after exposure. While these results yield a highly promising description of the mouse model, further investigations into the mechanisms behind the observed phenotype are necessary to understand how TRIM32 might function in human skin. The following sections will describe several approaches that can be used to understand the activity of TRIM32 in keratinocytes, skin, and cSCC.

i. **The effect of Trim32 on the MAPK signaling pathways.** Chapter 1 discussed the multiple cell signaling cascades shown to be important in regulating UV-induced keratinocyte proliferation. Among them, the MAPK proteins play a significant but sometimes controversial role in determining cell fate. Given the importance of both Trim32 and MAPKs in the UV response of mouse skin, investigations into the activity of p38α, JNK1, JNK2, and ERK1/2 in *Trim32*$^{+/-}$ and *Trim32*$^{-/-}$ keratinocytes are warranted. In order to do so, initial *in vitro* experiments on isolated primary keratinocytes from neonatal mice could be performed, allowing the for a focus on the response of this specific cell type (Lichti et al., 2008). Both WT keratinocytes and WT keratinocytes transduced with *Trim32* siRNA would be used as controls (Liu et al., 2014), with the latter determining if the phenotypes observed in *Trim32*$^{-/-}$ mice are due to long-term cellular changes. Furthermore, *Trim32*$^{-/-}$ and *Trim32*$^{tg/tg}$ mice could be crossed with one another to perform an add-back experiment that is specific to keratinocytes. This would have the added benefit of helping to eliminate secondary effects of the transgene (such as the insertion site) as an explanation for phenotypes observed in the *Trim32*$^{tg/tg}$ mice.

Once isolated, primary keratinocytes will be irradiated with a low to medium dose of UVB (0.25 – 0.40 kJ/m^2). In order to confirm the accuracy of this model, BrdU-incorporation could be measured in WT and *Trim32*$^{-/-}$ keratinocytes 0 to 48 hourrs after UVB irradiation and compared to the *in vivo* findings. Afterwards, cell lysate from the UVB treated keratinocytes will be collected, and the activity of MAPKs will be assessed via immunoblotting. Relative levels of phosphorylated p38α, JNK1, JNK2, and ERK1/2

will be compared between genotypes. Trim32 has not been previously shown to modulate MAPK activity, but given that both *Trim32*^{-/-} and p38α dominant negative mice show a reduction in UVB-induced tumorigenesis (Dickinson et al., 2011), I hypothesize that inhibition of Trim32 expression would decrease p38α phosphorylation. Likewise, a decrease in ERK1/2 phosphorylation would be expected as it has been shown to inhibit apoptosis in UVA-exposed HaCaT cells (He et al., 2004). Given the ambiguous role of the Jun-N terminal kinases (Muthusamy and Piva, 2010), assessing the phosphorylation levels of JNK1 and JNK2 in UVB-irradiated *Trim32*^{-/-} keratinocytes would further clarify the activity of these proteins during the UV response.

ii. The effect of Trim32 on NF-κB localization and transcriptional activity. One of the first studies on Trim32 used a mouse keratinocyte cell line to overexpress Trim32 and established a correlation between an increase in Trim32 expression and an increase in NF-κB transcriptional activity (Albor et al., 2006). In the same report, Trim32 was shown to induce the ubiquitination and subsequent degradation of Piasy, and a decrease in Piasy protein levels was associated with an increase in NF-κB transcriptional activity. While these studies are informative, the effect of endogenous Trim32 on the NF-κB pathway remains to be determined.

Using the same methods that will be employed to understand the relationship between Trim32 and the MAPK pathway, the effect of TRIM32 deficiency on UVB-induced activation of NF-κB can be determined. After UV irradiation, IκBα, an inhibitor of NF-κB, is phosphorylated by the IKK complex and degraded via the proteasome (Richmond,

2002). Exposure to UV light also induces translocation of NF-κB to the nucleus, where it is capable of activating transcription (Helenius et al., 1999; Tsuchiya et al., 2010). Activation of NF-κB can occur via several independent signaling pathways, some of which include the degradation of IκBα, others involving the activation of p38α and NF-κB independent of IκBα degradation (Bender et al., 1998; Chang et al., 2011; Lewis and Spandau, 2007). Immunoblotting for the UVB-induced phosphorylation of IKKβ and IκBα in *Trim32^{-/-}* and WT primary keratinocytes would shed light on the pathways affected by Trim32. I hypothesize that TRIM32 deficiency would downregulate the phosphorylation of IKKβ and IκBα shortly after UVB exposure, which would prevent the degradation of IκBα. As a consequence, NF-κB would be sequestered in the cytosol, which could be determined using immunofluorescence. In addition, the localization and protein levels of NF-κB and IκBα could be determined *in vivo* using the acute UVB exposures described in Materials and Methods. Removal of the *Trim32* gene would hypothetically inhibit nuclear localization of NF-κB and the degradation of IκBα *in vivo*, which would lead to the observed decrease in proliferation after UVB irradiation.

As a transcription factor, NF-κB regulates the expression of several genes important for a complete UV response. These genes include the potent cytokines IL-6, TNFα, IL-1β, and VEGF (Abeyama et al., 2000). To assess the effect of TRIM32 deficiency on the expression of these cytokines, isolated primary keratinocyte will be treated with UVB as described above, and total RNA will be collected using RNA*later* and phenol/chloroform extract. Analysis of expression levels will be performed by qRT-PCR. Given the previously establish role of Trim32 in the activation of NF-κB, I hypothesize that a

67

deficiency in TRIM32 will inhibit UVB-induced expression of IL-6, TNFα, IL-1β, and VEGF. Combined with the results of the MAPK activation assays, we would be able to further our understanding of the crosstalk between the MAPK and NF-κB signaling pathways. Several publications have shown that the two pathways interact with each other, but the exact outcome is dependent on the cell line, presence of pretreatments, UV type, and UV dose (Kato et al., 2003; Lewis and Spandau, 2007; Ravi et al., 2008). In addition, Trim32-activation of NF-κB may occur independent from the MAPK pathway and IκBα-degradation. If so, those findings would highlight a new and unique mechanisms for NF-κB activation.

iii. The effect of Trim32 on p53 localization and transcriptional activity. After treating the colon cancer cell lines HCT116 and RKO with the chemotherapeutic agents etoposide or 5-FU, p53 was shown to directly upregulate the transcription of Trim32 (Liu et al., 2014). In response, Trim32 induced the ubiquitination and degradation of p53 in a RING domain-dependent manner, resulting in a negative feedback loop. While these findings are intriguing, the effect of Trim32 on UVB-induce p53 activation remains to be determined. In order to answer this question, WT and $Trim32^{-/-}$ keratinocytes could be treated with UVB *in vitro*, and the localization of p53 could be assessed using immunofluorescence. After UVB irradiation, p53 is phosphorylated in a p38α-dependent manner and sequestered in the nucleus where it increases the expression of target gene such as *MDM2* (Chouinard et al., 2002). I hypothesize that $Trim32^{-/-}$ keratinocytes would display an increase in UVB-induced nuclear localization of p53 and an increase in UVB-induced *MDM2* expression. This could lead to the observed decrease in UVB-

induced proliferation. While these findings might clarify the role Trim32 has in regulating p53 activity in normal keratinocytes, they may not relate to the activity of Trim32 in cSCC since the majority of cSCCs are homozygous for p53 inactivating mutations (Giglia-Mari and Sarasin, 2003). Still, the results would be important for understanding the pathways involved during the early phases of the disease.

iv. Trim32, DNA damage repair, and gene silencing. There is currently no evidence to suggest that Trim32 affects a cell's capacity to repair UVB-induced pyrimidine dimers. However, a strong decrease in the number of tumors produced as a result of UVB treatments was observed in *Trim32*^{-/-} mice, signifying that Trim32 may be important during initiation and possibly DNA repair. Therefore, the speed of repair for UVB-induced cyclobutane pyrimidine dimers could be measured using immunofluorescence in keratinocytes isolated from both *Trim32*^{-/-} mice and in *Trim32*^{-/-} skin. Likewise, the repair of 6-4 photoproducts could be measured using an ELISA. My hypothesis is that the speed at which these lesions are repaired is unaffected by Trim32 expression levels and that the main activity of Trim32 in the UV response is during promotion.

Possibly the most interesting findings concerning the activity of Trim32 it its capacity to modulate the miRNA specificity of the RISC complex (Schwamborn et al., 2009). Specifically, Trim32 was shown to increase the affinity of Ago1 for let-7a, a potent tumor suppressor that regulates the expression of several oncogenes (Büssing et al., 2008). This ability was demonstrated in neural progenitor cells, but it stands to reason that it might be present in keratinocytes as well. While determining the effect Trim32 has on

miRNA-induced gene silencing is outside the scope of this project, the results might lead to a novel mechanism for a protein in cancer. If miRNAs such as let-7a are shown to be regulated by Trim32 in normal keratinocytes and during the development and progression of cSCC, it would reveal a fascinating dual function for the protein, in which the N-terminal RING domain mediates ubiquitination and degradation, and the C-terminal NHL repeats mediate gene silencing. This finding would further emphasize the importance of Trim32 in not only cancer, but also throughout development and homeostasis.

Chapter VI: SUMMARY AND CONCLUSIONS

As of May 2016, there was less than 100 publications that involved furthering our understanding of Trim32 (http://www.ncbi.nlm.nih.gov/pubmed/). Even with this limited knowledge, the importance of Trim32 in the human body has been demonstrated using a diverse array of disorders and diseases, including muscular dystrophy, ciliopathy, HIV infection, and cancer. Through the application of several cell lines and mouse models, multiple teams of investigators have shown that Trim32 can interact with or regulate several key proteins such as p53, c-Myc, Ago1, and NF-κB. The loss of *Trim32* in both humans and mice can lead to stark phenotypes, with one recent study even implicating the gene in anxiety and depression (Ruan et al., 2014). These findings suggest an intriguing avenue of discovery available for those investigating the function of Trim32.

The data presented in this thesis are limited to the characterization of the TRIM32 deficient and *Trim32* transgenic mouse strains. Our initial goal of determining the role of Trim32 in two-stage chemical carcinogenesis was met with mixed and inconclusive results, but still strongly hinted at the oncogenic role Trim32 might play during chemical carcinogenesis. Further experiments using pure background strains would certainly clarify the effect Trim32 has on DMBA-induced initiation and TPA-induced promotion, and would be informative in determining how the PKCε pathway is affected by changes in Trim32 expression. These results would be interesting, but may not be translatable to human cSCC. Therefore, we decided to focus on UVB-induced carcinogenesis. We

observed dramatic reductions in tumor development when the expression of Trim32 was limited. The delay in tumor formation and decrease in tumor number and size occurred in mice homozygous or heterozygous for the *Trim32* null allele. This haploinsufficiency displayed by the *Trim32* gene further highlights its important role in the cell. Closer examinations into the mechanisms behind this phenotype could lead to a greater understanding of cutaneous squamous cell carcinoma, while opening up the possibility of new targetable pathways for SCC prevention and therapies.

CHAPTER VII: REFERENCES

Abel, E.L., Angel, J.M., Kiguchi, K., and DiGiovanni, J. (2009). Multi-stage chemical carcinogenesis in mouse skin: Fundamentals and applications. Nat Protoc. *4*, 1350–1362.

Abeyama, K., Eng, W., Jester, J.V., Vink, A.A., Edelbaum, D., Cockerell, C.J., Bergstresser, P.R., and Takashima, A. (2000). A role for NF-kappaB-dependent gene transactivation in sunburn. J. Clin. Invest. *105*, 1751–1759.

Albor, A., and Kulesz-Martin, M. (2007). Novel initiation genes in squamous cell carcinomagenesis: A role for substrate-specific ubiquitylation in the control of cell survival. Mol. Carcinog. *46*, 585–590.

Albor, A., El-Hizawi, S., Horn, E.J., Laederich, M., Frosk, P., Wrogemann, K., and Kulesz-Martin, M. (2006). The interaction of Piasy with Trim32, an E3-ubiquitin ligase mutated in limb-girdle muscular dystrophy type 2H, promotes Piasy degradation and regulates UVB-induced keratinocyte apoptosis through NFkappaB. J Biol Chem *281*, 25850–25866.

Armstrong, B.K., and Kricker, A. (2001). The epidemiology of UV induced skin cancer. J. Photochem. Photobiol. B *63*, 8–18.

Arwert, E.N., Mentink, R.A., Driskell, R.R., Hoste, E., Goldie, S.J., Quist, S., and Watt, F.M. (2012). Upregulation of CD26 expression in epithelial cells and stromal cells during wound-induced skin tumour formation. Oncogene *31*, 992–1000.

Aziz, M.H., Manoharan, H.T., Sand, J.M., and Verma, A.K. (2007a). Protein kinase Cepsilon interacts with Stat3 and regulates its activation that is essential for the development of skin cancer. Mol. Carcinog. *46*, 646–653.

Aziz, M.H., Manoharan, H.T., and Verma, A.K. (2007b). Protein Kinase Cε, which Sensitizes Skin to Sun's UV Radiation–Induced Cutaneous Damage and Development of Squamous Cell Carcinomas, Associates with Stat3. Cancer Res. *67*, 1385–1394.

Baeuerle, P.A., and Baltimore, D. (1996). NF-kappa B: ten years after. Cell *87*, 13–20.

Benavides, F., Oberyszyn, T.M., VanBuskirk, A.M., Reeve, V.E., and Kusewitt, D.F. (2009). The hairless mouse in skin research. J. Dermatol. Sci. *53*, 10–18.

Bender, K., Göttlicher, M., Whiteside, S., Rahmsdorf, H.J., and Herrlich, P. (1998). Sequential DNA damage-independent and -dependent activation of NF-kappaB by UV. EMBO J. *17*, 5170–5181.

Bernacki, R.J., Bansal, S.K., and Gurtoo, H.L. (1987). Combinations of mesna with cyclophosphamide or adriamycin in the treatment of mice with tumors. Cancer Res. *47*, 799–802.

Blumberg, P.M. (1991). Complexities of the protein kinase C pathway. Mol. Carcinog. *4*, 339–344.

Brewer, J.D., Colegio, O.R., Phillips, P.K., Roenigk, R.K., Jacobs, M.A., Van de Beek, D., Dierkhising, R.A., Kremers, W.K., McGregor, C.G.A., and Otley, C.C. (2009). Incidence of and risk factors for skin cancer after heart transplant. Arch. Dermatol. *145*, 1391–1396.

Brodland, D.G., and Zitelli, J.A. (1992). Surgical margins for excision of primary cutaneous squamous cell carcinoma. J. Am. Acad. Dermatol. *27*, 241–248.

Brougham, N.D.L.S., Dennett, E.R., Cameron, R., and Tan, S.T. (2012). The incidence of metastasis from cutaneous squamous cell carcinoma and the impact of its risk factors. J. Surg. Oncol. *106*, 811–815.

Büssing, I., Slack, F.J., and Grosshans, H. (2008). let-7 microRNAs in development, stem cells and cancer. Trends Mol. Med. *14*, 400–409.

Cadet, J., Berger, M., Decarroz, C., Wagner, J.R., van Lier, J.E., Ginot, Y.M., and Vigny, P. (1986). Photosensitized reactions of nucleic acids. Biochimie *68*, 813–834.

Chahoud, J., Semaan, A., Chen, Y., Cao, M., Rieber, A.G., Rady, P., and Tyring, S.K. (2015). Association Between β-Genus Human Papillomavirus and Cutaneous Squamous Cell Carcinoma in Immunocompetent Individuals-A Meta-analysis. JAMA Dermatol.

Chang, E.-J., Kundu, J.K., Liu, L., Shin, J.-W., and Surh, Y.-J. (2011). Ultraviolet B radiation activates NF-κB and induces iNOS expression in HR-1 hairless mouse skin: role of IκB kinase-β. Mol. Carcinog. *50*, 310–317.

Chen, Y.R., Wang, X., Templeton, D., Davis, R.J., and Tan, T.H. (1996). The role of c-Jun N-terminal kinase (JNK) in apoptosis induced by ultraviolet C and gamma radiation. Duration of JNK activation may determine cell death and proliferation. J. Biol. Chem. *271*, 31929–31936.

Chiang, A.P., Beck, J.S., Yen, H.-J., Tayeh, M.K., Scheetz, T.E., Swiderski, R.E., Nishimura, D.Y., Braun, T.A., Kim, K.-Y.A., Huang, J., Elbedour, K., Carmi, R., Slusarski, D.C., Casavant, T.L., Stone, E.M., and Sheffield, V.C. (2006). Homozygosity mapping with SNP arrays identifies TRIM32, an E3 ubiquitin ligase, as a Bardet-Biedl syndrome gene (BBS11). Proc. Natl. Acad. Sci. U. S. A. *103*, 6287–6292.

Chouinard, N., Valerie, K., Rouabhia, M., and Huot, J. (2002). UVB-mediated activation of p38 mitogen-activated protein kinase enhances resistance of normal human keratinocytes to apoptosis by stabilizing cytoplasmic p53. Biochem. J. *365*, 133–145.

Ciechanover, A. (1994). The ubiquitin-proteasome proteolytic pathway. Cell *79*, 13–21.

Connolly, S.M., Baker, D.R., Coldiron, B.M., Fazio, M.J., Storrs, P.A., Vidimos, A.T., Zalla, M.J., Brewer, J.D., Smith Begolka, W., Berger, T.G., Bigby, M., Bolognia, J.L., Brodland, D.G., Collins, S., Cronin Jr., T.A., Dahl, M.V., Grant-Kels, J.M., Hanke, C.W., Hruza, G.J., James, W.D., Lober, C.W., McBurney, E.I., Norton, S.A., Roenigk, R.K., Wheeland, R.G., and Wisco, O.J. (2012). AAD/ACMS/ASDSA/ASMS 2012 appropriate use criteria for Mohs micrographic surgery: A report of the American Academy of Dermatology, American College of Mohs Surgery, American Society for Dermatologic Surgery Association, and the American Society for Mohs Surgery. J. Am. Acad. Dermatol. *67*, 531–550.

Cox, A.D., Fesik, S.W., Kimmelman, A.C., Luo, J., and Der, C.J. (2014). Drugging the undruggable RAS: Mission Possible? Nat. Rev. Drug Discov. *13*, 828–851.

Dickinson, S.E., Olson, E.R., Zhang, J., Cooper, S.J., Melton, T., Criswell, P.J., Casanova, A., Dong, Z., Hu, C., Saboda, K., Jacobs, E.T., Alberts, D.S., and Bowden, G.T. (2011). p38 MAP kinase plays a functional role in UVB-induced mouse skin carcinogenesis. Mol. Carcinog. *50*, 469–478.

DiGiovanni, J., S.Bhatt, T., and E.Walker, S. (1993). C57BL/6 mice are resistant to tumor promotion by full thickness skin wounding. Carcinogenesis *14*, 319–321.

D'Orazio, J., Jarrett, S., Amaro-Ortiz, A., and Scott, T. (2013). UV Radiation and the Skin. Int. J. Mol. Sci. *14*, 12222–12248.

English, D.R., Armstrong, B.K., Kricker, A., Winter, M.G., Heenan, P.J., and Randell, P.L. (1998). Demographic characteristics, pigmentary and cutaneous risk factors for squamous cell carcinoma of the skin: A case-control study. Int. J. Cancer *76*, 628–634.

Fatima, M., Kumari, R., Schwamborn, J.C., Mahadevan, A., Shankar, S.K., Raja, R., and Seth, P. (2016). Tripartite containing motif 32 modulates proliferation of human neural precursor cells in HIV-1 neurodegeneration. Cell Death Differ. *23*, 776–786.

Forbes, P.D., Davies, R.E., and Urbach, F. (1978). Experimental ultraviolet photocarcinogenesis: wavelength interactions and time-dose relationships. Natl. Cancer Inst. Monogr. 31–38.

Fridell, R.A., Harding, L.S., Bogerd, H.P., and Cullen, B.R. (1995). Identification of a novel human zinc finger protein that specifically interacts with the activation domain of lentiviral Tat proteins. Virology *209*, 347–357.

Fritsche, E., Schäfer, C., Calles, C., Bernsmann, T., Bernshausen, T., Wurm, M., Hübenthal, U., Cline, J.E., Hajimiragha, H., Schroeder, P., Klotz, L.-O., Rannug, A., Fürst, P., Hanenberg, H., Abel, J., and Krutmann, J. (2007). Lightening up the UV response by identification of the arylhydrocarbon receptor as a cytoplasmatic target for ultraviolet B radiation. Proc. Natl. Acad. Sci. *104*, 8851–8856.

Frosk, P., Weiler, T., Nylen, E., Sudha, T., Greenberg, C.R., Morgan, K., Fujiwara, T.M., and Wrogemann, K. (2002). Limb-girdle muscular dystrophy type 2H associated with

mutation in TRIM32, a putative E3-ubiquitin-ligase gene. Am. J. Hum. Genet. *70*, 663–672.

Garrick, D., Fiering, S., Martin, D.I., and Whitelaw, E. (1998). Repeat-induced gene silencing in mammals. Nat. Genet. *18*, 56–59.

Giglia-Mari, G., and Sarasin, A. (2003). TP53 mutations in human skin cancers. Hum. Mutat. *21*, 217–228.

Gordon, J.W., and Ruddle, F.H. (1981). Integration and stable germ line transmission of genes injected into mouse pronuclei. Science *214*, 1244–1246.

Hart, R.W., Setlow, R.B., and Woodhead, A.D. (1977). Evidence that pyrimidine dimers in DNA can give rise to tumors. Proc. Natl. Acad. Sci. U. S. A. *74*, 5574–5578.

Hashimoto, Y.U., Tajima, O., Osada, S., and Kuroki, T. (1994). Expression of protein kinase C isoforms in skin papilloma and carcinoma of mice. Cancer Lett. *83*, 245–248.

He, Y.-Y., Huang, J.-L., and Chignell, C.F. (2004). Delayed and sustained activation of extracellular signal-regulated kinase in human keratinocytes by UVA: implications in carcinogenesis. J. Biol. Chem. *279*, 53867–53874.

Heffner, C.S., Herbert Pratt, C., Babiuk, R.P., Sharma, Y., Rockwood, S.F., Donahue, L.R., Eppig, J.T., and Murray, S.A. (2012). Supporting conditional mouse mutagenesis with a comprehensive cre characterization resource. Nat. Commun. *3*, 1218.

Helenius, M., Mäkeläinen, L., and Salminen, A. (1999). Attenuation of NF-κB Signaling Response to UVB Light during Cellular Senescence. Exp. Cell Res. *248*, 194–202.

Hildesheim, J., Awwad, R.T., and Fornace, A.J. (2004). p38 Mitogen-activated protein kinase inhibitor protects the epidermis against the acute damaging effects of ultraviolet irradiation by blocking apoptosis and inflammatory responses. J. Invest. Dermatol. *122*, 497–502.

Hillje, A.-L., Worlitzer, M.M.A., Palm, T., and Schwamborn, J.C. (2011). Neural Stem Cells Maintain Their Stemness through Protein Kinase C ζ-Mediated Inhibition of TRIM32. STEM CELLS *29*, 1437–1447.

Hillje, A.-L., Pavlou, M. a. S., Beckmann, E., Worlitzer, M.M.A., Bahnassawy, L., Lewejohann, L., Palm, T., and Schwamborn, J.C. (2013). TRIM32-dependent transcription in adult neural progenitor cells regulates neuronal differentiation. Cell Death Dis. *4*, e976.

Hirai, S., Izumi, Y., Higa, K., Kaibuchi, K., Mizuno, K., Osada, S., Suzuki, K., and Ohno, S. (1994). Ras-dependent signal transduction is indispensable but not sufficient for the activation of AP1/Jun by PKC delta. EMBO J. *13*, 2331–2340.

Hodges, A., and Smoller, B.R. (2002). Immunohistochemical Comparison of P16 Expression in Actinic Keratoses and Squamous Cell Carcinomas of the Skin. Mod. Pathol. *15*, 1121–1125.

Hogerlinden, M. van, Rozell, B.L., Ährlund-Richter, L., and ToftgÅrd, R. (1999). Squamous Cell Carcinomas and Increased Apoptosis in Skin with Inhibited Rel/Nuclear Factor-κB Signaling. Cancer Res. *59*, 3299–3303.

Horn, E.J., Albor, A., Liu, Y., El-Hizawi, S., Vanderbeek, G.E., Babcock, M., Bowden, G.T., Hennings, H., Lozano, G., Weinberg, W.C., and Kulesz-Martin, M. (2004). RING protein Trim32 associated with skin carcinogenesis has anti-apoptotic and E3-ubiquitin ligase properties. Carcinogenesis *25*, 157–167.

Jansen, A.P., Verwiebe, E.G., Dreckschmidt, N.E., Wheeler, D.L., Oberley, T.D., and Verma, A.K. (2001a). Protein kinase C-epsilon transgenic mice: a unique model for metastatic squamous cell carcinoma. Cancer Res. *61*, 808–812.

Jansen, A.P., Dreckschmidt, N.E., Verwiebe, E.G., Wheeler, D.L., Oberley, T.D., and Verma, A.K. (2001b). Relation of the induction of epidermal ornithine decarboxylase and hyperplasia to the different skin tumor–promotion susceptibilities of protein kinase Cα, -δ and -ϵ transgenic mice. Int. J. Cancer *93*, 635–643.

Kamiya, T., Makino, J., Hara, H., Inagaki, N., and Adachi, T. (2011). Extracellular-superoxide dismutase expression during monocytic differentiation of U937 cells. J. Cell. Biochem. *112*, 244–255.

Kano, S., Miyajima, N., Fukuda, S., and Hatakeyama, S. (2008). Tripartite motif protein 32 facilitates cell growth and migration via degradation of Abl-interactor 2. Cancer Res. *68*, 5572–5580.

Kappes, U.P., Luo, D., Potter, M., Schulmeister, K., and Rünger, T.M. (2006). Short- and long-wave UV light (UVB and UVA) induce similar mutations in human skin cells. J. Invest. Dermatol. *126*, 667–675.

Karagas, M.R., Greenberg, E.R., Spencer, S.K., Stukel, T.A., and Mott, L.A. (1999). Increase in incidence rates of basal cell and squamous cell skin cancer in New Hampshire, USA. New Hampshire Skin Cancer Study Group. Int. J. Cancer J. Int. Cancer *81*, 555–559.

Karia, P.S., Han, J., and Schmults, C.D. (2013). Cutaneous squamous cell carcinoma: Estimated incidence of disease, nodal metastasis, and deaths from disease in the United States, 2012. J Am Acad Dermatol *68*, 957–966.

Karin, M., and Gallagher, E. (2005). From JNK to pay dirt: jun kinases, their biochemistry, physiology and clinical importance. IUBMB Life *57*, 283–295.

Katiyar, S.K., Agarwal, R., Wood, G.S., and Mukhtar, H. (1992). Inhibition of 12-O-Tetradecanoylphorbol-13-acetate-caused   Tumor   Promotion   in   7,12-

Dimethylbenz[a]anthracene-initiated SENCAR Mouse Skin by a Polyphenolic Fraction Isolated from Green Tea. Cancer Res. *52*, 6890–6897.

Kato, T., Delhase, M., Hoffmann, A., and Karin, M. (2003). CK2 Is a C-Terminal IkappaB Kinase Responsible for NF-kappaB Activation during the UV Response. Mol. Cell *12*, 829–839.

Kielbassa, C., Roza, L., and Epe, B. (1997). Wavelength dependence of oxidative DNA damage induced by UV and visible light. Carcinogenesis *18*, 811–816.

Kishikawa, M., Koyama, K., Iseki, M., Kobuke, T., Yonehara, S., Soda, M., Ron, E., Tokunaga, M., Preston, D.L., Mabuchi, K., and Tokuoka, S. (2005). Histologic characteristics of skin cancer in Hiroshima and Nagasaki: background incidence and radiation effects. Int. J. Cancer *117*, 363–369.

van Kranen, H.J., de Gruijl, F.R., de Vries, A., Sontag, Y., Wester, P.W., Senden, H.C., Rozemuller, E., and van Kreijl, C.F. (1995). Frequent p53 alterations but low incidence of ras mutations in UV-B-induced skin tumors of hairless mice. Carcinogenesis *16*, 1141–1147.

Kubo, Y., Urano, Y., Matsumoto, K., Ahsan, K., and Arase, S. (1997). Mutations of theINK4aLocus in Squamous Cell Carcinomas of Human Skin. Biochem. Biophys. Res. Commun. *232*, 38–41.

Kudryashova, E., Wu, J., Havton, L.A., and Spencer, M.J. (2009). Deficiency of the E3 ubiquitin ligase TRIM32 in mice leads to a myopathy with a neurogenic component. Hum. Mol. Genet. *18*, 1353–1367.

Kudryashova, E., Struyk, A., Mokhonova, E., Cannon, S.C., and Spencer, M.J. (2011). The common missense mutation D489N in TRIM32 causing limb girdle muscular dystrophy 2H leads to loss of the mutated protein in knock-in mice resulting in a Trim32-null phenotype. Hum. Mol. Genet. *20*, 3925–3932.

Laat, W.L. de, Jaspers, N.G.J., and Hoeijmakers, J.H.J. (1999). Molecular mechanism of nucleotide excision repair. Genes Dev. *13*, 768–785.

Lansbury, L., Bath-Hextall, F., Perkins, W., Stanton, W., and Leonardi-Bee, J. (2013). Interventions for non-metastatic squamous cell carcinoma of the skin: systematic review and pooled analysis of observational studies. BMJ *347*, f6153.

Leonardi-Bee, J., Ellison, T., and Bath-Hextall, F. (2012). Smoking and the risk of nonmelanoma skin cancer: systematic review and meta-analysis. Arch. Dermatol. *148*, 939–946.

Lewis, D.A., and Spandau, D.F. (2007). UVB activation of NF-kappaB in normal human keratinocytes occurs via a unique mechanism. Arch. Dermatol. Res. *299*, 93–101.

Lewis, J.G., and Adams, D.O. (1987). Early inflammatory changes in the skin of SENCAR and C57BL/6 mice following exposme to 12-O-tetradecanoylphorbol-13-acetat. Carcinogenesis *8*, 889–898.

Li, G., Mitchell, D.L., Ho, V.C., Reed, J.C., and Tron, V.A. (1996). Decreased DNA repair but normal apoptosis in ultraviolet-irradiated skin of p53-transgenic mice. Am. J. Pathol. *148*, 1113–1123.

Lichti, U., Anders, J., and Yuspa, S.H. (2008). Isolation and short-term culture of primary keratinocytes, hair follicle populations and dermal cells from newborn mice and keratinocytes from adult mice for in vitro analysis and for grafting to immunodeficient mice. Nat. Protoc. *3*, 799–810.

Liu, J., Zhang, C., Wang, X.L., Ly, P., Belyi, V., Xu-Monette, Z.Y., Young, K.H., Hu, W., and Feng, Z. (2014). E3 ubiquitin ligase TRIM32 negatively regulates tumor suppressor p53 to promote tumorigenesis. Cell Death Differ. *21*, 1792–1804.

Lofgren, J.L.S., Erdman, S.E., Hewes, C., Wong, C., King, R., Chavarria, T.E., Discua, A.R., Fox, J.G., and Maurer, K.J. (2012). Castration eliminates conspecific aggression in group-housed CD1 male surveillance mice (Mus musculus). J. Am. Assoc. Lab. Anim. Sci. JAALAS *51*, 594–599.

Lu, Y.-P., Lou, Y.-R., Yen, P., Mitchell, D., Huang, M.-T., and Conney, A.H. (1999). Time Course for Early Adaptive Responses to Ultraviolet B Light in the Epidermis of SKH-1 Mice. Cancer Res. *59*, 4591–4602.

Martinez J, Otley CC, Stasko T, and et al (2003). Defining the clinical course of metastatic skin cancer in organ transplant recipients: A multicenter collaborative study. Arch. Dermatol. *139*, 301–306.

Maschke, M., Kastrup, O., Esser, S., Ross, B., Hengge, U., and Hufnagel, A. (2000). Incidence and prevalence of neurological disorders associated with HIV since the introduction of highly active antiretroviral therapy (HAART). J. Neurol. Neurosurg. Psychiatry *69*, 376–380.

Maubec, E., Petrow, P., Scheer-Senyarich, I., Duvillard, P., Lacroix, L., Gelly, J., Certain, A., Duval, X., Crickx, B., Buffard, V., Basset-Seguin, N., Saez, P., Duval-Modeste, A.-B., Adamski, H., Mansard, S., Grange, F., Dompmartin, A., Faivre, S., Mentré, F., and Avril, M.-F. (2011). Phase II study of cetuximab as first-line single-drug therapy in patients with unresectable squamous cell carcinoma of the skin. J. Clin. Oncol. Off. J. Am. Soc. Clin. Oncol. *29*, 3419–3426.

McGrath, J.A., and Uitto, J. (2010). Anatomy and Organization of Human Skin. In Rook's Textbook of Dermatology, T.B.M. Dermatologist BS, FRCP Emeritus Consultant, S.B. Dermatologist MB, BChir, MD,, FRCP Consultant, N.C.Bs. Visitingessor MB, ChB, FRCP(Lond &.Edin) Consultant Dermatologist, and C.G.Bs. Dermatologist MD, FRCP, FRCPathessor of Dermatology Consultant, eds. (Wiley-Blackwell), pp. 1–53.

Mellor, H., and Parker, P.J. (1998). The extended protein kinase C superfamily. Biochem. J. *332 (Pt 2)*, 281–292.

Melnikova, V.O., Pacifico, A., Chimenti, S., Peris, K., and Ananthaswamy, H.N. (2005). Fate of UVB-induced p53 mutations in SKH-hr1 mouse skin after discontinuation of irradiation: relationship to skin cancer development. Oncogene *24*, 7055–7063.

Mills, K.J., Bocckino, S.B., Burns, D.J., Loomis, C.R., and Smart, R.C. (1992). Alterations in protein kinase C isozymes alpha and beta 2 in activated Ha-ras containing papillomas in the absence of an increase in diacylglycerol. Carcinogenesis *13*, 1113–1120.

Mishra, M., Taneja, M., Malik, S., Khalique, H., and Seth, P. (2010). Human immunodeficiency virus type 1 Tat modulates proliferation and differentiation of human neural precursor cells: implication in NeuroAIDS. J. Neurovirol. *16*, 355–367.

Mouret, S., Baudouin, C., Charveron, M., Favier, A., Cadet, J., and Douki, T. (2006). Cyclobutane pyrimidine dimers are predominant DNA lesions in whole human skin exposed to UVA radiation. Proc. Natl. Acad. Sci. U. S. A. *103*, 13765–13770.

Muthusamy, V., and Piva, T.J. (2010). The UV response of the skin: a review of the MAPK, NFκB and TNFα signal transduction pathways. Arch. Dermatol. Res. *302*, 5–17.

Neri, M., Selvatici, R., Scotton, C., Trabanelli, C., Armaroli, A., De Grandis, D., Levy, N., Gualandi, F., and Ferlini, A. (2013). A patient with limb girdle muscular dystrophy carries a TRIM32 deletion, detected by a novel CGH array, in compound heterozygosis with a nonsense mutation. Neuromuscul. Disord. NMD *23*, 478–482.

Nishigori, C., Hattori, Y., and Toyokuni, S. (2004). Role of Reactive Oxygen Species in Skin Carcinogenesis. Antioxid. Redox Signal. *6*, 561–570.

Nisole, S., Stoye, J.P., and Saib, A. (2005). TRIM family proteins: retroviral restriction and antiviral defence. Nat Rev Micro *3*, 799–808.

Ozato, K., Shin, D.-M., Chang, T.-H., and Morse, H.C. (2008). TRIM family proteins and their emerging roles in innate immunity. Nat Rev Immunol *8*, 849–860.

Panteleyev, A.A., van der Veen, C., Rosenbach, T., Müller-Röver, S., Sokolov, V.E., and Paus, R. (1998). Towards Defining the Pathogenesis of the Hairless Phenotype. J. Invest. Dermatol. *110*, 902–907.

Pelleitier, M., and Montplaisir, S. (1975). The nude mouse: a model of deficient T-cell function. Methods Achiev. Exp. Pathol. *7*, 149–166.

Popp, S., Waltering, S., Herbst, C., Moll, I., and Boukamp, P. (2002). UV-B-type mutations and chromosomal imbalances indicate common pathways for the development of Merkel and skin squamous cell carcinomas. Int. J. Cancer *99*, 352–360.

Potter, G.B., Beaudoin, G.M.J., DeRenzo, C.L., Zarach, J.M., Chen, S.H., and Thompson, C.C. (2001). The hairless gene mutated in congenital hair loss disorders encodes a novel nuclear receptor corepressor. Genes Dev. *15*, 2687–2701.

Ramachandran, H., Schäfer, T., Kim, Y., Herfurth, K., Hoff, S., Lienkamp, S.S., Kramer-Zucker, A., and Walz, G. (2014). Interaction with the Bardet-Biedl Gene Product TRIM32/BBS11 Modifies the Half-life and Localization of Glis2/NPHP7. J. Biol. Chem. *289*, 8390–8401.

Ramos, M.C., Steinbrenner, H., Stuhlmann, D., Sies, H., and Brenneisen, P. (2004). Induction of MMP-10 and MMP-1 in a squamous cell carcinoma cell line by ultraviolet radiation. Biol. Chem. *385*, 75–86.

Ratushny, V., Gober, M.D., Hick, R., Ridky, T.W., and Seykora, J.T. (2012). From keratinocyte to cancer: the pathogenesis and modeling of cutaneous squamous cell carcinoma. J. Clin. Invest. *122*, 464–472.

Ravi, D., Muniyappa, H., and Das, K.C. (2008). Caffeine inhibits UV-mediated NF-kappaB activation in A2058 melanoma cells: an ATM-PKCdelta-p38 MAPK-dependent mechanism. Mol. Cell. Biochem. *308*, 193–200.

Reddig, P.J., Dreckschmidt, N.E., Ahrens, H., Simsiman, R., Tseng, C.P., Zou, J., Oberley, T.D., and Verma, A.K. (1999). Transgenic mice overexpressing protein kinase Cdelta in the epidermis are resistant to skin tumor promotion by 12-O-tetradecanoylphorbol-13-acetate. Cancer Res. *59*, 5710–5718.

Reddig, P.J., Dreckschmidt, N.E., Zou, J., Bourguignon, S.E., Oberley, T.D., and Verma, A.K. (2000). Transgenic mice overexpressing protein kinase C epsilon in their epidermis exhibit reduced papilloma burden but enhanced carcinoma formation after tumor promotion. Cancer Res. *60*, 595–602.

Reed, D.R., Bachmanov, A.A., and Tordoff, M.G. (2007). Forty mouse strain survey of body composition. Physiol. Behav. *91*, 593–600.

Rehman, I., Lowry, D.T., Adams, C., Abdel-Fattah, R., Holly, A., Yuspa, S.H., and Hennings, H. (2000). Frequent codon 12 Ki-ras mutations in mouse skin tumors initiated by N-methyl-N′-nitro-N-nitrosoguanidine and promoted by mezerein. Mol. Carcinog. *27*, 298–307.

Reigneau, M., Robert, C., Routier, E., Mamelle, G., Moya-Plana, A., Tomasic, G., and Mateus, C. (2015). Efficacy of neoadjuvant cetuximab alone or with platinum salt for the treatment of unresectable advanced nonmetastatic cutaneous squamous cell carcinomas. Br. J. Dermatol. *173*, 527–534.

Reiners, J.J., and Singh, K.P. (1997). Susceptibility of 129/SvEv mice in two-stage carcinogenesis protocols to 12-O-tetradecanoylphorbol-13-acetate promotion. Carcinogenesis *18*, 593–597.

Reiners, J.J., Nesnow, S., and Slaga, T.J. (1984). Murine susceptibility to two-stage skin carcinogenesis is influenced by the agent used for promotion. Carcinogenesis *5*, 301–307.

Richmond, A. (2002). NF-κB, chemokine gene transcription and tumour growth. Nat. Rev. Immunol. *2*, 664–674.

Rogers, H.W., Weinstock, M.A., Harris, A.R., Hinckley, M.R., Feldman, S.R., Fleischer, A.B., and Coldiron, B.M. (2010). Incidence estimate of nonmelanoma skin cancer in the United States, 2006. Arch. Dermatol. *146*, 283–287.

Roh, J.-L., Sung, M.-W., and Kim, K.H. (2005). Suppression of accelerated tumor growth in surgical wounds by celecoxib and indomethacin. Head Neck *27*, 326–332.

Rojas, I.-G., Padgett, D.A., Sheridan, J.F., and Marucha, P.T. (2002). Stress-Induced Susceptibility to Bacterial Infection During Cutaneous Wound Healing. Brain. Behav. Immun. *16*, 74–84.

Rowe, D.E., Carroll, R.J., and Day, C.L. (1992). Prognostic factors for local recurrence, metastasis, and survival rates in squamous cell carcinoma of the skin, ear, and lip. Implications for treatment modality selection. J. Am. Acad. Dermatol. *26*, 976–990.

Ruan, C.-S., Wang, S.-F., Shen, Y.-J., Guo, Y., Yang, C.-R., Zhou, F.H., Tan, L.-T., Zhou, L., Liu, J.-J., Wang, W.-Y., Xiao, Z.-C., and Zhou, X.-F. (2014). Deletion of TRIM32 protects mice from anxiety- and depression-like behaviors under mild stress. Eur. J. Neurosci. *40*, 2680–2690.

Ryu, Y.S., Lee, Y., Lee, K.W., Hwang, C.Y., Maeng, J.-S., Kim, J.-H., Seo, Y.-S., You, K.-H., Song, B., and Kwon, K.-S. (2011). TRIM32 Protein Sensitizes Cells to Tumor Necrosis Factor (TNFα)-induced Apoptosis via Its RING Domain-dependent E3 Ligase Activity against X-linked Inhibitor of Apoptosis (XIAP). J. Biol. Chem. *286*, 25729–25738.

Saccone, V., Palmieri, M., Passamano, L., Piluso, G., Meroni, G., Politano, L., and Nigro, V. (2008). Mutations that impair interaction properties of TRIM32 associated with limb-girdle muscular dystrophy 2H. Hum. Mutat. *29*, 240–247.

Sadek, H., Azli, N., Wendling, J.L., Cvitkovic, E., Rahal, M., Mamelle, G., Guillaume, J.C., Armand, J.P., and Avril, M.F. (1990). Treatment of advanced squamous cell carcinoma of the skin with cisplatin, 5-fluorouracil, and bleomycin. Cancer *66*, 1692–1696.

Sano, S., Chan, K.S., Kira, M., Kataoka, K., Takagi, S., Tarutani, M., Itami, S., Kiguchi, K., Yokoi, M., Sugasawa, K., Mori, T., Hanaoka, F., Takeda, J., and DiGiovanni, J. (2005). Signal Transducer and Activator of Transcription 3 Is a Key Regulator of Keratinocyte Survival and Proliferation following UV Irradiation. Cancer Res. *65*, 5720–5729.

Schaffer, B.S., Grayson, M.H., Wortham, J.M., Kubicek, C.B., McCleish, A.T., Prajapati, S.I., Nelon, L.D., Brady, M.M., Jung, I., Hosoyama, T., Sarro, L.M., Hanes, M.A., Rubin, B.P., Michalek, J.E., Clifford, C.B., Infante, A.J., and Keller, C. (2010). Immune Competency of a Hairless Mouse Strain for Improved Preclinical Studies in Genetically-Engineered Mice. Mol. Cancer Ther. *9*, 2354–2364.

Schieke, S.M., Ruwiedel, K., Gers-Barlag, H., Grether-Beck, S., and Krutmann, J. (2005). Molecular crosstalk of the ultraviolet a and ultraviolet B signaling responses at the level of mitogen-activated protein kinases. J. Invest. Dermatol. *124*, 857–859.

Schwamborn, J.C., Berezikov, E., and Knoblich, J.A. (2009). The TRIM-NHL protein TRIM32 activates microRNAs and prevents self-renewal in mouse neural progenitors. Cell *136*, 913–925.

Sherr, C.J. (2004). Principles of Tumor Suppression. Cell *116*, 235–246.

Short, K.M., and Cox, T.C. (2006). Subclassification of the RBCC/TRIM Superfamily Reveals a Novel Motif Necessary for Microtubule Binding. J. Biol. Chem. *281*, 8970–8980.

Simanainen, U., Ryan, T., Li, D., Suarez, F.G., Gao, Y.R., Watson, G., Wang, Y., and Handelsman, D.J. (2015). Androgen receptor actions modify skin structure and chemical carcinogen-induced skin cancer susceptibility in mice. Horm. Cancer *6*, 45–53.

Simon, M.M., Aragane, Y., Schwarz, A., Luger, T.A., and Schwarz, T. (1994). UVB Light Induces Nuclear Factor κB (NFκB) Activity Independently from Chromosomal DNA Damage in Cell-Free Cytosolic Extracts. J. Invest. Dermatol. *102*, 422–427.

Soames, A.R., Lavender, D., Foster, J.R., Williams, S.M., and Wheeldon, E.B. (1994). Image analysis of bromodeoxyuridine (BrdU) staining for measurement of S-phase in rat and mouse liver. J. Histochem. Cytochem. *42*, 939–944.

Soufir, N., Daya-Grosjean, L., Salmonière, P. de L., Moles, J.-P., Dubertret, L., Sarasin, A., and Basset-Seguin, N. (2000). Association Between INK4a-ARF and p53 Mutations in Skin Carcinomas of Xeroderma Pigmentosum Patients. J. Natl. Cancer Inst. *92*, 1841–1847.

Stern, R.S., and PUVA Follow-Up Study (2012). The risk of squamous cell and basal cell cancer associated with psoralen and ultraviolet A therapy: a 30-year prospective study. J. Am. Acad. Dermatol. *66*, 553–562.

Stoye, J.P., Fenner, S., Greenoak, G.E., Moran, C., and Coffin, J.M. (1988). Role of endogenous retroviruses as mutagens: The hairless mutation of mice. Cell *54*, 383–391.

Sundberg, J.P., Sundberg, B.A., and Beamer, W.G. (1997). Comparison of chemical carcinogen skin tumor induction efficacy in inbred, mutant, and hybrid strains of mice:

morphologic variations of induced tumors and absence of a papillomavirus cocarcinogen. Mol. Carcinog. *20*, 19–32.

Thomas-Ahner, J.M., Wulff, B.C., Tober, K.L., Kusewitt, D.F., Riggenbach, J.A., and Oberyszyn, T.M. (2007). Gender Differences in UVB-Induced Skin Carcinogenesis, Inflammation, and DNA Damage. Cancer Res. *67*, 3468–3474.

Tornaletti, S., and Pfeifer, G.P. (1994). Slow repair of pyrimidine dimers at p53 mutation hotspots in skin cancer. Science *263*, 1436–1438.

Tournier, C., Hess, P., Yang, D.D., Xu, J., Turner, T.K., Nimnual, A., Bar-Sagi, D., Jones, S.N., Flavell, R.A., and Davis, R.J. (2000). Requirement of JNK for stress-induced activation of the cytochrome c-mediated death pathway. Science *288*, 870–874.

Tsuchiya, Y., Asano, T., Nakayama, K., Kato Jr., T., Karin, M., and Kamata, H. (2010). Nuclear IKKβ Is an Adaptor Protein for IκBα Ubiquitination and Degradation in UV-Induced NF-κB Activation. Mol. Cell *39*, 570–582.

Uribe, P., and Gonzalez, S. (2011). Epidermal growth factor receptor (EGFR) and squamous cell carcinoma of the skin: Molecular bases for EGFR-targeted therapy. Pathol. - Res. Pract. *207*, 337–342.

Van Laethem, A., Nys, K., Van Kelst, S., Claerhout, S., Ichijo, H., Vandenheede, J.R., Garmyn, M., and Agostinis, P. (2006). Apoptosis signal regulating kinase-1 connects reactive oxygen species to p38 MAPK-induced mitochondrial apoptosis in UVB-irradiated human keratinocytes. Free Radic. Biol. Med. *41*, 1361–1371.

Veness, M.J. (2006). Defining patients with high-risk cutaneous squamous cell carcinoma. Australas. J. Dermatol. *47*, 28–33.

Venugopal, R., and Jaiswal, A.K. (1996). Nrf1 and Nrf2 positively and c-Fos and Fra1 negatively regulate the human antioxidant response element-mediated expression of NAD(P)H:quinone oxidoreductase1 gene. Proc. Natl. Acad. Sci. U. S. A. *93*, 14960–14965.

Wani, M.A., Zhu, Q.Z., El-Mahdy, M., and Wani, A.A. (1999). Influence of p53 tumor suppressor protein on bias of DNA repair and apoptotic response in human cells. Carcinogenesis *20*, 765–772.

Wehner, M.R., Shive, M.L., Chren, M.-M., Han, J., Qureshi, A.A., and Linos, E. (2012). Indoor tanning and non-melanoma skin cancer: systematic review and meta-analysis. BMJ *345*, e5909.

Wheeler, D.L., Martin, K.E., Ness, K.J., Li, Y., Dreckschmidt, N.E., Wartman, M., Ananthaswamy, H.N., Mitchell, D.L., and Verma, A.K. (2004). Protein Kinase C ε Is an Endogenous Photosensitizer That Enhances Ultraviolet Radiation-Induced Cutaneous

Damage and Development of Squamous Cell Carcinomas1. Cancer Res. *64*, 7756–7765.

Wheeler, D.L., Li, Y., and Verma, A.K. (2005). Protein kinase C epsilon signals ultraviolet light-induced cutaneous damage and development of squamous cell carcinoma possibly through Induction of specific cytokines in a paracrine mechanism. Photochem. Photobiol. *81*, 9–18.

Wilgus, T.A., Ross, M.S., Parrett, M.L., and Oberyszyn, T.M. (2000). Topical application of a selective cyclooxygenase inhibitor suppresses UVB mediated cutaneous inflammation. Prostaglandins Other Lipid Mediat. *62*, 367–384.

Williams, A., Harker, N., Ktistaki, E., Veiga-Fernandes, H., Roderick, K., Tolaini, M., Norton, T., Williams, K., and Kioussis, D. (2008). Position effect variegation and imprinting of transgenes in lymphocytes. Nucleic Acids Res. *36*, 2320–2329.

APPENDIX I: COAUTHORED PUBLICATION

NF-κB Repression by PIAS3 Mediated RelA SUMOylation

Yuangang Liu, Rebecca Bridges, Aaron Wortham, and Molly Kulesz-Martin

A. Contribution

My main contribution to this publication was the generation of RelA and PIASy expression vectors and the initial work demonstrating the SUMOylation of RelA by PIASy.

B. Abstract

Negative regulation of the NF-κB transcription factor is essential for tissue homeostasis in response to stress and inflammation. NF-κB activity is regulated by a variety of biochemical mechanisms including phosphorylation, acetylation, and ubiquitination. In this study, we provide the first experimental evidence that NF-κB is regulated by SUMOylation, where the RelA subunit of NF-κB is SUMOylated by PIAS3, a member of the PIAS (protein inhibitor of activated STAT) protein family with E3 SUMO ligase activity. PIAS3-mediated NF-κB repression was compromised by either RelA mutant resistant to SUMOylation or PIAS3 mutant defective in SUMOylation. PIAS3-mediated SUMOylation of endogenous RelA was induced by NF-κB activation thus forming a

negative regulatory loop. The SUMOylation of endogenous RelA was enhanced in IκBα null as compared with wild type fibroblasts. The RelA SUMOylation was induced by TNFα but not leptomycin B mediated RelA nuclear translocation. Furthermore, RelA mutants defective in DNA binding were not SUMOylated by PIAS3, suggesting that RelA DNA binding is a signal for PIAS3-mediated SUMOylation. These results support a novel negative feedback mechanism for NF-κB regulation by PIAS3-mediated RelA SUMOylation.

C. Introduction

NF-κB is a transcription factor that mediates cellular response to inflammation, immune response, and stress [1]. Deregulation of NF-κB is one of the common features in many pathological disorders including inflammatory diseases and cancer. NF-κB is a dimeric protein which can be comprised of a variety of combinations of Rel family DNA binding proteins including RelA (p65), RelB, c-Rel, p50, and p52. A heterodimer of RelA and p50 is the most common combination in the canonical NF-κB signaling pathway. In unstimulated cells, NF-κB is held in check by the inhibitor of NF-κB (IκBα) which sequesters NF-κB in the cytoplasm and prevents NF-κB DNA binding. Upon stimulation, IκBα is phosphorylated by IκB kinases, leading to its degradation. The degradation of IκBα allows the free NF-κB to translocate to the nucleus where it functions as a transcription factor to induce the expression of proinflammatory cytokines, chemokines, and factors for cell proliferation and survival [2].

Aberrant activation of NF-κB is detrimental to the host and may lead to a variety of inflammation related diseases like cancer, psoriasis and arthritis. Thus, as in many other signal transduction pathways, there are multiple feedback mechanisms to balance the activity of NF-κB. A well-established mechanism is NF-κB dependent induction of IκBα which disrupts NF-κB DNA binding and shuttles nuclear NF-κB back to cytoplasm, thus forming a negative regulation loop [3], [4], [5]. A20 is another NF-κB induced gene that inhibits NF-κB activity by degrading receptor interacting protein (RIP), an essential mediator for the activation of the TNF receptor-associated signaling complex in the cytoplasm [6]. In addition to negative regulation by NF-κB inducible genes, NF-κB is negatively regulated by CYLD, a deubiquitinase that represses the activation of the IKK complex by removing K63-linked ubiquitin chains from TRAFs and NEMO [7], [8], [9].

In addition to protein ubiquitination, growing evidence suggests that several proteins in the NF-κB pathway are regulated by SUMOylation [10]. SUMOylation is a posttranslational modification involving covalent conjugation of small ubiquitin-like modifier proteins (SUMO) to target proteins. In contrast to protein ubiquitination, which generally tags proteins for proteasome-mediated degradation, SUMOylation modulates protein localization, protein/protein interaction, transcriptional regulation, as well as protein stabilization. SUMOylation of IκBα inhibits NF-κB activation by blocking IκBα ubiquitination and degradation [11]. In response to genotoxic stress but not inflammatory challenge, NF-κB is activated by PIASy-mediated NEMO SUMOylation [12].

Mammalian PIAS has four family members including PIAS1, PIAS2 (PIASx), PIAS3, and PIASy [13]. PIAS proteins have four conserved structural domains and motifs: a SAP domain for chromatin binding, PINIT motif for localization, SP-RING domain for E3-SUMO ligation, and a SUMO-interacting motif for SUMO binding. While PIASy-mediated NEMO SUMOylation contributes to NF-κB activation [12], PIAS1 and PIAS3 inhibit NF-κB activity by direct binding to the RelA subunit of NF-κB [14], [15]. PIAS1 binds to the C-terminal transactivation domain of RelA and blocks RelA binding to DNA in vitro and in vivo [14]. PIAS3 binds to the N-terminal DNA binding domain of RelA and interferes with RelA binding to the CBP coactivator [15]. In our previous studies, we also found that PIASy represses NF-κB activity in mouse keratinocytes and represses the expression of CCL20 chemokine in response to TNFα and/or IL-17A [16]. Although SUMO modification has been suggested as a mechanism for transcriptional repression conserved from yeast to human [17], RelA SUMOylation and its role in transcriptional regulation have not been defined.

In this study, we provide in vitro (cell free) and in vivo evidence that RelA is SUMOylated. RelA is predominantly SUMOylated by PIAS3, among PIAS family proteins. PIAS3-mediated NF-κB repression is compromised by either RelA mutant resistant to SUMOylation or PIAS3 mutant defective in SUMOylation. The SUMOylation of endogenous RelA by PIAS3 is induced by NF-κB activation. Furthermore, PIAS3-mediated RelA SUMOylation was dependent on RelA DNA binding. These data suggest PIAS3-mediated RelA SUMOylation as a novel negative regulatory mechanism for NF-κB regulation.

D. Materials and Methods

i. Plasmids. Flag-tagged RelA/p65 was constructed by cloning the RelA/p65 coding sequence from HA-tagged RelA (kindly provided by S. Ghosh, Yale University) into pCMVTag2B vector (Stratagene). V5-tagged RelA was constructed by cloning RelA coding sequence from Flag-tagged RelA vector into pCDNA-v5 vector (Invitrogen). RelA mutants (121/122K>R, 37K>R, 39E>I, 36Y>A) and catalytically dead PIAS3 mutant (299C>S) were generated by targeted mutagenesis (Stratagene). His-tagged RelA and PIAS3 were cloned into pET-24a expression vector for the production of PIAS3 and RelA recombinant protein in BL-21 E. coli cells. Flag-tagged Pias1and PIAS3 cDNA were kindly provided by Shaiu Ke, UCLA. His-tagged SUMO3 and constitutively active IKK2 were kindly provided by Paul Fraser [18] and Anjana Rao [19], respectively.

ii. Cell Culture and Transfection. Human embryonic kidney 293T (HEK293T) cells (Invitrogen), mouse 3T3 fibroblasts [20], IκBα null fibroblasts and wild type fibroblasts [3], [4], [5] were cultured in Dulbecco's modified Eagle's medium supplemented with 10% fetal calf serum. Cells were transfected in serum free OptiMEM medium (Invitrogen) at 90% confluence using Transfectin (Bio-Rad) according to the manufacturer's instructions.

iii. Expression and Purification of Recombinant Bacterial Proteins. BL-21 cells containing the 6×his- and 6×his-Flag expression vectors noted above were grown to log phase in 300 ml Luria broth and induced with 1 mM IPTG (Fisher) for 1 hour. The cells were centrifuged at 5000 rpm for 5 mins at 4°C. The pellet was diluted in nickel lysis

buffer (50 mM NaH2PO4, 300 mM NaCl, 20 mM imidazole, pH 8.0), treated with lysozyme (1 mg/ml) for 20 minutes on ice, and sonicated. The crude lysate was clarified by centrifugation at 10,000 rpm for 20 min. The lyaste was incubated with 1 mL of Ni-NTA agarose slurry (Invitrogen) in nickel lysis buffer for 1 hr at 4°C. The beads were washed three times with 6 ml nickel wash buffer (50 mM NaH2PO4, 300 mM NaCl, 60 mM imidazole, pH 8.0), and eluted in 500 μL fractions using the nickel elution buffer (50 mM NaH2PO4, 300 mM NaCl, 250 mM imidazole, pH 8.0). The eluants were dialyzed against DNAB buffer (50 mM NaCl, 20 mM Tris [pH7.2]; 4% glycerol; 0.1% Triton-100; 1 mM EDTA). The purity and concentration of purified proteins were verified by Coomassie stain and immunoblotting.

iv. *In vivo* SUMOylation Assay. Murine 3T3 cells were transfected with His6-tagged SUMO vector, V5-tagged RelA vector, and Flag-tagged PIAS vectors, and other vectors as indicated. 24 hrs after transfection, cells were washed twice with PBS and harvested in 1 ml of PBS. Fifty percent of cells collected were lysed in RIPA buffer and used for direct immunoblotting. The remainder was lysed in denaturing lysis buffer (6 ml of 6 M guanidinium-HCl, 0.1 M Na2HPO4/NaH2PO4, 0.01 M Tris/HCl, pH 8.0, 5 mM, imidazole and 10 mM beta-mercaptoethanol). 50 μl of Ni2+-NTA-agarose beads (Qiagen) were then added and lysates were rotated at room temperature (RT) for 4 h. The beads were washed for 5 min between each step at room temperature with each of the following buffers, successively: Buffer A (6 M guanidinium-HCl, 0.1 M Na2HPO4/NaH2PO4, 0.01 M Tris/HCl, pH 8.0 plus 10 mM b-mercaptoethanol); Buffer B (8 M urea, 0.1 M Na2HPO4/NaH2PO4, 0.01 M Tris/HCl, pH 8.0, 10 mM b-mercaptoethanol); and Buffer

C (8 M urea, 0.1 M Na2HPO4/NaH2PO4, 0.01 M Tris/HCl, pH 6.3, 10 mM b-mercaptoethanol plus 0.2% Triton X-100). After the last wash His6-tagged SUMOylated products were eluted by incubating the beads in 75 ml of 200 mM imidazole, 0.15 M Tris/HCl pH 6.7, 30% glycerol, 0.72 M b-mercaptoethanol, 5%SDS for 20 min with vigorous shaking. The eluates were subjected to immunoblotting with anti-RelA antibody (C-20, Santa Cruz) or anti-V5 antibody (Abcam).

v. *In vitro* SUMOylation Assay. His-tagged RelA, RelA 122R mutant, and PIAS3 proteins were produced in BL-21 E. coli transformed with the corresponding pET-24a expression vectors by IPTG induction for 1 hour at room temperature. The His-tagged proteins were purified by Ni-NTA affinity purification in lysis buffer (50 mM NaHPO4 pH8, 300 mM NaCl, 10 mM imidazole). The eluted proteins were dialyzed against binding buffer (50 mM Tris [pH7.2]; 4% glycerol; 0.1% Triton-100; 1 mM EDTA; 50 mM NaCl). The in vitro SUMOylation assay was performed in 40 µl of reaction buffer (20 mM HEPES [pH 7.4], 50 mM MgCl2, 20 mM ATP) with 0.1 µg of SAE1/SAE2 (Boston Biochem), 0.1 µg of Ubc9 (Boston Biochem), 6 ug of SUMO3, 15 ng of RelA, and 0.2 µg of PIAS3 at 37C for one hour. The reaction was terminated by 5✕ SDS sample buffer. The SUMOylated products were visualized by immunoblotting with anti-RelA antibody.

vi. Luciferase Assay. Mouse 3T3 cells were plated in 24 well plates and transfected with NF-κB reporter, and β-galactosidase reporter vectors. 24 hrs post-transfection, cells were lysed in luciferase assay buffer (0.1 M NaPO4 [pH 8.0], 4 mM ATP, 1 mM pyrophosphate, 1 mM MgCl, 20 mM DTT) supplemented with 0.2% Triton-100. Cleared

supernatants were used for luciferase measurement. The β-galactosidase activity was measured by Tropix galacto-light beta-galactosidase assay (Applied Biosystems) for data normalization. The relative NF-kB luciferase activity was calculated by dividing the signal of NF-kB reporter by that of β-galactosidase.

vii. His-SUMO3 Lentivirus. His-SUMO3 [18] was cloned into XhoI/EcoRI sites of pSL35 lentiviral vector [21]. His-SUMO3 lentiviruses were generated using the four-plasmid system by cotransfection of 293T cells with pSL3, which expresses the vesicular stomatitis virus G envelope protein; pSL4, which expresses the HIV-1 gag/pol genes; pSL5, which expresses the rev gene; and pSL35 containing His-SUMO3. Lentivruses were harvested at 48 and 72 h after the transfection and concentrated by ultracentrifugation at 500,000×g for 90 min. The recombinant virus titer was determined for use of minimal viral particles to achieve ≥90% infection of IκBα null fibroblasts and wild type fibroblasts.

viii. DNA Affinity Immunoblot. RelA DNA binding activity was measured by DNA affinity immunoblotting, a sensitive in vitro technique for measurement of endogenous DNA binding proteins [22]. A 200 µg aliquot of nuclear extract was mixed with biotinylated NF-κB consensus binding sequence, biotin-CATAAGTCATGAGTTGAGGGGACTTTCC CAGGC in 1× DNA binding buffer [20 mM Tris (pH 7.2), 1 mM EDTA, and 0.06% Triton X-100 supplemented with 5 mM DTT, and 10 µg salmon sperm DNA), with a final NaCl level equal to 250 mM and glycerol level equal to 4%] in cold room for 30 minutes. The DNA bound proteins were captured by

streptavidin magnasphere paramagnetic particles (Promega) and analyzed by immunoblotting.


E. Results

i. RelA SUMOylation by PIAS3. To determine whether RelA is SUMOylated by PIAS proteins, we evaluated in vivo RelA SUMOylation in murine 3T3 cells transiently transfected with V5-tagged RelA, Flag-tagged PIAS proteins, and His-tagged SUMO3. Analysis of nickel-affinity purified RelA from the cell lysate revealed several slowly migrating forms of RelA (**Figure 14A**). As the slowly migrating forms of RelA were dependent on co-transfection of his-tagged SUMO3 (**Figure 15**), they represent SUMOylated RelA species with one or more SUMO3 molecules. Although RelA SUMOylation by PIAS1 and PIASy was detectable, PIAS3 showed the most potent effect on RelA SUMOylation. PIAS3-dependent RelA SUMOylation was also detected in other cell types such as HEK293 and H1299 cells (**Figure 16**). To test whether endogenous RelA is SUMOylated by PIAS3, we evaluated RelA SUMOylation by in vivo SUMOylation assay in 3T3 cells transiently transfected with Flag-tagged PIAS and His-tagged SUMO3. The SUMOylation of endogenous RelA by either PIAS1 or PIASy was barely detectable (Figure 1B). The endogenous RelA was SUMOylated by PIAS3 only after NF-κB activation by treatment of cells with TNFα (**Figure 14B**). Taken together, these data provide evidence that RelA is SUMOylated and that RelA SUMOylation is mediated by PIAS3.
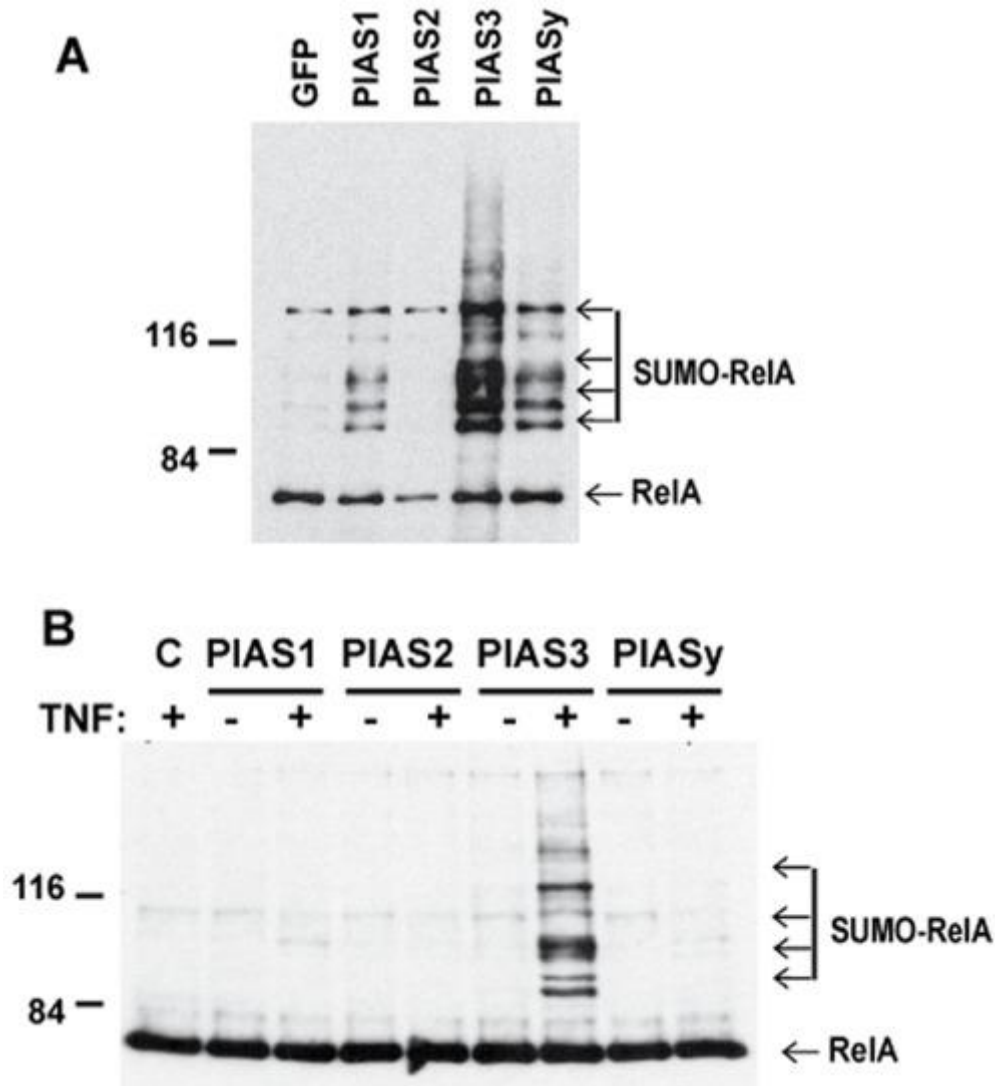
Figure 14. RelA is predominantly SUMOylated by PIAS3. A) SUMOylation of overexpressed RelA by PIAS proteins. Mouse 3T3 fibroblast cells were transfected with V5-tagged RelA, His-tagged SUMO3, and Flag-tagged PIAS vectors as indicated. SUMOylated RelA was measured by in vivo SUMOylation assay with anti-V5 antibody. B) TNFα-dependent SUMOylation of endogenous RelA in mouse 3T3 fibroblast cells. Mouse 3T3 cells were transfected with His-tagged SUMO3 and Flag-tagged PIAS vectors as indicated. The cells were treated with TNFα (20 ng/ml) for 4 hours after overnight transfection. SUMOylated RelA was measured by in vivo SUMOylation assay with anti-RelA antibody.
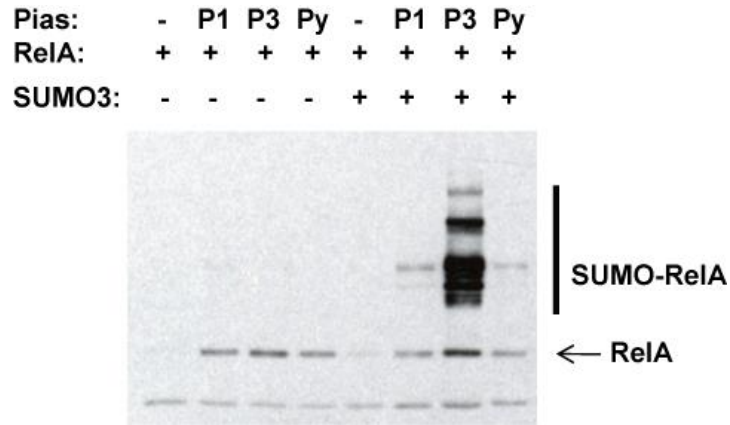
Figure 15. PIAS3 mediated RelA SUMOylation is SUMO3 dependent. 293T cells were transfected with v5 tagged RelA, flag-tagged PIAS, and his-tagged SUMO3 as indicated. SUMOylated RelA was measured by nickle pull down followed by immunoblotting with anti-V5 antibody.
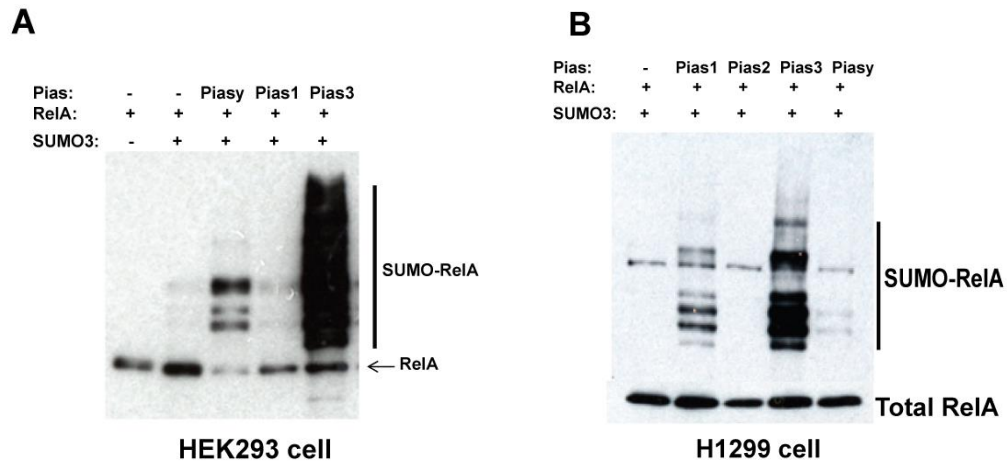

Figure 16. RelA SUMOylation by PIAS3 in HEK293 and H1299 cells. HEK293 cells (A) or H1299 cells (B) were transfected with V5-tagged RelA, His-tagged SUMO3, and Flag-tagged PIAS vectors as indicated. SUMOylated RelA was measured by nickle pull down followed by immunoblotting with anti-V5 antibody.

ii. Lysine 37, 121/122 are the Major SUMOylation Sites in RelA. Protein SUMOylation generally targets lysine residues in a ψKXE consensus sequence [23], where ψ is a hydrophobic amino acid residue, X represents any residue, E is an acidic residue, and K is a lysine residue to which SUMO moiety is covalently bound. There is no perfectly matched ψKXE consensus sequence in RelA protein. However, several nearly matched ψKXE consensus sequences in RelA protein are 37K(YKCE), 121/122K (VKKRD), and 222K (QKED). *In vivo* SUMOylation analysis of these RelA mutants revealed that PIAS3-mediated RelA SUMOylation was compromised by RelA mutations from lysine to arginine at 37 and 121/122 respectively (**Figure 17A**). PIAS3-mediated RelA SUMOylation was virtually abolished by compound mutation of 37K and 121/122K, indicating that lysine residues at 37 and 121/122 are involved in PIAS3-mediated RelA SUMOylation. To further define the role of PIAS3 in RelA SUMOylation, we conducted in vitro SUMOylation assays with purified RelA and PIAS3 proteins. As expected, RelA SUMOylation was abolished in the absence of either E1 enzyme (SAE1) or E2 enzyme (Ubc9) in the in vitro SUMOylation reaction. Consistent with the in vivo SUMOylation assays and RelA mutational analysis, RelA SUMOylation in vitro was enhanced by PIAS3 (**Figure 17B**) and RelA SUMOylation was compromised by 121/122 K>R mutation.

iii. RelA SUMOylation Dependent NF-kB Repression. Protein SUMOylation has been associated with a number of cellular activities including transcriptional repression by altering protein interactions [24]. To test the effects of PIAS3-mediated RelA SUMOylation, NF-κB luciferase activity was measured in 293T cells transfected with
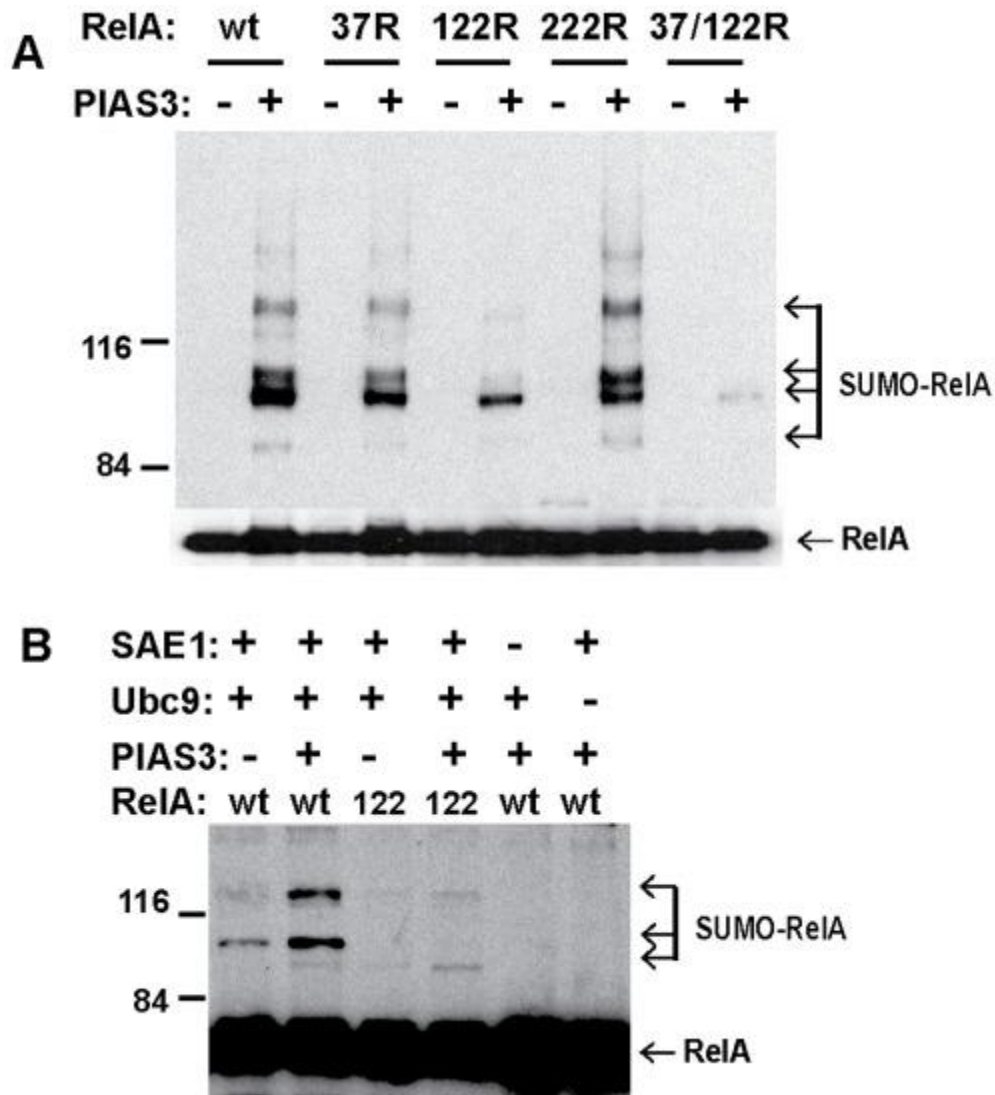
Figure 17. Identification of preferred RelA SUMOylation site. A) Mouse 3T3 cells were transfected with His-tagged SUMO3, v5-tagged RelA mutants 37R, 122R (121K>R/122K>R), and 222R as indicated, and Flag-tagged PIAS3 plasmids. The SUMOylated RelA was measured by nickel pull down followed by immunoblotting with V5 antibody. The total RelA protein was measured by direct immunoblotting with V5 antibody. B) Analysis of PIAS3-dependent RelA SUMOylation by in vitro SUMOylation assay. The in vitro SUMOylation assay was conducted with Purified E1 (SAE1), Ubc9, PIAS3, wild type RelA (wt), and RelA 122R mutant (122) as indicated. The SUMOylated RelA was detected by immunoblotting with anti-RelA antibody.

wild type RelA and SUMO defective RelA (SD-RelA, RelA with K>R mutations at 37, 121, and 122) (**Figure 18A**). NF-κB activation by wild type RelA was significantly repressed by PIAS3 overexpression. However, PIAS3-dependent NF-κB repression was compromised in the SUMOylation defective RelA mutant. As lysine is the accept site not only for SUMOylation but also for acetylation, methylation, and ubiquitination, these modifications may potentially contribute to altered NF-κB activity of SUMO defective RelA. To further define the contribution of RelA SUMOylation to NF-κB repression, NF-κB luciferase activity was compared in 293T cells transfected with wild type PIAS3 and catalytically dead PIAS3 mutant (CD-PIAS3, PIAS3 with C>S mutation at 299) (**Figure 18B**). The catalytically dead PIAS3 mutant failed to mediate RelA SUMOylation in response to NF-kB activation by constitutively active IKK2. These results suggest PIAS3-mediated RelA SUMOylation as a mechanism of NF-κB transcriptional repression.

iv. PIAS3 Mediated RelA SUMOylation is Induced by NF-κB Activation. Because PIAS3-mediated RelA SUMOylation was associated with NF-κB inhibition, we evaluated RelA SUMOylation as a potential mechanism for NF-κB negative regulation after activation by either TNFα treatment or co-transfection of constitutively active IKK2. Similar to TNFα treatment, the SUMOylation of endogenous RelA was induced by IKK2 co-transfection (**Figure 19A**). Analysis of NF-κB activity in the corresponding cells confirmed NF-κB activation by either TNFα treatment or IKK2 co-transfection (**Figure 19B**). In addition, the NF-κB activation by TNFα or IKK2 was repressed by PIAS3. This suggests that NF-κB activation is required for PIAS3-mediated RelA SUMOylation.
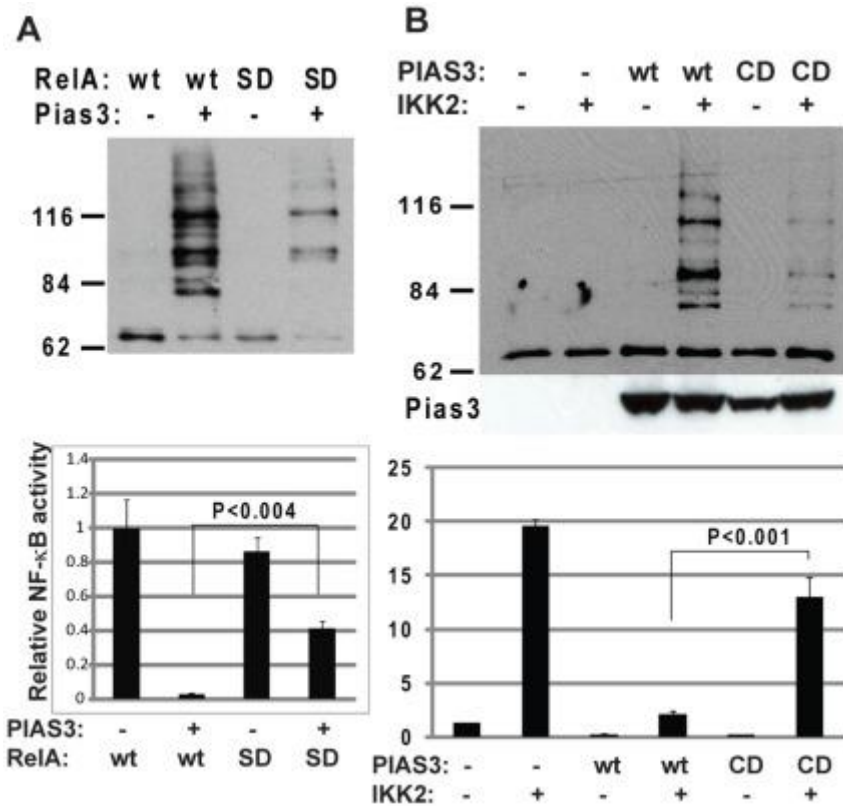
Figure 18. RelA SUMOylation-mediated NF-κB repression. A) Effects of RelA SUMO-dead mutation on PIAS3-mediated NF-κB repression. HEK 293T cells were transfected with his-tagged SUMO3, v5-tagged SUMO-dead mutant (SD, RelA with K>R mutations at 37, 121, and 122) and its wild type control (wt) in the presence or absence of Flag-tagged PIAS3. The SUMOylated RelA was measured by in vivo SUMOylation assay with anti-V5 antibody (upper panel). The corresponding NF-κB luciferase activity was measured (lower panel). B) Effects of PIAS3 catalytically dead mutation on PIAS3 mediated NF-κB repression. HEK 293T cells were transfected with wild type PIAS3 (WT), PIAS3 catalytically dead mutant (CD, PIAS3 with C>S mutation at 299), in the presence or absence of constitutively active IKK2. The SUMOylation of endogenous RelA was measured by in vivo SUMOylation assay with anti-RelA antibody (Upper panel). The corresponding NF-κB luciferase activity was measured (lower panel).
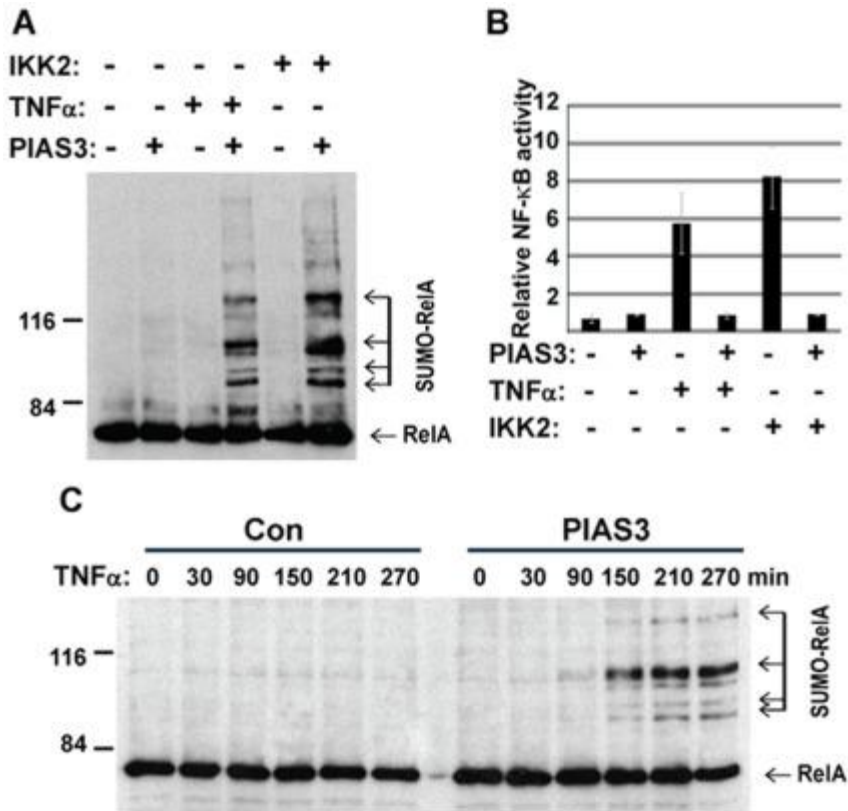
Figure 19. Endogenous RelA SUMOylation by PIAS3 is induced by NF-κB activation. A) HEK 293T were transfected with his-SUMO3 plus PIAS3 or GFP control plasmid as indicated. NF-κB activation was achieved by either co-transfection of constitutive IKK2 or TNFα treatment (20 ng/ml for 4 hours). SUMOylated RelA was measured by nickle pull down followed by immunoblotting with anti-RelA antibody. B) NF-κB repression by PIAS3. The NF-κB activity of cells described in panel A was measured by NF-κB luciferase assay. C) The time course of RelA SUMOylation in response to NF-κB activation. HEK 293T cells were transfected with his-SUMO3 plus PIAS3 or control GFP plasmid as indicated. The cell lysates were collected for in vivo SUMOylation assay at indicated time points after TNFα treatment (20 ng/ml). SUMOylated RelA was detected by nickel pull down followed by immunoblotting

Because NF-κB activation is repressed by PIAS3, RelA SUMOylation by PIAS3 is likely a mechanism for NF-κB negative regulation.

To further define the role of NF-κB activation in RelA SUMOylation, we examined the kinetics of PIAS3-mediated RelA SUMOylation in response to TNFα treatment. PIAS3-mediated RelA SUMOylation was observed 150 minutes after TNFα treatment and increased with time after TNFα treatment (**Figure 19C**). These results are consistent with RelA SUMOylation by PIAS3 as a negative regulatory mechanism for NF-κB.
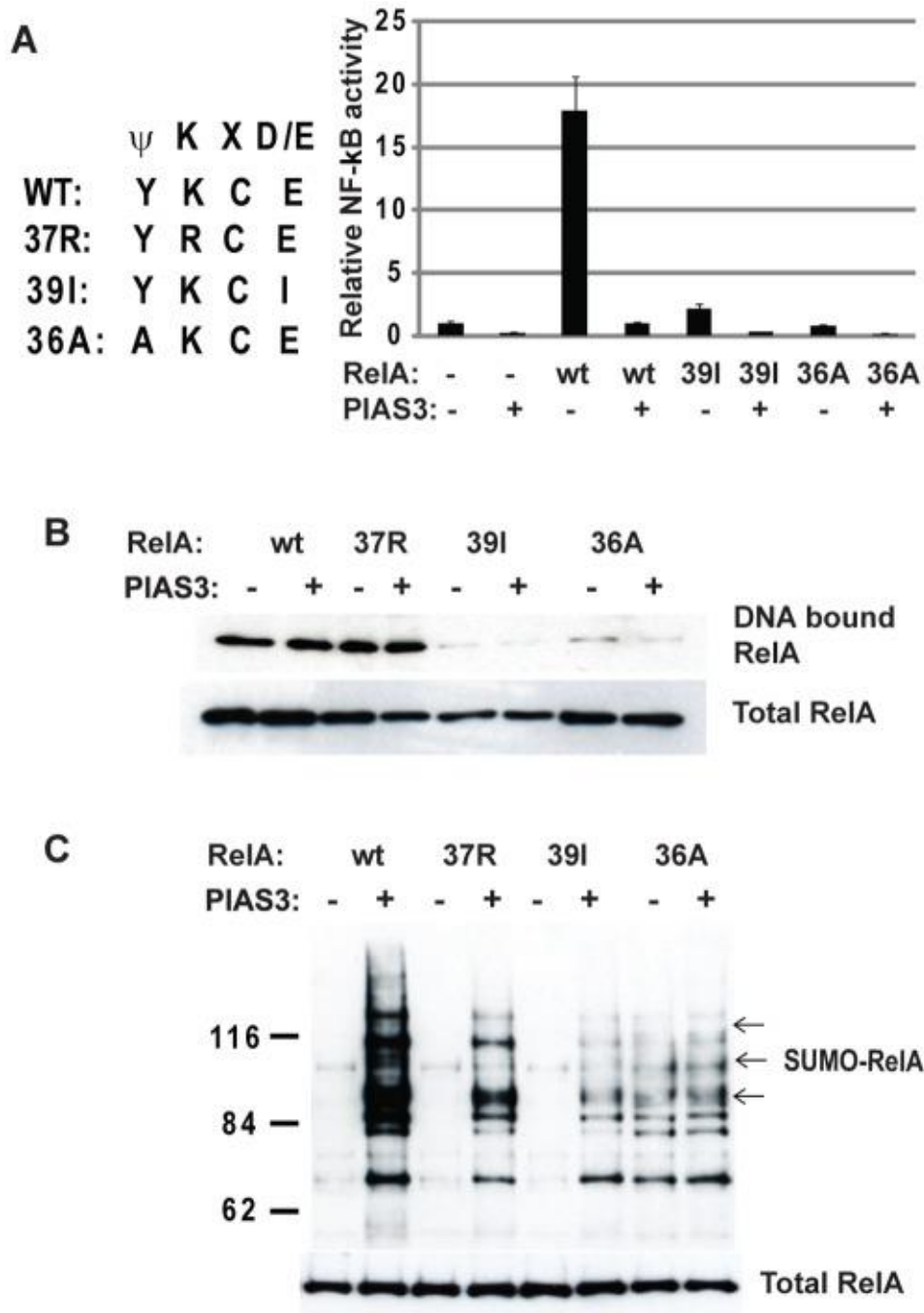
v.   DNA Binding Dependent RelA SUMOylation by PIAS3. The central mechanism of NF-κB regulation is through the NF-κB negative regulator, IκBα, which sequesters NF-κB in the cytoplasm and dissociates NF-κB from DNA in the nucleus [2]. To further define the role of PIAS3-mediated RelA SUMOylation as a negative regulator of activated NF-κB in the nucleus, we evaluated RelA SUMOylation in cells with IκBα null background. To overcome low transfection frequency of IκBα null cells compared to wild type cells, we established cell lines with stable expression of His-tagged SUMO3. In the absence of TNFα, RelA SUMOylation was barely detected in either wild type or IκBα null cell lines. RelA SUMOylation was induced in both wild type and IκBα null cell lines upon TNFα treatment. IκBα null cells showed much stronger RelA SUMOylation than its wild type counterpart (**Figure 20A**). To test whether enhanced RelA SUMOylation in IκBα null cells is associated with increased RelA nuclear accumulation or RelA DNA binding capability, we evaluated RelA SUMOylation in wild type and IκBα null cells treated with leptomycin B to block RelA nuclear export. Upon leptomycin B treatment,

102
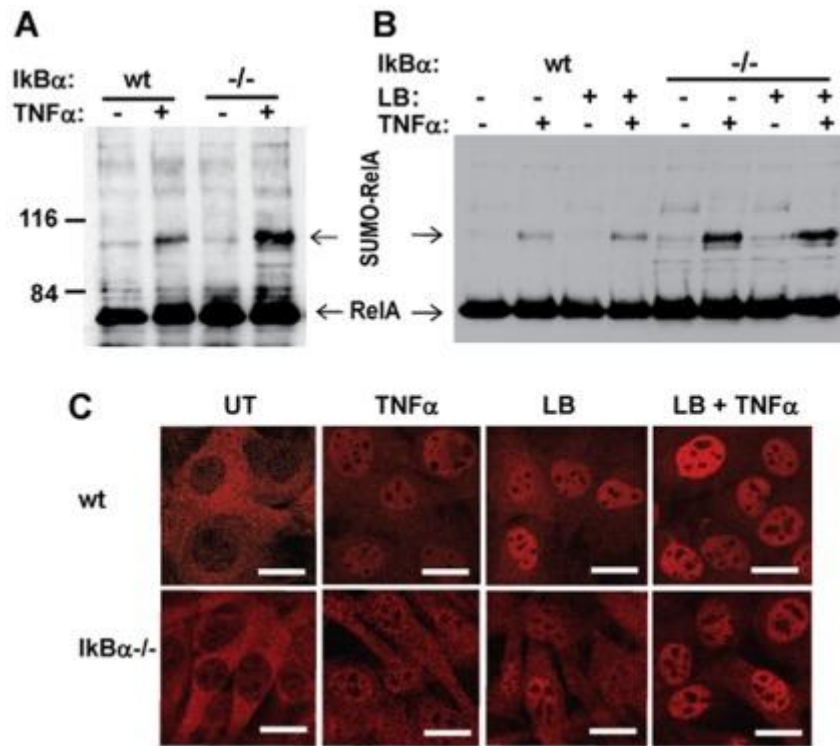
Figure 20. PIAS3-mediated RelA SUMOylation is enhanced by IκBα deficiency. IκBα null and wild type fibroblasts were stably transduced with His-tagged SUMO3 lentivirus. The SUMO3 transduced cells were treated with 20 ng/ml TNFα for 2 hours without (A) or with (B) 10 ug/ml leptomycin B for 2 hours, and subjected to in vivo SUMOylation assay. The SUMOylated RelA was detected by immunoblotting with anti-RelA antibody. C) RelA localization in response to TNFα and/or leptomycin B treatment. RelA protein was stained with anti-RelA antibody. The bar equals 20 microns.

RelA accumulated in the nucleus in both wild type and IκBα null cells (**Figure 20**). However, RelA SUMOylation was detected only after TNFα treatment, not in either cell line treated with leptomycin B alone, showing that nuclear accumulation of RelA was insufficient for RelA SUMOylation.

Because dissociation of RelA DNA binding is another function of IκBα, we evaluated whether RelA DNA binding is required for PIAS3-mediated SUMOylation of RelA by using RelA mutants (39E>I and 36Y>A) defective in DNA binding [25]. The 39E>I and 36Y>A mutants, conferred defects in NF-κB activation as expected (**Figure 21A**). Consistent with previous DNA binding data [25], the39E>I and 36Y>A mutants failed to bind NF-κB consensus DNA binding sequence whereas the DNA binding activity of 37K>R mutant was not affected (**Figure 21B**). Compared with wild type RelA and SUMOylation compromised mutant at 37K, PIAS3-mediated RelA SUMOylation was abolished by both 39E>I and 36Y>A mutants (**Figure 21B**). It is of interest to note that weak RelA SUMOylation was induced independent of PIAS3 in the 36Y>A mutant (**Figure 21C**), likely due to the generation a perfectly matched SUMO consensus site (ψKXE), converting a polar amino acid to a hydrophobic amino acid. Even so, PIAS3-dependent RelA SUMOylation was abolished by the same mutation. The abolition of PIAS3-mediated RelA SUMOylation by different RelA mutants defective in DNA binding suggests that DNA bound RelA is the preferred target for SUMOylation by PIAS3.

Figure 21. PIAS3-mediated RelA SUMOylation is dependent on RelA DNA binding. A) HEK 293T cells were transfected with Flag-tagged PIAS3, V5-tagged RelA and RelA mutants defective in DNA binding (39I and 36A) as indicated. The transactivation activity was measured by NF-κB luciferase activity. B) The nuclear extracts from HEK 293T cells transfected with indicated plasmids were subjected to DNA affinity immunoblotting with biotinylated NF-κB consensus binding DNA. DNA bound RelA was measured by immunoblotting with anti V5 antibody. C) The cell lysates from HEK293T cells transfected with indicated RelA mutants were collected for in vivo SUMOylation assay and detected by anti-V5 antibody for SUMOylated RelA (B).

F. Discussion

NF-κB is known to be tightly negatively regulated by IκBα, which dissociates NF-κB from DNA and sequesters it in the cytoplasm [3], [4], [5], [26]. In this study, we provide experimental evidence for a novel mechanism for negative regulation of NF-κB by PIAS3-mediated RelA SUMOylation. PIAS3-mediated SUMOylation of endogenous RelA was observed to increase with time after TNFα stimulation, and RelA DNA binding-defective

mutants were resistant to PIAS3-mediated SUMOylation. The dependence of SUMOylated RelA upon DNA binding capability as shown by DNA binding defective mutants, and upon TNFα stimulation and not simply nuclear localization after leptomycin B treatment, suggests a biochemical mechanism for NF-κB transcriptional repression.

PIAS3 has been reported to repress NF-κB activity through interfering with RelA binding to transcriptional co-activators [15]. However, PIAS3-mediated RelA SUMOylation was not considered a factor, largely due to the lack of perfectly matched SUMO consensus motifs in the RelA protein sequence and lack of detectable SUMOylated RelA under the conditions of that study. In our study, we demonstrate RelA SUMOylation by PIAS3 under both overexpressed and physiological conditions. While RelA could be weakly SUMOylated by other PIAS proteins like PIAS1 and PIASy, endogenous RelA was SUMOylated specifically by PIAS3, indicating PIAS3 as a primary mediator for RelA SUMOylation. Approaches to knockdown PIAS3 function by shRNA targeting of PIAS3

have been unsuccessful, so far, to address PIAS3dependence of RelA SUMOylation, in part possibly due to PIAS redundancy and shRNA efficiency. However, endogenous RelA SUMOylation specifically mediated by PIAS3 was demonstrated using the catalytically dead PIAS3 mutant.

Although protein SUMOylation is associated with many cellular activities, transcriptional repression is the primary consequence of protein SUMOylation. In fact, SUMO consensus sequence (ψKXE) was identified as a synergy control motif for transcriptional repression even before being recognized as a SUMO consensus sequence [27]. The identification of RelA SUMOylation has been hampered by the lack of perfectly matched ψKXE consensus sequence in RelA protein [15]. Recent global analysis of SUMOylated endogenous proteins revealed that one third of SUMO sites are not perfectly matched to ψKXE consensus sequences [28]. In this study, we have identified two imperfectly matched SUMOylation sites, 37K (YKCE), 121/122K (VKKRD) in RelA protein. Compound mutation of these sites abolished PIAS3-mediated RelA SUMOylation, and compromised PIAS3-mediated NF-κB repression (**Figure 17 and Figure 18**). Compromised NF-κB repression by PIAS3 mutant defective in E3 SUMO ligase activity further supported the role of PIAS3-mediated RelA SUMOylation in NF-κB repression (**Figure 18B**). These data suggest that RelA SUMOylation is a mechanism for NF-κB negative regulation, consistent with the known role of SUMOylation in transcriptional repression.

So far, the mechanism of RelA SUMOylation-mediated transcriptional repression is largely unknown. A number of transcriptional repressors and corepressors are either SUMOylated or associated with SUMOylated proteins through their SUMO interacting motif, thus enabling formation of transcription repression complexes [17], [26]. SUMOylation contributes to heterochromatin establishment and maintenance in yeast and Drosophila [29], [30]. A number of transcriptional repressors are either SUMOylated or capable of binding to the SUMO moiety through the SUMO interacting motif (SIM), including HDAC1 [31], CtBP [32], ZEB1 [26] and CoREST [33]. However, it has been a challenge to identify SUMOylation-dependent formation of transcription repression complexes. By sequential chromatin immunoprecipitation, Shuai's group elegantly demonstrated PIAS1-dependent recruitment of heterochromatin protein 1 and DNA methyltransferase to the Foxp3 promoter [34]. These lines of evidence suggest that PIAS3-mediated RelA SUMOylation may provide a scaffold for the recruitment of transcriptional repressors with SUMO binding motifs thus leading to transcriptional repression. In addition to SUMOylation, the RelA SUMO sites are modified by methylation by SET7/9 [35] and acetylation by p300 and PCAF [36]. Further study to understand the relationship among these modifications is needed to define the mechanism of RelA SUMOylation in NF-κB transcriptional regulation.

Like many important signaling pathways, the NF-κB pathway is exquisitely regulated by multiple negative feedback regulatory mechanisms, such as the induction of IκBα to sequester NF-κB in the cytoplasm [5] and A20 to block NEMO activation [37]. In addition to NF-κB repression by RelA SUMOylation, we also demonstrated that PIAS3-

mediated RelA SUMOylation was induced by NF-κB activation (**Figure 20**). The induction of RelA SUMOylation by NF-κB activation and the repression of NF-κB activity by RelA SUMOylation suggest that PIAS3-mediated RelA SUMOylation is a negative feedback mechanism for NF-kB regulation. This notion was further supported by the evidence from IκBα null cells, in which RelA SUMOylation was significantly enhanced, suggesting its compensatory role in NF-kB negative regulation.

It remains a challenge to define the molecular pathways that lead to RelA SUMOylation in response to NF-κB activation. The evidence from RelA mutants defective in DNA binding suggests that DNA-bound RelA is the preferred target for PIAS3-mediated RelA SUMOylation. In this study, RelA mutants (39E>I and 36Y>A) defective in DNA binding [25] also abolished PIAS3-mediated SUMOylation. Coincidently, both mutations reside in the N-terminal RelA SUMO consensus motif (36YKCE39). The abolition of PIAS3-mediated RelA SUMOylation by these mutations is very unlikely due to the disruption of the SUMO consensus site. Compared with the SUMOylation of 37K>R mutant, 39E>I mutation showed more severe effect on PIAS3-mediated RelA SUMOylation. Furthermore, 36Y>A mutation that generates a perfect SUMOylation motif, also abolished PIAS3-mediated RelA SUMOylation despite its enhancement of PIAS3-independent RelA SUMOylation. The abolition of PIAS3-mediated RelA SUMOylation by these various RelA DNA binding mutants suggests that RelA DNA binding is a determining factor in PIAS3-mediated RelA SUMOylation. In vitro, RelA DNA complex can be rapidly dissociated by IκBα, which reduces the half-life of the RelA DNA complex from 45 to 3 minutes [38]. RelA binding to DNA is negatively regulated by IκBα [3],

which therefore reduces the pool of DNA-bound RelA available for SUMOylation. In the absence of IκBα negative regulation, increased DNA-bound RelA is available for SUMOylation. Thus, SUMOylation of RelA could be a mechanism to halt sustained NF-κB activation that is beyond the capacity of IκBα to control. The SUMOylation of DNA-bound RelA provides a molecular basis to form heterchromatic foci at promoters of genes regulated by NF-κB, to repress transcription, thus safeguarding against sustained transcriptional activation. Future studies will be needed to illustrate the mechanisms of RelA SUMOylation in NF-κB negative regulation in specific cell contexts, including defining NF-κB downstream genes affected by SUMOylation of RelA, and the associated transcriptional repressors in complex with SUMOylated RelA.

G. References

1. Ghosh S, Karin M. 109 Suppl. Cell; 2002. Missing pieces in the NF-kappaB puzzle. pp. S81–96.

2. Hoffmann A, Baltimore D. Circuitry of nuclear factor kappaB signaling. Immunol Rev. 2006;210:171–186.

3. Arenzana-Seisdedos F, Thompson J, Rodriguez MS, Bachelerie F, Thomas D, et al. Inducible nuclear expression of newly synthesized I kappa B alpha negatively regulates DNA-binding and transcriptional activities of NF-kappa B. Mol Cell Biol. 1995;15:2689–2696.

4. Arenzana-Seisdedos F, Turpin P, Rodriguez M, Thomas D, Hay RT, et al. Nuclear localization of I kappa B alpha promotes active transport of NF-kappa B from the nucleus to the cytoplasm. J Cell Sci 110 (Pt. 1997;3):369–378.

5. Hoffmann A, Levchenko A, Scott ML, Baltimore D. The IkappaB-NF-kappaB signaling module: temporal control and selective gene activation. Science. 2002;298:1241–1245.

6. Wertz IE, O'Rourke KM, Zhou H, Eby M, Aravind L, et al. De-ubiquitination and ubiquitin ligase domains of A20 downregulate NF-kappaB signaling. Nature. 2004;430:694–699.

7. Brummelkamp TR, Nijman SM, Dirac AM, Bernards R. Loss of the cylindromatosis tumor suppressor inhibits apoptosis by activating NF-kappaB. Nature. 2003;424:797–801.

8. Kovalenko A, Chable-Bessia C, Cantarella G, Israel A, Wallach D, et al. The tumor suppressor CYLD negatively regulates NF-kappaB signalling by deubiquitination. Nature. 2003;424:801–805.

9. Trompouki E, Hatzivassiliou E, Tsichritzis T, Farmer H, Ashworth A, et al. CYLD is a deubiquitinating enzyme that negatively regulates NF-kappaB activation by TNFR family members. Nature. 2003;424:793–796.

10. Girdwood DW, Tatham MH, Hay RT. SUMO and transcriptional regulation. Semin Cell Dev Biol. 2004;15:201–210.

11. Desterro JM, Rodriguez MS, Hay RT. SUMO-1 modification of IkappaBalpha inhibits NF-kappaB activation. Mol Cell. 1998;2:233–239.

12. Mabb AM, Wuerzberger-Davis SM, Miyamoto S. PIASy mediates NEMO sumoylation and NF-kappaB activation in response to genotoxic stress. Nat Cell Biol. 2006;8:986–993.

13. Shuai K, Liu B. Regulation of gene-activation pathways by PIAS proteins in the immune system. Nat Rev Immunol. 2005;5:593–605.

14. Liu B, Yang R, Wong KA, Getman C, Stein N, et al. Negative regulation of NF-kappaB signaling by PIAS1. Mol Cell Biol. 2005;25:1113–1123.

15. Jang HD, Yoon K, Shin YJ, Kim J, Lee SY. PIAS3 suppresses NF-kappaB-mediated transcription by interacting with the p65/RelA subunit. J Biol Chem. 2004;279:24873–24880.

16. Liu Y, Lagowski JP, Gao S, Raymond JH, White CR, et al. Regulation of the psoriatic chemokine CCL20 by E3 ligases Trim32 and Piasy in keratinocytes. J Invest Dermatol. 2010;130:1384–1390.

17. Garcia-Dominguez M, Reyes JC. SUMO association with repressor complexes, emerging routes for transcriptional control. Biochim Biophys Acta. 2009;1789:451–459.

18. Dorval V, Fraser PE. Small ubiquitin-like modifier (SUMO) modification of natively unfolded proteins tau and alpha-synuclein. J Biol Chem. 2006;281:9919–9924.

19. Mercurio F, Zhu H, Murray BW, Shevchenko A, Bennett BL, et al. IKK-1 and IKK-2: cytokine-activated IkappaB kinases essential for NF-kappaB activation. Science. 1997;278:860–866.

20. Schneider BL, Bowden GT, Sutter C, Schweizer J, Han KA, et al. 7,12-Dimethylbenz[a]anthracene-induced mouse keratinocyte malignant transformation independent of Harvey ras activation. JInvest Dermatol. 1993;101:595.

21. Liu Y, Lagowski J, Sundholm A, Sundberg A, Kulesz-Martin M. Microtubule disruption and tumor suppression by mitogen-activated protein kinase phosphatase 4. Cancer Res. 2007;67:10711–10719.

22. Liu Y, Asch H, Kulesz-Martin MF. Functional quantification of DNA-binding proteins p53 and estrogen receptor in cells and tumor tissues by DNA affinity immunoblotting. Cancer Res. 2001;61:5402.

23. Rodriguez MS, Dargemont C, Hay RT. SUMO-1 conjugation in vivo requires both a consensus modification motif and nuclear targeting. J Biol Chem. 2001;276:12654–12659.
24. Hay RT. SUMO: a history of modification. Mol Cell. 2005;18:1–12.

25. Wissink S, van Heerde EC, Schmitz ML, Kalkhoven E, van der Burg B, et al. Distinct domains of the RelA NF-kappaB subunit are required for negative cross-talk and direct interaction with the glucocorticoid receptor. J Biol Chem. 1997;272:22278–22284.

26. Wang J, Scully K, Zhu X, Cai L, Zhang J, et al. Opposing LSD1 complexes function in developmental gene activation and repression programs. Nature. 2007;446:882–887.

27. Iniguez-Lluhi JA, Pearce D. A common motif within the negative regulatory regions of multiple factors inhibits their transcriptional synergy. Mol Cell Biol. 2000;20:6040–6050.

28. Matic I, Schimmel J, Hendriks IA, van Santen MA, van de Rijke F, et al. Site-specific identification of SUMO-2 targets in cells reveals an inverted SUMOylation motif and a hydrophobic cluster SUMOylation motif. Mol Cell. 2010;39:641–652.

29. Shin JA, Choi ES, Kim HS, Ho JC, Watts FZ, et al. SUMO modification is involved in the maintenance of heterochromatin stability in fission yeast. Mol Cell. 2005;19:817–828.

30. Hari KL, Cook KR, Karpen GH. The Drosophila Su(var)2–10 locus regulates chromosome structure and function and encodes a member of the PIAS protein family. Genes Dev. 2001;15:1334–1348.

31. David G, Neptune MA, DePinho RA. SUMO-1 modification of histone deacetylase 1 (HDAC1) modulates its biological activities. J Biol Chem. 2002;277:23658–23663.

32. Lin X, Sun B, Liang M, Liang YY, Gast A, et al. Opposed regulation of corepressor CtBP by SUMOylation and PDZ binding. Mol Cell. 2003;11:1389–1396.

33. Ouyang J, Shi Y, Valin A, Xuan Y, Gill G. Direct binding of CoREST1 to SUMO-2/3 contributes to gene-specific repression by the LSD1/CoREST1/HDAC complex. Mol Cell. 2009;34:145–154.

34. Liu B, Tahk S, Yee KM, Fan G, Shuai K. The ligase PIAS1 restricts natural regulatory T cell differentiation by epigenetic repression. Science. 2010;330:521–525.

35. Li Y, Reddy MA, Miao F, Shanmugam N, Yee JK, et al. Role of the histone H3 lysine 4 methyltransferase, SET7/9, in the regulation of NF-kappaB-dependent inflammatory genes. Relevance to diabetes and inflammation. J Biol Chem. 2008;283:26771–26781.

36. Kiernan R, Bres V, Ng RW, Coudart MP, El Messaoudi S, et al. Post-activation turn-off of NF-kappa B-dependent transcription is regulated by acetylation of p65. J Biol Chem. 2003;278:2758–2766.
37. Werner SL, Kearns JD, Zadorozhnaya V, Lynch C, O'Dea E, et al. Encoding NF-kappaB temporal control in response to TNF: distinct roles for the negative regulators IkappaBalpha and A20. Genes Dev. 2008;22:2093–2101.

38. Zabel U, Baeuerle PA. Purified human I kappa B can rapidly dissociate the complex of the NF-kappa B transcription factor with its cognate DNA. Cell. 1990;61:255–265.